2018

Impact of Submerged Aquatic Vegetation on Water Quality in Cache Slough Complex, Sacramento-San Joaquin Delta: a Numerical Modeling Study

Xun Cai
College of William and Mary - Virginia Institute of Marine Science, ncai@vims.edu

IMPACT OF SUBMERGED AQUATIC VEGETATION ON WATER QUALITY IN CACHE SLOUGH COMPLEX, SACRAMENTO-SAN JOAQUIN DELTA: A NUMERICAL MODELING STUDY

A Thesis

Presented to

The Faculty of the School of Marine Science

The College of William and Mary in Virginia

In Partial Fulfillment

of the Requirements for the Degree of

Master of Science

---

by

Xun Cai

August 2018

APPROVAL PAGE

This thesis is submitted in partial fulfillment of

the requirements for the degree of

Master of Science

Xun Cai

Approved by the Committee, July 2017

Yinglong Joseph Zhang, PhD
Committee Chair / Advisor

Jian Shen, PhD
Co-Advisor

Carlton H. Hershner

Ping Wang

Eli Ateljevich
California Department of Water Resources
Sacramento, CA, USA

TABLE OF CONTENTS

Acknowledgements

This thesis has been made possible by an incredibly supportive network of mentors, colleagues, friends and family. First and foremost, I would like to express my deepest thanks to my advisor, Dr. Joseph Zhang, for his constant supports and encouragements. He demonstrated the patience, enthusiasm, and guidance of only the highest quality from a mentor, in addition to being a motivational speaker, a challenger and even an editor. I would also like to thank my co-advisor, Dr. Jian Shen for his advice, flexibility, availability, and patience over the past three years. Also, thanks are due to my committee members Dr. Carlton Hershner, Dr. Eli Ateljevich and Dr. Ping Wang for their knowledge and recommendations while working on my master's thesis. Their review and input were fundamental to the successful completion of my study. My fellow lab mates, Dr. Zhengui Wang and Qubin Qin, deserve special thanks for helping me on my intensive processing thesis work. I'd like to thank Dr. Roger Mann for serving as moderator in the defense.

A special thank-you to the VIMS Office of Academic Studies, especially Associate Dean Linda Schaffner, Ombud Faculty Dr. Deborah Steinburg, Ombud Student Dr. Julia Moriarty, Registrar and Assistant to the Associate Dean Jennifer Hay, and Graduate Program Business Manager Cathy Cake for being so supportive and responsive to students.

I would like to thank the VIMS community, especially Fei Da, Fei Ye, Weiling Sun, Lizzy Clyne, Karinna Nunez, Xiaodong Wang, Wenlong Chen, Nathalie Schieder, Mac Sisson (for his diligent editing effort), Zhuo Liu, Rico Wang and my classmates. You made graduate school fun and my foreign life less lonely. I would also like to thank the CCRM members, especially Administrative Coordinator Dawn Fleming for everything that she did for me. Furthermore, I'd like to thank my English training volunteers, especially Jim Hutchins, and his wife, Mary Margaret, who have become one of my best friends and like my family in this country. I will always be thankful for the VIMS folks who taught me life skills and science beyond what is presented in this thesis.

Finally, I would like to thank my family, for supporting my dreams throughout my life, even though we were thousands of miles apart. I am especially thankful to my parents for constantly motivating me to do my best, and to my grandparents who raised and kept me company for the first 15 years of my life.

This work is financially supported by California Department of Water Resources and VIMS Graduate Research Grants. We have also received generous help from EPA's Chesapeake Bay Program, which has made their SAV code available to Dr. Harry Wang who passed it onto us. This code served as a starting point for the new SAV model developed in this thesis.

List of Figures

List of Tables

Abstract

Submerged aquatic vegetation (SAV) plays a significant role in many aquatic systems, and impacts both physical and ecological quantities. It can baffle currents, attenuate waves, recycle nitrogen and phosphorus from the sediment bed, perform ecosystem function as a primary producer, and provide critical habitat for many aquatic species. Conversely, the invasive SAV, Egeria densa (Brazilian waterweed), in the San Francisco Bay & Delta has been a nuisance since its introduction into the system in the 1960s. It has displaced most of the native submersed aquatic plant species in the Delta and restructured the ecosystem, thus threatening the survival of several endangered native fishes such as Delta Smelt. Its impacts on the ecological system remain largely unknown and the need for assessment is growing.

This multi-interdisciplinary study, incorporating biogeochemistry, hydrodynamics, and numerical computing and field survey data, accomplishes two main goals. The first goal is to develop a new SAV model imbedded into the unstructured-grid SCHISM-ICM framework. In addition to the advantages of directly simulating the SAV impact on hydrodynamics using high-resolution unstructured grids, this new SAV model can also simulate the competition between SAV and phytoplankton for light and nutrient supplies. The second goal is to apply the new model to Cache Slough Complex, Sacramento-San Joaquin Delta, to estimate the impact on the water quality from intervening SAV removal. Removal of SAV is already being studied in Little Hastings Tract and this study can serve to develop hypotheses for monitoring and ultimately guidance for managing SAV removal in the Bay-Delta region.

We benchmark the new SAV model with the tests on the SAV biomass, growth and impacts on light supply and nutrient budget in the water column and sediment bed, respectively. Starting from a uniform biomass distribution, we simulate the evolution of biomass over seasonal scales and validate the calculated distribution with the observed distribution. The model is able to successfully simulate the SAV die-off process in areas where it is known to be unable to colonize.

By applying the fully coupled SCHISM-ICM-SAV model in the Cache Slough Complex area, the changes of the water quality state variables due to SAV are estimated over spatial and seasonal scales. Generally, SAV increases the accumulation of phytoplankton by locally reducing flushing and thus increasing the residence time, but in the meantime, reduces its local growth rate due to light shading and nutrient competition. A combination of direct impact from SAV and indirect impact through changed phytoplankton results in changes in other water quality variables: dissolved oxygen and nutrients. SAV tends to increase oxygen and organic nutrients while decreasing inorganic nutrients. For this system, the feedback loop from SAV to the hydrodynamics plays the most important role in the water quality variables among all feedback loops.

Impact of Submerged Aquatic Vegetation on Water Quality in Cache Slough Complex, Sacramento-San Joaquin Delta: A Numerical Modeling Study

Chapter 1 Introduction

1.1. Background

1.1.1 SAV Effects on the Aquatic System

SAV (submerged aquatic vegetation) is a term used to describe rooted vascular plants that grow completely under the water surface (Thayer and Fonseca, 1984). It is defined as any combination of seagrasses, oligohaline grasses, attached macroalgae and drift algae that cover 10 to 100 percent of a substrate (Maglio and Hershorin, 2013). SAV has a large influence on physical and ecological environments (Carpenter and Lodge, 1986). It can affect the basic physical parameters, such as light and temperature, as the SAV canopy attenuates light exponentially with depth, making the temperature gradient underneath 20 times greater than outside (Westlake, 1964; Owens et al., 1967; Dale and Gillespie, 1977). More importantly, SAV affects the hydrodynamics in aquatic systems, including changes in flow structure, wave attenuation, and additional turbulence production, and thus alters the circulation pattern and sediment transport (Darby, 1999; Mendez and Losada, 2004). The magnitude of wave orbital velocity is reduced throughout the depth (Tsujimoto and Kitamura, 1995). A reduction of almost 40% of wave height was measured in emergent wetland plants in Lake Ontario, Canada (Tschirky et al., 2001). Additional production and increase of three-dimensional coherent large eddies occur on the top and lateral boundary of the emergent vegetation (Ikeda and Kanazawa, 1996; Tsujimoto and Kitamura, 1995). As the established SAV beds slow down the water flow and decrease shear stress, sedimentation and retention of the bed material are increased, which in turn decreases turbidity caused by suspended sediments and increases water clarity (De Boer, 2007). SAV is documented to be one of the important factors in turbidity decline; for example, 21-70% turbidity decline trend is attributed to the SAV expansion in the Sacramento-San Joaquin Delta (Hestir et al., 2016). Because of the influence on hydrodynamics, abundance of SAV tends to trap the sediments and thus modifies the river beds into shallower environments (Yarrow et al., 2009).

SAV beds, usually ranked among the most productive habitats in marine and estuarine environments, act as "ecosystem engineer" (Latta et al., 2012; Moore, 2004). SAV can have a larger oxygenate rate in water than phytoplankton and the rhizospheres (Pokorný and Rejmánková, 1983; Oremland and Taylor, 1977). Also, SAV serves as a huge nutrient recycler in the water; for example, it removes inorganic carbon, nitrogen and phosphorus through assimilation into organic matter and precipitation as carbonate salts and pH-mediated P co-precipitation on the leaves, (Wetzel, 1960; Dierberg et al., 2002). SAV-dominated lakes and rivers can have a mean total phosphorus mass removal of 1.2 g/m^2 per year (Knight et al., 2003). Furthermore, SAV, accounting for 4 to 93% of host macrophyte productivity, provides habitat to a rich array of microbes, algae and fishes, and plays an important role in biotic interaction in the ecosystem (Allanson, 1973; Howard-Williams and Allanson, 1981). On the other hand, it is also a nuisance species that clogs the waterways in the Sacramento-San Joaquin Delta, as we will discuss in Section 1.1.3.

1.1.2 San Francisco Bay and Delta

The system of interest in this study is the San Francisco Bay and Delta ('Bay-Delta' hereafter). San Francisco Bay is located at northern California coast and is the second largest estuary in the US west coast, while the Sacramento-San Joaquin Delta ('Delta' hereafter) is a web of channels and reclaimed islands by the confluence of the Sacramento and San Joaquin Rivers, lying east of the Suisun Bay (Nichols et al., 1986; Lund et al., 2007). The Bay-Delta system is a typical shallow and coastal plain estuary (Nichols et al., 1986; Cloern, 1987). The central channel is 10-20 m while the subtidal shoals are less than 3 m in depth (Nichols et al., 1986). It is dominated by semidiurnal tide and the tidal range of nearly ~2m at the Golden Gate (http://tidesandcurrents.noaa.gov). The averaged maximum temperature is 34.6℃, and the minimum temperature is 3.4℃(Center, 2010).

The Delta contributes about 90 percent of the freshwater inflow into Suisun Bay that goes through San Pablo Bay and San Francisco Bay to the Pacific (Smith, 1987). Annual discharge is

characterized with a high winter runoff and low summer runoff (Jassby and Cloern, 2000). The annual variability in the freshwater inflow plays an important role on the Bay-Delta system; for example, doubling freshwater outflow from the Delta would move the salinity gradient about 8 km seaward (Latta et al., 2012). The seasonal freshwater discharge from Delta mostly influences the northern reach, while the south bay receives negligible amount of freshwater inflow and is controlled by tide and wind (Smith, 1987; Peterson et al., 1975). Due to the annual freshwater discharge, the northern reach exhibits a clear gravitational circulation pattern, while the south bay is lagoon-like and generally well-mixed (Cloern, 1987; Latta et al., 2012). The northern reach generally has a turbidity maximum in summer, while the south bay has substantially lower suspended particulate matter concentration (Conomos and Peterson, 1977). The seasonal riverine input of suspended sediments, with maxima during winter storms, is composed of lithogenous materials (Conomos and Peterson, 1977). A large spatial gradient in turbidity occurs in the Bay, with highest suspended particulate matter concentrations in the upper estuary, and lowest at the estuary mouth (Cloern, 1987).

The Bay-Delta is commonly characterized as an estuary of exceptionally low productivity as compared to many estuaries in the world (Boynton et al., 1982). Historically, the Bay-Delta is characteristic of a high nutrient, low primary production -- phytoplankton growth is considered to be limited primarily by light, and its biomass accumulation is controlled by grazing while also affected by hydrodynamic entrapment and tidal stirring (Alpine and Cloern, 1992; Dugdale et al., 2007; Kimmerer, 2004; Cloern et al., 1985; Cloern, 1987). Over the past decades, the role of nutrients has been received renewed attention, due to the increase of nutrient loading, the change in phytoplankton species and the change in the food-web (Glibert, 2010; Glibert et al., 2011; Glibert et al., 2014). A major source of nutrients to the Bay-Delta come from the sewage effluents from wastewater treatment plants (WWTP) on the upper Sacramento River, with nitrogen (NH_4^+) discharges at the rate of 14 - 15 tons per day, and at the concentration of more than 20 mg/L in the 2000s, compared to ~ 10 mg/L in the 1980s (Glibert, 2010; Glibert et al., 2011). Approximately 90% of the total N in the northern Bay originates from this single

point source under average flow conditions (Jassby, 2008). Increasing clarity of waters, which may be stimulated by the proliferation of aquatic water weeds, as well as the emergence of harmful algal blooms and altered food webs has brought the issue of nutrient dynamics to the forefront in the Delta (Dahm, 2016). There are other lesser known Delta nutrient sources of nutrients than the loadings from the river input, such as agricultural drainage from farms within the Delta, or what might be coming from the sediments within the Delta's aquatic ecosystems (Dahm, 2016).

1.1.3 SAV in the Sacramento-San Joaquin Delta

In the Sacramento-San Joaquin Delta *invasive* freshwater species Egeria densa (Brazilian waterweed) has been reported to have displaced most of the native submersed aquatic plant species within the Delta (Lund et al., 2007; Schaeffer et al., 2007).

Egeria densa is native to southeastern Brazil, Uruguay, Argentina, and possibly Paraguay, whose stem can easily fragment roots and develop into new shoots, so rapidly that the species often outgrows a suitable aquatic system (Haynes, 1988). Stems are approximately 3 mm thick and commonly less than 1 m in height, but can reach up to 1.8 m to 3 m (Qbank, 2014). Slow-flowing or still water in ditches, sloughs, canals, rivers, ponds, lakes, and reservoirs, especially rich-nutrient substrates, are ideal habitats for Egeria densa (Branquart et al., 2013). Experiments suggest that Egeria densa has a low light compensation point (7.5–16.2 μmol m-2 s-1), thus allowing it to grow in turbid water and to compete in various habitats (Rodrigues and Thomaz, 2010). Canopies of Egeria densa on the water surface favor the twice daily tidal changes in water level in Delta, and the dense canopies can provide shade, allowing Egeria densa to thrive even under intense summer insolation (Santos et al., 2011). In summary, Delta provides a favorable environment for Egeria densa to grow and spread.

Egeria densa has been one of the typical nuisance species in the Bay-Delta. Especially in the Delta, a heavy infestation of this kind of invasive freshwater SAV has the potential to increase flow impediment in waterways, cause unintended flooding, clog pumps and boat propellers, and do harm to the

watershed system (Feijoó et al., 1996). When Egeria densa aggressively invade new aquatic environments, its dense subsurface canopies displace the native aquatic vegetation by blocking the light penetration, while benefiting species with tolerance for low light or less sensitivity to light (Yarrow et al., 2009). Egeria densa is reported to have altered aquatic plant community structure and composition in Delta as it supports the persistence of some species, but reduces the likelihood of establishment of some other species (Santos et al., 2011). Secondly, the change in light and nutrients caused by Egeria densa may also affect the plankton community (Darrin, 2009). Chlorophyll-a is found to be lower in some Egeria densa beds, as the canopy tends to shade out phytoplankton lower in the water column (Mazzeo et al., 2003; Yarrow et al., 2009). For zooplankton, Egeria densa beds may act as a refuge against the abundance of planktivorous fish and as a feeding zone (Mazzeo et al., 2003). Egeria densa has been reported to negatively affect fish populations and communities, as heavy infestations confer no oxygen benefit to fish or other animals (Yarrow et al., 2009).

Several types of SAV research have been conducted in the Bay-Delta, to study SAV transplant, to quantify SAV influence on turbidity, and to include SAV as parts of some conceptual ecosystem model. Zimmerman et al. (1995) examined the survival, metabolism and growth of Zostera marina transplants along depth gradients in Keil Cove and Paradise Cove in the extremely turbid San Francisco Bay estuary. They found that while light availability is the key limiting factor for eelgrass transplants in San Francisco Bay, the role of carbon reserves and transplant timing may also influence transplant survival. Schoellhamer et al. (2012) developed a conceptual model of sedimentation in the Delta, involving SAV as ecosystem engineers that can create a positive feedback loop by decreasing suspended sediment, increasing water column light, which in turn enables more vegetation. As for the plant Egeria densa, which invaded some of the open waters of the Delta in the early1960s (Jassby and Cloern 2000), the conceptual model demonstrates how Egeria densa can successfully invade the Delta and reduce turbidity, because in the open water where SAV successfully colonizes, hydrodynamic energy and bed shear stress are reduced. The conceptual model is used to identify information gaps that needed to be resolved in an

accurate sediment transport model. Hestir et al. (2015) investigated the effect of primarily invasive SAV expansion on a concomitant decline in turbidity in the Delta, isolating the effects of decreasing sediment supply from the watershed from increasing SAV coverage. Airborne hyperspectral remote sensing and long-term monitoring turbidity data were used to determine SAV cover and correct the influence from decreasing sediment supply. The conclusion of this study is that SAV is an important factor in the turbidity decline, and contributes to 21–70 % of the total declining turbidity trend and has negative impact on juvenile delta smelt feeding.

Note that in the last couple of years, there is more diversity among the freshwater SAV species. Still we can use Egeria densa here as one of the representatives in this research; other species can be incorporated in future work with different parametrization.

1.2. Observation

1.2.1 Available Data from San Francisco Bay and Delta

A plethora of *in situ* data is available for model setup, calibration and evaluation in Bay-Delta. Notably, California Department of Water Resources (DWR) and the United States Geological Survey (USGS) operate a maintain on extensive hydrologic and water quality network including stations in the study region. It was possible to obtain some water quality data such as chlorophyll-a and dissolved oxygen through the California Data Exchange Center, a real-time data warehouse operated by DWR that includes contributed data from many agencies (http://cdec.water.ca.gov/cdecstation2/). In addition, we were able to obtain some nutrient data at some stations of Delta from the Water Data Library (WDL), the main data archive for the DWR North Central Regional Office (http://wdl.water.ca.gov/waterdatalibrary/). Besides DWR, USGS also provides temperature, salinity, chlorophyll-a, dissolved oxygen and nutrient data for several stations in the region.

For the setup of Cache Slough Complex domain presented in chapter 3, most of the boundary hydrodynamic forcings of water level, flow velocity, and temperature are taken from the CDEC data (LIS, BKS, RYI, HWB) from 2015 to 2016. The nutrients loading for both boundary and point/non-point sources is taken from WDL and USGS (WDL 145 (http://wdl.water.ca.gov/waterdatalibrary/includes/include_wqstation_details.cfm?qst_id=145), USGS 11455315 (https://waterdata.usgs.gov/ca/nwis/uv?site_no=11455315), USGS 11455350 (https://waterdata.usgs.gov/ca/nwis/uv/?site_no=11455350&PARAmeter_cd=00065,00060)). UC Davis CSTARS estimated coverage for SAV distribution from DWR report (2017) is used for SAV model setup and model validation.

1.2.2 Data Analysis

Before developing and applying the SAV model, the open water method using high-frequency dissolved oxygen data is used to estimate gross primary production of the entire ecosystem (Staehr et al., 2012). In addition, the phytoplankton primary production can be estimated from available high-frequent chlorophyll-a using a similar method (Qin and Shen, 2017). The advection effect is assumed to be small in both methods. With the gross primary production and phytoplankton primary production known, SAV primary production can be estimated from the difference between these two productions.

1.2.3 Preliminary results from Data Analysis

We examine data at two Delta stations where high-frequency data are available. Station LIS is located on the upper riverside of Yolo Bypass at Lisbon Weir and is a typical upper estuary station in a channel. Station FRK is located at the middle of Franks Tract in the Central Delta, and is known for the luxuriant vegetation (Durand, 2017). Besides the overall annual variation of primary production, higher in summer and lower in winter for both total production and phytoplankton production, we can see from

Figure 1-1 that the phytoplankton contributes to less than 30% of the total primary production at both stations. As both SAV and FAV (Floating Aquatic Vegetation) are found in the Delta, even with a conservative assumption that SAV only accounts for half of the vegetation, the contribution of SAV to the total primary production may be over 35%. In addition, at both stations, phytoplankton contribution tends to be higher during winter-spring time but lower during summer. Therefore we hypothesize that during summer-fall time, SAV competes with phytoplankton and is dominant in those areas, whereas during winter-spring time, SAV declines and so phytoplankton may account for a bigger proportion of the ecosystem.

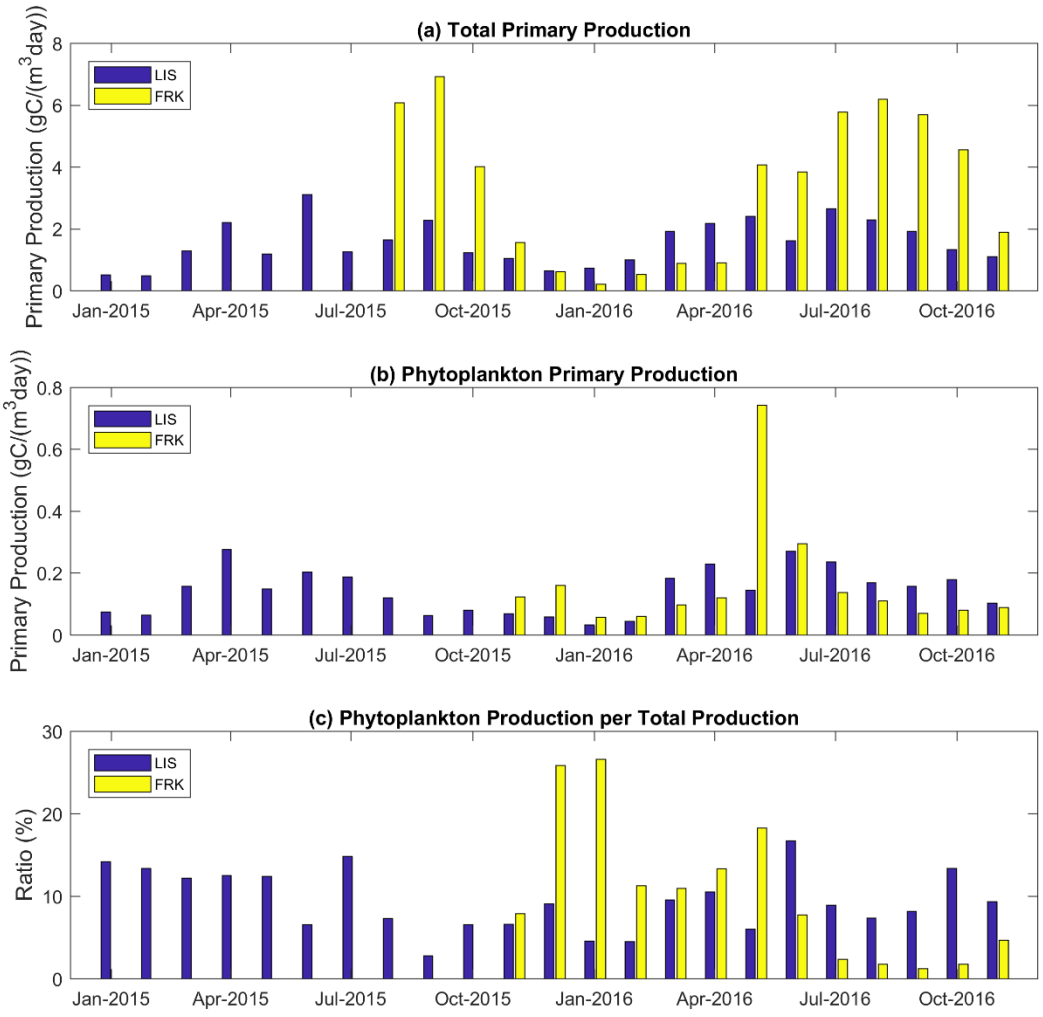

Figure 1-1: Monthly averaged (a) total primary production and (b) phytoplankton production from the open water methods (note that FRK data starts from Nov. 2015). (c) Ratio of phytoplankton primary production to the total production. Blue bar represents the results of station LIS (cf. Figure 3-2) while the yellow bar represents the station FRK (in Franks Tract in the central Delta).

1.3. Conclusion and Preview of this Thesis

SAV affects the aquatic system both physically and ecologically. It changes the hydrodynamics by attenuating wave, reducing flow velocity and bottom shear stress, as well as increasing sedimentation. On the ecological side, it is an important primary producer, generating oxygen and altering the nutrient budget. It can also provide habitat for many organisms and juvenile fish.

The Bay-Delta has seen large impacts from human activities. As a result, invasive plants and fishes have become a bigger issue in the recent years. In particular, invasive species Egeria densa has displaced most of the native species. Egeria densa can form huge canopies in slow-flowing or still water. It has dominated certain areas in Delta and threatened the endangered Delta smelt population.

By analyzing the high-frequency dissolved oxygen and chlorophyll-a data with the open water method, the contribution of phytoplankton to the total primary production in two Delta regions is found to be lower than 30% overall, and even lower in summer-fall seasons. This further demonstrates the significance of SAV in the aquatic system as a primary producer, and its ability to alter the ecosystem as an invasive species. We hypothesize that during summer-fall time, SAV competes with phytoplankton and is dominant in those areas, whereas during winter-spring time, SAV declines and so phytoplankton may account for a relatively larger proportion of the ecosystem. This hypothesis will be tested in Chapter 3.

The overarching goal of this thesis is two-fold: (1) to develop a new version of SAV model imbedded into the fully coupled hydrodynamic-water quality modeling framework of SCHISM-ICM; (2) to apply this SAV model to Cache Slough Complex in the Delta for demonstration purpose first before we

apply it to the entire system in the future. Through simulation experiments we will estimate the impact of SAV removal on the hydrodynamic and water quality conditions.

Chapter 2 introduces the development of this new version of SAV model. It also shows the benchmark tests results concerning the biomass dynamics, growth and impacts of SAV. Chapter 3 applies the new SAV model to Cache Slough Complex. The model is validated with comparisons with field data and estimates. In particular, the distribution of SAV biomass is shown to qualitatively match the observed SAV distribution. We then conduct several sensitivity experiments to understand the feedback from SAV to the hydrodynamic and water quality variables. We will examine (a) the spatial variabilities of the water quality state variables, (b) spatial variabilities of the annually-averaged differences with and without SAV, (c) seasonal patterns of SAV-phytoplankton interactions, (d) SAV-induced local kinetic changes on the nutrients and dissolved oxygen, and (e) the feedback of SAV canopy heights to the hydrodynamics.

Chapter 2 Development of SAV Model

2.1. Introduction

2.1.1 Background of SAV Modeling

Much progress has been made in the recent 30 years in simulating the impact of vegetation on flow, wave transformation and turbulence, starting from a simple empirical relationship on Manning's Law to model flow resistance, which has little impact on the flow structure above and within the canopies (Chow, 1959). More recently, vegetation is idealized as vertical round rods, and the SAV bed is considered as clusters of cylinders (Shimizu and Tsujimoto, 1994; Naot et al., 1996; Lopez and Garcia 2001; Wu et al., 2007). The assumption for the model is that the introduced vegetation in the turbulent channel flow will lead to an additional drag force and production of turbulence energy (Shimizu and Tsujimoto, 1993). In this way, the model introduces an external drag force term in the mean flow momentum equation, and include the additional production of turbulence into the turbulence closure scheme (Shimizu and Tsujimoto, 1993; Naot et al., 1996; Wu et al., 2007).

Shimuzu and Tsujimoto (1994) modified the steady Reynolds-averaged Navier-Stokes (RANS) equations using a $k-\varepsilon$ model for turbulence closure (where k is the turbulent kinetic energy and ε is the dissipation rate of turbulent kinetic energy). Naot et al. (1996) developed a phenomenological model with an algebraic stress model (ASM) of turbulence to study the turbulent flow in a compound wide rectangular open channel with vegetated domain, with the vegetation modeled as an internal resistance that exerts drag force and produces turbulence energy. The characteristics of flow and free shear layers at the edge of the vegetated domain were modeled, and the importance of the pattern of vegetation placement on the shading factors was highlighted. However, as a steady flow model, it is unable to simulate the dynamic evolution of large-scale horizontal eddies. Nadaoka and Yagi (1998) developed a two-dimensional depth-integrated model (SDS-2DH) to compute shallow water turbulence for flow in a channel with vegetation bank. A so-called sub-depth scale and a large-scale was introduced to

respectively model turbulence in both vertical and horizontal directions. The sub-depth scale turbulence was modeled by a $k - l$ type parameterization, including the turbulence generated by the vegetation, while the large-scale horizontal turbulence was calculated explicitly using the technique of large eddy simulation (LES). The model reasonably captured a series of large horizontal eddies, important momentum exchanges across the lateral boundary of vegetation zone and the effects of flow geometry on the large-scale eddy development, with a better performance than the depth-integrated $k - \varepsilon$ model. However, the two-dimensional depth-integrated LES model is only applicable to a shallow water environment with emergent vegetation. Su and Li (2002) developed an LES model based on 3D equations to simulate the hydrodynamic behavior of turbulent flow in an open channel with a domain of vegetation that produces transversal shear. The LES results successfully simulate the dynamic development of large eddies and the associated intermittent turbulence.

In conclusion, several approaches have been proposed to simulate the impact of submerged or emergent vegetation on the flows: steady or unsteady 1D RANS equations for uniform flows, 2D depth-integrated RANS, and momentum equations with a hydrostatic or non-hydrostatic pressure in the vertical direction, with considerably different computational costs (Shimizu and Tsujimoto 1994; Naot et al., 1996; Nadaoka and Yagi 1998; Su and Li 2002; Wu et al., 2007). A key seems to be to improve the turbulence closure to better capture the vegetated flow structure and transport processes.

Besides modeling the impact of SAV on the flow and waves, efforts have also been made on simulating SAV biomass, distribution and its interaction and feedback to the nutrient cycle and sediments.

A computer model was developed to simulate photosynthesis and growth of eelgrass by Wetzel and Neckles (1986) in the lower Chesapeake Bay, and this model simulated the biologically controlled processes with theoretical non-linear functions and incorporated the physical-chemical interactions with empirical or statistical relationships. Bach (1993) combined an eelgrass sub-model and a phytoplankton sub-model in a modeling system, where both sub-models interact with each other since the water transparency depends on the phytoplankton concentration and also affects the eelgrass biomass. This

model was able to simulate the seasonal and regional variations in eelgrass production and its biomasses above and below ground.

Initial efforts to evaluate the nutrient controls from SAV relied on living-resources habitat criteria (Dennison et al., 1993; Cerco and Cole, 1993). This approach had two shortcomings: (1) the model can only make qualitative, not quantitative improvements; (2) the model is unable to account for the feedback between the improved SAV abundance and the surrounding environment. Cerco and Moore (2001) incorporated an SAV sub-model into an eutrophication model, which directly simulates SAV abundance, distribution, and the interactions between SAV and the environment. This model can simulate environmental variables that affect SAV abundance, especially light attenuation, and provides a first approximation of feedback between SAV biomass and suspended solids concentrations with an empirical function of SAV biomass and settling velocity. However, the model does not perform well in reproducing inter-annual variations in abundance, because it is not able to robustly simulate event-scale processes, such as storm surge, or include aging, reproduction, and propagation in the population dynamics. Jin et al. (2007) applied the SAV model of Cerco et al. (2002) to the Lake Okeechobee Environment Model (LOEM), with only three state variables: shoots (aboveground biomass), roots (belowground biomass), and epiphytes (attached growth). The model was shown to represent the spatial and temporal variations of SAV in the lake well.

2.1.2 SCHISM Modeling System

2.1.2.1 Features of SCHISM

The SCHISM (Semi-implicit Cross-scale Hydroscience Integrated System Model) is a derivative product of the original SELFE (Semi-implicit Eulerian Lagrangian Finite Element) model (Zhang and Baptista, 2008) and has been implemented by Dr. Y. Joseph Zhang and other developers across the world. It is an open-source community-supported modeling system based on unstructured grids, designed for

seamless simulation of 3D baroclinic circulation across creek-lake-river-estuary-shelf-ocean scales. Main features of SCHISM include a semi-implicit time stepping scheme applied in a hybrid finite-element and finite-volume framework to solve the Navier-Stokes equations in hydrostatic form, and as a result, the time step is not restricted by the CFL (Courant-Friedrichs-Lewy) condition, thus improving numerical efficiency. The Eulerian-Lagrangian method is used to treat the momentum advection to further boost numerical efficiency and stability.

As a finite-element model, SCHISM uses flexible unstructured grids in the horizontal and flexible coordinate systems in the vertical dimension (Zhang et al., 2015). Hybrid triangular-quad elements are used in the horizontal to take advantage of the superior boundary-fitting capability of triangles and efficiency/accuracy of quads in representing certain features such as channels. The setup of the vertical grid structure in SCHISM allows two options: (1) hybrid SZ grid (terrain-following generalized S-coordinates and Z-coordinates), or (2) a spatially varying LSC^2 vertical grid based on local water depths (Zhang et al., 2015), which further enhances SCHISM's efficiency in cross-scale applications. The recent extension to large-scale eddying regime enables a seamless cross-scale capability from creek to ocean on a single grid (Zhang et al., 2016).

SCHISM has been widely tested against standard oceanic and coastal benchmarks and applied to many estuarine and coastal systems around the globe, in the context of general circulation, tsunami, storm-surge inundation, water quality, oil spill, sediment transport, coastal ecology, and wave-current interaction. The whole modeling system is parallelized via domain decomposition and MPI (Message Passing Interface). Examples of unique features of SCHISM relevant to this study are:

- Finite element/volume formulation
- Unstructured mixed triangular/quadrangular grid in the horizontal dimension
- Hybrid SZ coordinates or new LSC^2 in the vertical dimension
- Semi-implicit time stepping with no CFL stability constraints to enhance numerical efficiency
- Natural treatment of wetting and drying suitable for inundation studies

- Mass conservative, monotone, higher-order transport solvers
- No bathymetry smoothing necessary
- Very tolerant of bad-quality meshes in the non-eddying regime

SAV impact on hydrodynamic is simulated in the SCHISM hydrodynamics part (Zhang et al., submitted). The new vegetation-related terms are treated implicitly, which greatly enhances the stability. The model has gone through the benchmark tests with lab data and has been applied to the Delta system with SAV beds in the Franks Tract Area (Zhang et al., submitted).

2.1.2.2 SAV Impacts on Hydrodynamics in SCHISM

SAV impact on hydrodynamic is incorporated into the SCHISM hydrodynamics part by Zhang et al. (submitted). The SAV-induced drag force is included in the momentum equations. With the SAV-induced drag force, the impact on flow velocity and settling of suspended solids can be simulated. The Reynolds averaged equations are expressed as:

$$\text{Continuity equation: } \nabla \cdot \mathbf{u} + \frac{\partial w}{\partial z} = 0 \tag{2-1}$$

$$\text{Transport equation: } \frac{\partial C}{\partial t} + \nabla \cdot (\mathbf{u}C) = \frac{\partial}{\partial z}\left(\kappa \frac{\partial C}{\partial t}\right) + F_h \tag{2-2}$$

$$\text{Momentum equation: } \frac{D\mathbf{u}}{Dt} = \frac{\partial}{\partial z}\left(\nu \frac{\partial \mathbf{u}}{\partial z}\right) - g \cdot \nabla\eta(x, y, t) + \mathbf{f} \tag{2-3}$$

∇ is $(\frac{\partial}{\partial x}, \frac{\partial}{\partial y})$, and $\frac{D}{Dt}$ is material derivative.

(x, y) is horizontal Cartesian coordinates, z is vertical coordinate, positive upward (with z=0 at undisturbed surface), and t is time.

$\mathbf{u}(x, y, z, t)$ is horizontal velocity with Cartesian components (u, v) (m/s), w is vertical velocity (m/s).

C is tracer concentration (e.e., salinity, temperature etc), κ is vertical eddy diffusivity for tracers (m^2/s), and F_h includes horizontal diffusion and mass sources/sinks (m^2/s).

ν is vertical eddy viscosity (m^2/s), which is determined by the turbulence closure below.

$\eta(x, y, t)$ is free surface elevation (m), and $h(x, y)$ is bathymetric depth measured from a fixed datum (m).

f represents forcing terms in momentum treated explicitly in the numerical formulation – Coriolis force, baroclinic gradient, atmospheric pressure, earth tidal potential, horizontal viscosity and vegetation-induced drag force:

$$\mathbf{f} = f(v, -u) - \frac{g}{\rho_0}\int_z^\eta \nabla\rho d\zeta - \frac{\nabla p_A}{\rho_0} + \alpha g\nabla\psi + \mathbf{F_m} - \frac{\mathbf{F_{veg}}}{\rho_0} + other \quad (2\text{-}4)$$

p is hydrostatic pressure (Pa), and p_A is atmospheric pressure reduced to mean sea level (Pa).

ρ is water density (kg/m^3), g is acceleration of gravity (m/s^2), $\mathbf{F_m}$ is horizontal viscosity (m/s^2).

$\mathbf{F_{veg}}$ is horizontal vegetation-induced drag force in (x, y) direction. It is expressed as:

$$\mathbf{F_{veg}} = \rho_0 \cdot \alpha \cdot \mathbf{u}|\mathbf{u}| \cdot L(x, y, z) \quad (2\text{-}5)$$

$\alpha(x, y)$ is a vegetation related density variable (m^{-1}):

$$\alpha(x, y) = 0.5 \cdot D_v \cdot N_v \cdot C_{D_v} \quad (2\text{-}6)$$

where $\mathrm{D_v}$ is the stem diameter (m), $\mathrm{N_v}$ is vegetation density (number stems per m^2), $\mathrm{C_{D_v}}$ is a bulk drag coefficient with a typical value of 1.13 (Garcia et al., 2004; Nepf and Vivoni, 2000).

As SCHISM has the feature of 'polymorphism' with mixed 1D, 2D and 3D cells in a single grid (Zhang et al., 2016), it has different forms for the vegetation term in 2/3D:

$$L(x, y, z) = \begin{cases} \mathcal{H}(z_v - z), & 3D \\ 1, & 2D \end{cases} \quad (2\text{-}7)$$

where z_v is the z-coordinate of the canopy and $\mathcal{H}(x)$ is the Heaviside step function:

$$\mathcal{H}(x) = \begin{cases} 1, & x \geq 0 \\ 0, & x < 0 \end{cases} \tag{2-8}$$

SAV impact is also taken into account in the turbulence closure equations for turbulent kinetic energy K and a generic length-scale variable ψ:

$$\frac{DK}{Dt} = \frac{\partial}{\partial z}\left(\nu_k^{\psi} \frac{\partial K}{\partial z}\right) + \nu M^2 + \mu N^2 - \varepsilon + c_{fk}\alpha|\mathbf{u}|^3\mathcal{H}(z_v - z) \tag{2-9}$$

$$\frac{D\psi}{Dt} = \frac{\partial}{\partial z}\left(\nu_{\psi} \frac{\partial \psi}{\partial z}\right) + \frac{\psi}{K}(c_{\psi 1}\nu M^2 + c_{\psi 2}\mu N^2 - c_{\psi 3}F_w\varepsilon + c_{f\psi}\alpha|\mathbf{u}|^3\mathcal{H}(z_v - z)) \tag{2-10}$$

The generic length-scale is defined as:

$$\psi = (c_{\mu}^0)^p K^m \ell^n \tag{2-11}$$

where ℓ is the turbulence mixing length, $c_{\mu}^0 = 0.3^{1/2}$. p, m and n are specific constants leading to different closure models, and ν_k^{ψ} and ν_{ψ} are vertical turbulent diffusivities:

$$\nu_k^{\psi} = \frac{\nu}{\sigma_k^{\psi}} \tag{2-12}$$

$$\nu_{\psi} = \frac{\nu}{\sigma_{\psi}} \tag{2-13}$$

where the Schmidt numbers σ_k^{ψ} and σ_{ψ} are model-specific constants, and the vertical eddy viscosities and diffusivities are:

$$\nu = \sqrt{2}s_m K^{1/2}\ell \tag{2-14}$$

$$\mu = \sqrt{2}s_h K^{1/2}\ell \tag{2-15}$$

where the stability functions S_m and S_n are given by an Algebraic Stress Model.

$c_{\psi 1}$, $c_{\psi 2}$ and $c_{\psi 3}$ are model-specific constants (Umlauf and Burchard, 2003).

F_w is a wall proximity function.

M, N and ε are shear production, buoyancy production and dissipation rate of K.

c_{fk} and $c_{f\psi}$ are parameters with specific value for different turbulence schemes.

Boundary conditions are required for these governing equations. The kinetic boundary conditions at the free surface and the bottom are expressed as:

$$w = \frac{\partial \eta}{\partial t} + u\frac{\partial \eta}{\partial x} + v\frac{\partial \eta}{\partial y},\ z = \eta \tag{2-16}$$

$$w = -u\frac{\partial h}{\partial x} - v\frac{\partial h}{\partial y},\ z = -h \tag{2-17}$$

Where η is the free-surface elevation relative to the undisturbed free surface, where $z = 0$. h is the water depth.

At the sea surface, SCHISM enforces the balance between the internal Reynolds stress and the applied shear stress:

$$\nu\frac{\partial \mathbf{u}}{\partial z} = \boldsymbol{\tau_w},\ z = \eta \tag{2-18}$$

where τ_w is wind shear stress on free surface.

The no-slip condition at the sea or river bottom is replaced by a balance between the internal Reynolds stress and the bottom friction stress:

$$\nu\frac{\partial \mathbf{u}}{\partial z} = \boldsymbol{\tau_b},\ z = -h \tag{2-19}$$

The specific form of the bottom stress τ_b in the turbulent boundary layer is:

$$\boldsymbol{\tau_b} = C_{db} \cdot |\mathbf{u_b}| \cdot \mathbf{u_b} \tag{2-20}$$

Where $\mathbf{u}_b$ is the velocity (u_b, v_b) measured at the top of the bottom computational cell. The details of numerical method used to solve the differential equations (2-2) with vegetation effects can be found in Zhang et al. (submitted).

2.2. The New SAV Model

2.2.1 ICM (Integrated Compartment Model) with SCHISM

ICM, which was originally developed by U.S. Army Corps of Engineering (ASCE) Research and Development Center as one of the components of the water quality model package to study the eutrophication processes in the Chesapeake Bay, is a flexible, widely-applicable eutrophication model (Cerco and Cole, 1994). The fully coupled SCHISM-ICM represents a 3D hydrodynamic and eutrophication model, where SCHISM provides physical information and ICM simulates the spatial and temporal distribution of water quality parameters (Park et al., 1995). In the following we will briefly review the ICM first.

2.2.1.1 The Eutrophication Model

The ICM eutrophication model computes 23 state variables including physical parameters: salinity, temperature, total suspended sediment and multiple forms of algae, carbon, nitrogen, phosphorus, and silica, and each state variable can be individually activated or deactivated (Figure 2-1).

The governing mass-balance equation for each of the water quality state variables consists of physical transport of both advection and diffusion, and kinetic process:

$$\frac{\partial C}{\partial t}+\frac{\partial (uC)}{\partial x}+\frac{\partial (vC)}{\partial y}+\frac{\partial (wC)}{\partial z}=\frac{\partial}{\partial x}\left(K_x\frac{\partial C}{\partial x}\right)+\frac{\partial}{\partial y}\left(K_y\frac{\partial C}{\partial y}\right)+\frac{\partial}{\partial z}\left(K_z\frac{\partial C}{\partial z}\right)+K\cdot C+R \qquad (2\text{-}21)$$

C is the concentration of a water quality state variable.

u, v, w are velocity components in the X, Y and Z directions respectively.

K_x, K_y, K_z are turbulent diffusivities in the X, Y and Z directions respectively, ($K_z = \kappa$ in equation 2-2).

K is kinetic rate (time^{-1}) of a water quality state variable.

R is source and sink (mass $\cdot$ volume^{-1} $\cdot$ time^{-1}) of a water quality state variable.

The last three terms on the left-hand side and first three terms on the right-hand side account for the advection and diffusion, respectively, which are calculated using the advection-diffusion solver in SCHISM. The last two terms on the right-hand side represent the kinetic processes and external loads. The kinetic formulations vary for different state variables, and may also interact with the sediment processes.

2.2.1.2 The Sediment Flux Model

The sediment flux model developed by DiToro and Fitzpatrick (1993) was incorporated into the water quality model (Figure 2-1). The sediment model is driven by net settling of particulate organic carbon, nitrogen, phosphorus and silica from the overlying water and outputs the production of oxygen demand and inorganic nutrients flux to the water column. In the sediment flux model, benthic sediments are represented as two layers: a thin upper layer and a permanently anoxic lower layer. The upper layer can be anoxic or otherwise depending on the oxygen concentration in the overlying water. The depth of the upper layer is determined by the penetration of oxygen into the sediments and is only a small fraction of the total sediment bed. The anoxic lower layer occupies most of the bed and connects to a burial output. The model incorporates three basic processes: depositional flux of POM, diagenesis flux and sediment flux. The coupling of the sediment process model with the water quality model not only increases the predictive capability of the water quality parameters but also enables long-term simulation of changes in water quality conditions in response to the changes of nutrient loadings or SAV growth.

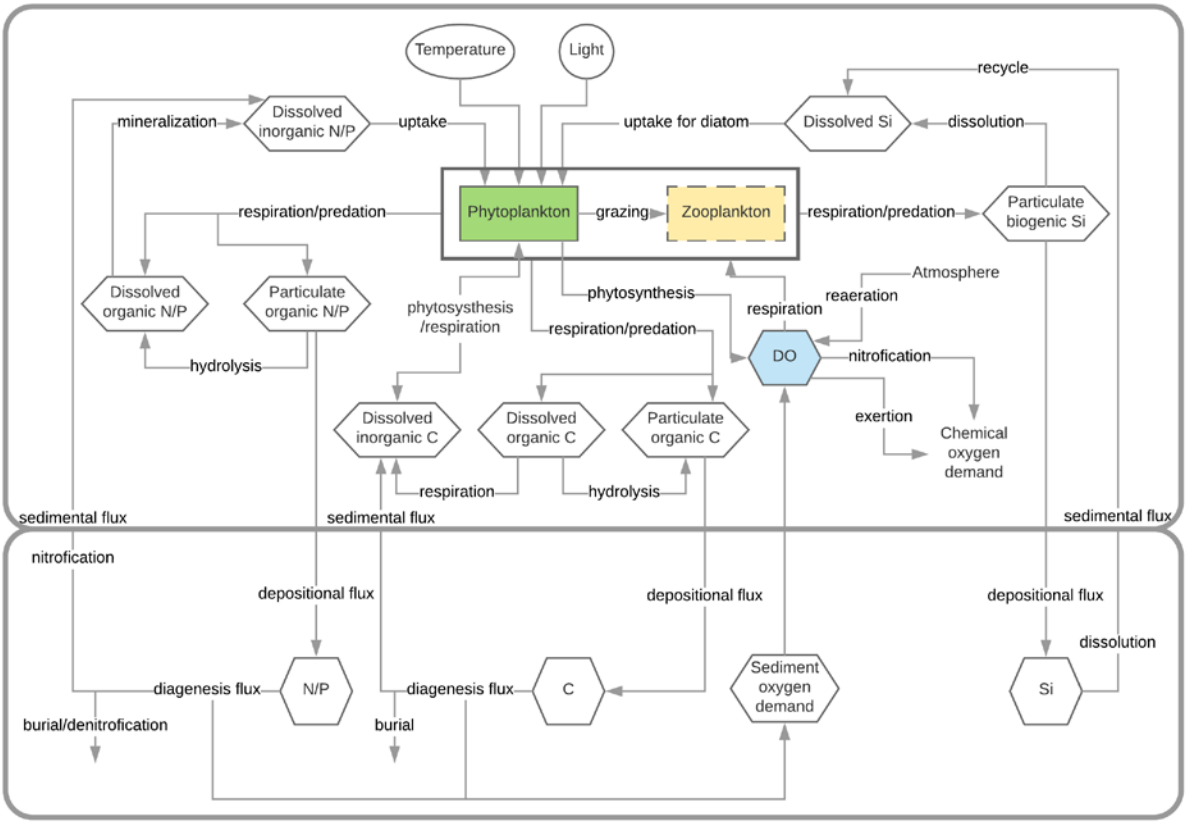

Figure 2-1: ICM eutrophication model schematic

2.2.2 SAV Model and Coupling

The SAV model used here largely follows the work of Cerco and Moore (2001) and Cerco et al. (2002), who first introduced this component into ICM during the tributary refinements phase of the Chesapeake Bay study.

Besides the biomass dynamics, the competition between SAV and phytoplankton for light and nutrient supply is also fully implemented in the new ICM-SAV. The canopy height as a function of biomass simulated by ICM-SAV is then sent back to the SCHISM hydro part.

Three state variables of the SAV model are leaves, stems, and roots, which represent the three major components of freshwater plants. Definition of these three parameters are:

- Leaves – the photosynthetic portions of the above-ground plant biomass
- Stems – the structural, non-photosynthetic portions of the above-ground plant biomass
- Roots – the below-ground portions of the plant biomass associated with anchoring the plant and with nutrient uptake

The kinetic mass balance equations for these variables are expressed as:

$$\frac{d\,LF}{dt} = Plf \cdot (1 - Fam) \cdot FPlf \cdot LF - BMlf \cdot LF \quad (2\text{-}22)$$

$$\frac{d\,ST}{dt} = Plf \cdot (1 - Fam) \cdot FPst \cdot LF - BMst \cdot ST \quad (2\text{-}23)$$

$$\frac{d\,RT}{dt} = Plf \cdot (1 - Fam) \cdot FPrt \cdot LF - BMrt \cdot RT \quad (2\text{-}24)$$

And the canopy height is expressed as a function of the biomass:

$$Hcan = rlf \cdot LF + rst \cdot ST + rrt \cdot RT + hcansav0 \quad (2\text{-}25)$$

where LF, ST, RT are biomass of leaves, stems, and roots (g C m^{-2}), and the production of stems and roots is expressed as a fraction of leave production.

Plf is leaf specific primary production rate (d^{-1}). Fam is fraction of leaf production devoted to active metabolism.

$FPlf, FPst, FPrt$ are fractions of leaf production routed to leaf, stem and root biomass.

$BMlf, BMst, BMrt$ are basal metabolism of leaf, stem and root biomass (d^{-1}).

$rlf, rst, rrt, hcansav0$ are coefficients to transfer SAV biomass to canopy height.

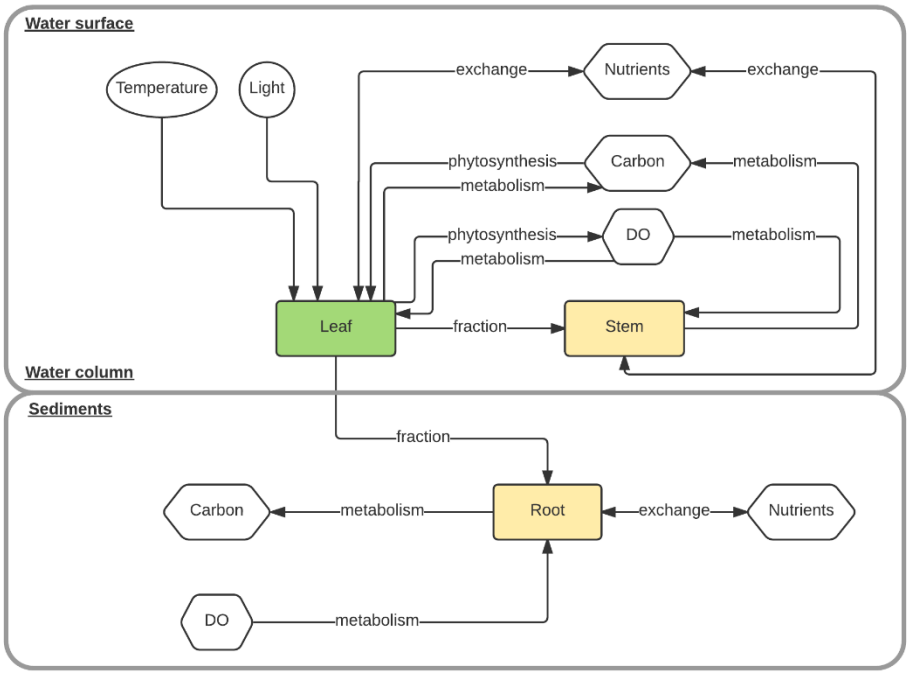

Figure 2-2: SAV model schematic

At the moment, multiple species can be modeled with multiple parameter sets for different regions, but no more than one species can be assigned to a model cell. Also, competitions between plant species are not considered in the current model. Epiphytes are neglected in this model because epiphytes are low in the freshwater environments of Delta. Interactions or competitions between deferent primary producers (SAV and phytoplankton) are modeled through the light and nutrient supply. Specifically, for the light supply, a long-established conceptual model suggests that light reaching SAV shoots is first attenuated by the dissolved and particulate matter, including suspended sediment, CDOM, chlorophyll-a in the water column, and the effects of self-shading (Kemp et al., 1983). However, the canopy of Egeria densa can often grow up to the water surface, so the impacts of phytoplankton on light limitation for SAV is minor in this case. Conversely, the canopy of SAV can block the light supply to phytoplankton, which will be incorporated to the light attenuation formula for phytoplankton simulation.

2.2.2.1 Plant Production

The production rate is computed using a temperature-dependent maximum rate and several limiting factors that are independently evaluated with light, nitrogen and phosphorus.

$$Plf = Pm(T) \cdot min(f(I), f(N), f(P))/Acdw \quad (2\text{-}26)$$

$Pm(T)$ is maximum production at temperature T (g C g^{-1} DW d^{-1}).

$f(I), f(N), f(P)$ are light limitation, nitrogen limitation, phosphorus limitation ($0 \leq f(I), f(N), f(P) \leq 1$).

$Acdw$ is plant carbon-to-dry-weight ratio (g C g^{-1} DW).

2.2.2.1.1 Maximum Production Function

$$Pm(T) = e^{-KTg1 \cdot (T-Topt)^2}, when\ T \leq Topt \quad (2\text{-}27)$$

$$Pm(T) = e^{-KTg2 \cdot (T-Topt)^2}, when\ T > Topt \quad (2\text{-}28)$$

T is temperature (°C).

$Topt$ is optimal temperature for SAV production (°C).

$KTg1, KTg2$ are coefficient of temperature effects below/above $Topt$ on production ($°C^{-2}$).

2.2.2.1.2 Light Limitation Function

Light limitation is based on the function of Jassby and Platt (1976) with consideration of attenuations due to dissolved and particulate matter, and the self-shading effect. Light reaching SAV shoots is first attenuated by dissolved and particulate matter, including total suspended solid and phytoplankton in the water column and SAV self-shading. Through the use of fine local resolution, the SAV leaf and stem are distributed into different vertical layers *k*=0,1,2, … *Nv*, where *k*=0 corresponds to the surface layer as shown in Figure 2-3. This SAV model is able to simulate the competition of phytoplankton and SAV on light supplies in each layer.

The light function $f(I)$ for leaf growth is expressed as:

$$f(I) = \frac{Iwc}{\sqrt{Iwc^2 + Ik^2}} \tag{2-29}$$

where $Ik = \frac{Pm(T)}{\alpha}$ is derived from maximum production (E m^{-2} d^{-1}). α is the initial slope of production versus irradiance curve (E^{-1} m^2).

The light intensity is given by:

$$Iwc = I_{n-1} \cdot e^{-Ke \cdot dep_n} \tag{2-30}$$

$$I_n = I_{n-1} e^{-Ke \cdot 2dep_n} \tag{2-31}$$

where Iwc is the irradiance at a certain layer (E m^{-2} d^{-1}), I_{n-1} is irradiance at the bottom of layer *n*-1 (E m^{-2} d^{-1}), I_n is irradiance on the bottom of this layer *n* (E m^{-2} d^{-1}), and dep_n is half of the layer thickness in this layer (m). Ksh is light attenuation by SAV absorption (m^2 g^{-1} C). The water column attenuation in layers occupied by SAV is expresses as:

$$Ke = Kw + Ksh \cdot (LF + ST) \tag{2-32}$$

where Kw is diffuse light attenuation within the water column (m^{-1}), which accounts for the attenuation from chlorophyll-a, total suspended solids and background attenuation.

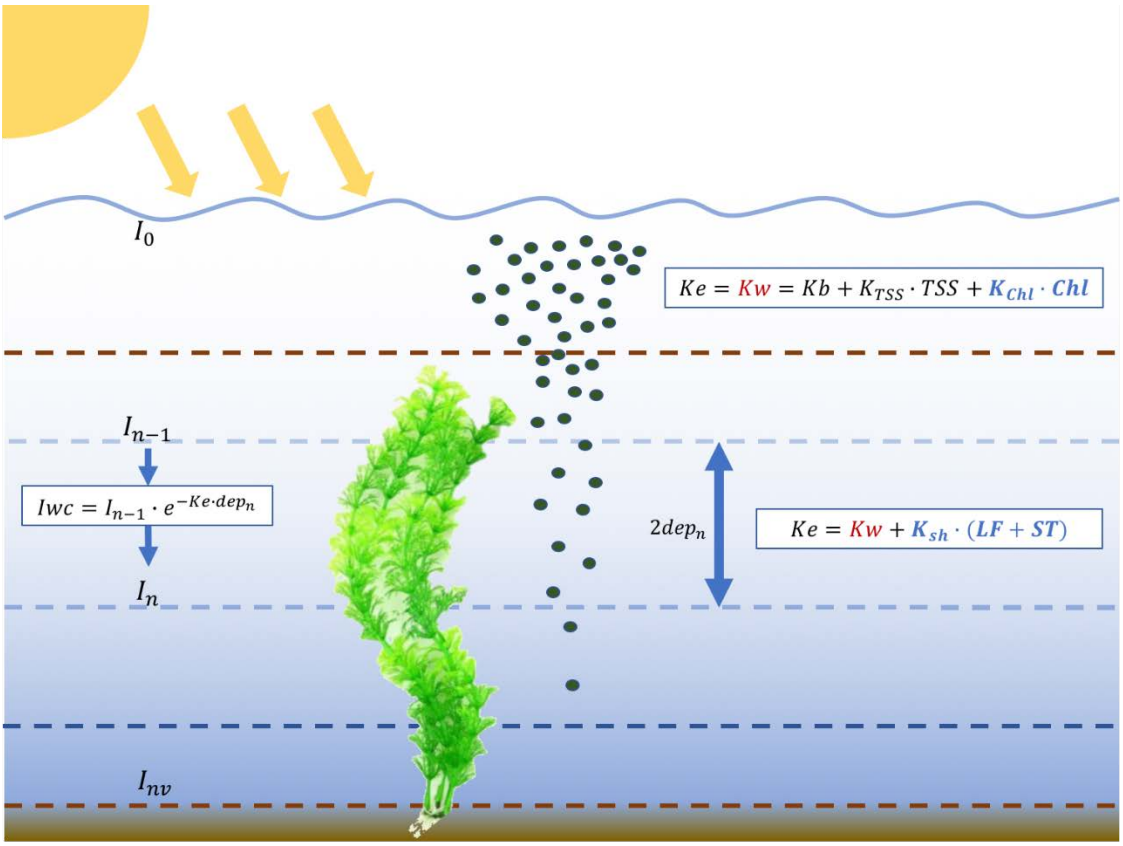

Figure 2-3: Light supply and attenuation over multiple vertical layers in SCHISM.

2.2.2.1.3 Nutrient Limitation Function

Nutrient limitation is evaluated from a formula that combines individual Monod-like functions for roots and shoots (Madden and Kemp, 1996). The limiting functions for nitrogen and phosphorus are:

$$f(N) = \frac{NH4w + NO3w + \frac{KHNw}{KHNs} \cdot NH4s}{KHNw + NH4w + NO3w + \frac{KHNw}{KHNs} \cdot NH4s} \quad (2\text{-}33)$$

$$f(P) = \frac{PO4w + \frac{KHPw}{KHPs} \cdot PO4s}{KHPw + PO4w + \frac{KHPw}{KHPs} \cdot PO4s} \quad (2\text{-}34)$$

$NH4w, NO3w, PO4w$ $NH4s, PO4s$ are nutrient concentrations in water column and in sediments, respectively (g m^{-3}) respectively. $KHNw, KHNs, KHPw, KHPs$ are half-saturation concentrations for nitrogen and phosphorus uptake from water column and sediments respectively (g m^{-3}).

2.2.2.2 Basal Metabolism

Basal metabolism is a function of temperature.

$$BM = BMr \cdot e^{KTb \cdot (T - Tr)} \quad (2\text{-}35)$$

BMr is metabolic rate at temperature Tr (d^{-1}).

Tr is reference temperature for metabolism (℃).

KTb is effect of temperature on metabolism ($℃^{-1}$).

Equation 2-35 is applicable to leaf, stem, and root with different constants.

2.2.2.3 SAV Interaction with Water Quality Parameters in Water Column

For SAV to interact with the water column nutrients, a fundamental assumption is made that plants have a uniform, constant composition, i.e. nitrogen and phosphorus in plant biomass are quantified as fractions of the carbonaceous biomass, so nutrients are taken up in stoichiometric relation to net production. Proportions of nutrients removed from the water column and sediments are determined by the relative nutrient limits in each pool. Active and basal metabolism returns some portion of nutrients to the sediments and water column.

Nitrogen, phosphorus, dissolved oxygen, and carbon are affected by the SAV interaction with the water column.

2.2.2.3.1 Nitrogen

The source/sink terms for ammonium, nitrate and organic nitrogen by SAV (use dissolved nitrogen as an example, and the rest have the same form) in water column where SAV occurs are expressed as (here we use dissolved nitrogen as an example, and the remainder have similar forms for labile and refractory particulate organic nitrogen):

$$\frac{dNH_4}{dt} = Anc \cdot FNI \cdot [(BMlf + Plf \cdot Fam) \cdot LF + BMst \cdot ST] - Anc \cdot (1 - FNsed) \cdot NPRsav \cdot Plf \cdot LF \quad (2\text{-}36)$$

$$\frac{dNO_3}{dt} = -Anc \cdot (1 - FNsed) \cdot (1 - NPRsav) \cdot Plf \cdot LF \quad (2\text{-}37)$$

$$\frac{dDON}{dt} = Anc \cdot FND \cdot [(BMlf + Plf \cdot Fam) \cdot LF + BMst \cdot ST] \quad (2\text{-}38)$$

Anc is SAV nitrogen to carbon ratio (g N g^{-1} C).

FNI, FND are ammonium and dissolved organic nitrogen fraction of metabolic nitrogen release ($0 \leq FNI, FNLD \leq 1$).

For ammonium and nitrate, both of which are available as nitrogenous nutrients, there is an empirical preference function ($NPRsav$) to determine the fraction of plant nitrogenous nutrients from each pool:

$$NPRsav = \frac{NH_4}{KHNprsav+NO_3} \cdot [\frac{NO_3}{KHNprsav+NH_4} + \frac{KHNprsav}{NH_4+NO_3}] \quad (2\text{-}39)$$

where $KHNprsav$ is the ammonium concentration at which half the SAV nitrogen uptake is ammonium (g N m^{-3}).

While ammonium and nitrate are also available from the sediment, the sediment concentration of ammonium is much larger than that of nitrate, so the preference for sediment nitrate is assumed to be zero. The nitrogenous nutrient fraction obtained from sediment is determined by the function:

$$FNsed = \frac{Nsed}{Nsed+\frac{KHNs}{KHNw}(NH4+NO3)} \quad (2\text{-}40)$$

where $Nsed$ is the bulk ammonium concentration in sediments (g N m^{-3}).

Nitrogen is utilized by SAV for its photosynthesis on leaf in the form of ammonia and nitrate. It is released to the water column by active and basal metabolism on leaf and basal metabolism on stem in the form of ammonium and three types of organic nitrogen – dissolved, labile particulate and refractory particulate. The factions of these four pools are specified as model parameters -- $FNI, FND, FNLP, FNRP$.

2.2.2.3.2 Phosphorus

Phosphate is the only available inorganic phosphorus form in the water column, and its source/sink terms are analogous to the equation for nitrogen, except that there is no preference function in the inorganic nutrient formula.

$$\frac{dPO_4}{dt} = Apc \cdot FPI \cdot [(BMlf + Plf \cdot Fam) \cdot LF + BMst \cdot ST] - Apc \cdot (1 - FPsed) \cdot Plf \cdot LF \qquad (2\text{-}41)$$

where Apc is SAV phosphorus to carbon ratio (g P g^{-1} C).

2.2.2.3.3 Dissolved Oxygen and Organic Carbon

Plant photosynthesis produces dissolved oxygen, while active and basal metabolism consume oxygen and releases three types of organic carbon (similarly for organic nitrogen). Metabolic fractions of oxygen consumption and organic carbon release are specified parameters analogous to nitrogen fractions.

The source/sink terms for dissolved oxygen, and three types of organic carbon (take dissolved organic carbon as an example) are expressed as:

$$\frac{d\,DO}{dt} = Aocr \cdot Plf \cdot LF - Aocr \cdot FDO \cdot [(BMlf + Plf \cdot Fam) \cdot LF + BMst \cdot ST] \qquad (2\text{-}42)$$

$$\frac{dDOC}{dt} = FCD \cdot [(BMlf + Plf \cdot Fam) \cdot LF + BMst \cdot ST] \qquad (2\text{-}43)$$

$Aocr$ is the mass ratio of oxygen to carbon produced in photosynthesis (g DO g^{-1} C).

$FDO, FCLD$ are fractions of metabolism expressed as oxygen consumption and released as dissolved organic carbon ($0 \leq FDO, FCD \leq 1$).

2.2.2.4 SAV Interaction with Nutrients and Dissolved Oxygen in Sediments

In the sediment bed, SAV production removes nutrients, in the form of ammonium and phosphate, while metabolism in the roots and tubers returns nutrients in organic form. Basal metabolism by roots and tubers consumes dissolved oxygen and releases organic carbon to the sediments.

Nitrogen, phosphorus, dissolved oxygen, and carbon are involved in the SAV interaction with the sediment.

2.2.2.4.1 Nitrogen

The source/sink term for ammonium uptake from the sediments is expressed as:

$$\frac{dNH_4}{dt} = -Anc \cdot FNsed \cdot Plf \cdot LF \quad (2\text{-}44)$$

The source/sink term for organic nitrogen released into the sediments is expressed as:

$$\frac{dORGN}{dt} = Anc \cdot BMrt \cdot RT \quad (2\text{-}45)$$

where $ORGN$ is sediment organic nitrogen (g N m^{-3}).

2.2.2.4.2 Phosphorus

The source/sink term for phosphate uptake from the sediments is expressed as:

$$\frac{dPO_4}{dt} = -Apc \cdot FPsed \cdot Plf \cdot LF \quad (2\text{-}46)$$

The source/sink term for organic phosphorus released into the sediments is expressed as:

$$\frac{dORGP}{dt} = Apc \cdot BMrt \cdot RT \quad (2\text{-}47)$$

where $ORGP$ is sediment organic phosphorus (g P m^{-3}).

2.2.2.4.3 Dissolved Oxygen and Organic Carbon

The source/sink term for oxygen consumption in the sediments is expressed as:

$$\frac{dDO}{dt} = -Aocr \cdot FDO \cdot BMrt \cdot RT \quad (2\text{-}48)$$

The source/sink term for organic carbon produced in the basal metabolism in the sediments is expressed as:

$$\frac{dORGC}{dt} = (1 - FDO) \cdot BMrt \cdot RT \quad (2\text{-}49)$$

where $ORGC$ is sediment organic carbon (g C m^{-3}).

All the parameters related to the SAV model can be found in Table 3-1.

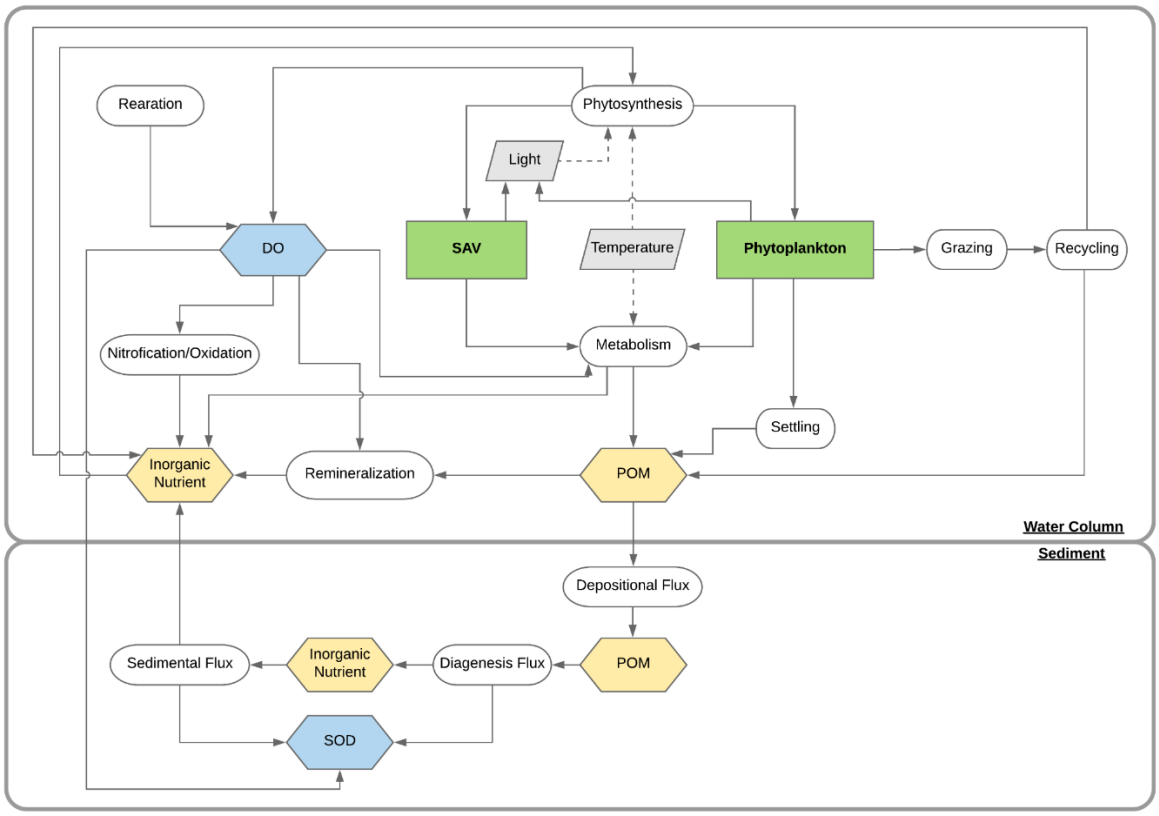

Figure 2-4: Coupled ICM-SAV model schematic

2.2.2.5 Numerical Scheme of SAV model

Since the equations for the stem and root take similar forms, here we only show stem as an illustration. The biomass function of leaf can be written as:

$$\frac{dLF}{dt} = Ksav \cdot LF \tag{2-50}$$

where *Ksav* is the net growth rate. Integrating this equation from step *n* to *n*+1 gives:

$$LF^{n+1} = LF^{n} \cdot e^{Ksav^{n} \cdot \Delta t} \tag{2-51}$$

The dynamic formulation of stem can be formally written as:

$$\frac{dST}{dt} = T \cdot LF + B \cdot ST \tag{2-52}$$

We use an implicit scheme to solve the kinetic equation as:

$$\frac{ST^{n+1} - ST^{n}}{\Delta t} = T^{n} \cdot LF^{n+1} + B^{n} \cdot ST^{n+1} \tag{2-53}$$

and therefore:

$$ST^{n+1} = \frac{T^{n} \cdot \Delta t}{1 - B^{n} \cdot \Delta t} \cdot LF^{n+1} + \frac{ST^{n}}{1 - B^{n} \cdot \Delta t} \tag{2-54}$$

2.3. Model Tests

In this section, we set up a toy model with small domain of ~1km, extracted from the Cache Slough Complex domain in Chapter 3. It uses two boundaries: Lisbon Weir and Cache Slough at Ryer Island with the same boundary conditions as the real domain as described in section 3.2.1.

2.3.1 Benchmark Test about SAV Biomass Dynamics

To test the calculation of SAV biomass dynamics, a benchmark test with some simplified assumptions is conducted. We recall that the original kinetic formula for leaf biomass dynamics is:

$$\frac{d\,LF}{dt} = Plf \cdot (1 - Fam) \cdot FPlf \cdot LF - BMlf \cdot LF \tag{2-55}$$

In this test, the limitation for growth from light or nutrients are all deactivated, so the growth rate Plf is an exponential function of temperature. Temperature is assumed to be constant at 25℃. The sunrise and sunset times determine the start and end of photosynthesis, which are assumed to be 7 am and 7 pm, respectively. In other words, outside this period, $Plf = 0$.

$$Plf = Pm(T) = e^{-KTg1 \cdot (T - Topt)^2} = e^{-0.003 \cdot (25 - 32)^2} \tag{2-56}$$

And the metabolism rate is:

$$BMlf = BMlfr \cdot e^{KTblf\cdot(T-Trlf)} = 0.02 \cdot e^{0.069\cdot(25-32)} \quad (2\text{-}57)$$

So that equation 2-55 for the daytime is:

$$\frac{d\,LF}{dt} = (e^{-0.003\cdot(25-32)^2} \cdot (1-0.2)\cdot 0.6 - 0.02 \cdot e^{0.069\cdot(25-32)}) \cdot LF \quad (2\text{-}58)$$

and for the nighttime is:

$$\frac{d\,LF}{dt} = (-0.02 \cdot e^{0.069\cdot(25-32)}) \cdot LF \quad (2\text{-}59)$$

If we assume that the initial biomass of leaf, stem, and root are all set to be 0.1 g/m^2 at t=0, then the solution for the first day from 12:00am to 7am is:

$$LF_{N1} = 0.1 \cdot e^{-0.0123\cdot t} \quad (2\text{-}60)$$

and from 7am until 7pm, the solution for daytime is:

$$LF_{D1} = LF_{N1}(t = 7am) \cdot e^{0.402\cdot t} \quad (2\text{-}61)$$

So in conclusion, the solution for leaf is:

$$LF_{Nn} = LF_{D(n-1)} \cdot e^{-0.0123\cdot t} \quad (2\text{-}62)$$

$$LF_{Dn} = LF_{Nn} \cdot e^{0.402\cdot t} \quad (2\text{-}63)$$

The equations for stem and root are similar, so we use stem as an example.

$$\frac{d\,ST}{dt} = Plf \cdot (1-Fam)\cdot FPst \cdot LF - BMst \cdot ST \quad (2\text{-}64)$$

where the stem metabolism rate is

$$BMst = BMstr \cdot e^{KTbst\cdot(T-Trlst)} = 0.02 \cdot e^{0.069\cdot(25-32)} \quad (2\text{-}62)$$

So the equation can be rewritten as following during daytime:

$$\frac{d\,ST}{dt} == \left(e^{-0.003\cdot(25-32)^2} \cdot (1-0.2)\cdot 0.3\right) \cdot LF - 0.02 \cdot e^{0.069\cdot(25-32)} \cdot ST \quad (2\text{-}63)$$

The implicit scheme reads:

$$\frac{ST^{n+1}-ST^{n}}{\Delta t} = 0.2072 \cdot LF^{n+1} - 0.0123 \cdot ST^{n+1} \quad (2\text{-}64)$$

And for nighttime, it is:

$$\frac{ST^{n+1}-ST^{n}}{\Delta t} = -0.0123 \cdot ST^{n+1} \quad (2\text{-}65)$$

With leaf biomass calculated at each time step and the initial stem biomass known, we can get the 'analytical' stem biomass at each time step, using $\Delta t = 120s = 0.0014day$.

Comparison of the model results with the analytical solutions in Figure 2-5 indicates that these two agree with each other well in terms of the growth and metabolism on each day. The errors are largely attributed to the differences in the assumed photosynthesis periods in the analytical solutions and the model. As Cerco and Moore (2001) indicated, the ratio between the net primary production of leaf, stem and root should be close to 6:3:1, and therefore the root biomass exhibits a non-monotonic behavior (Figure 2-5), as its biomass tries to adjust from its initial value to this canonical ratio.

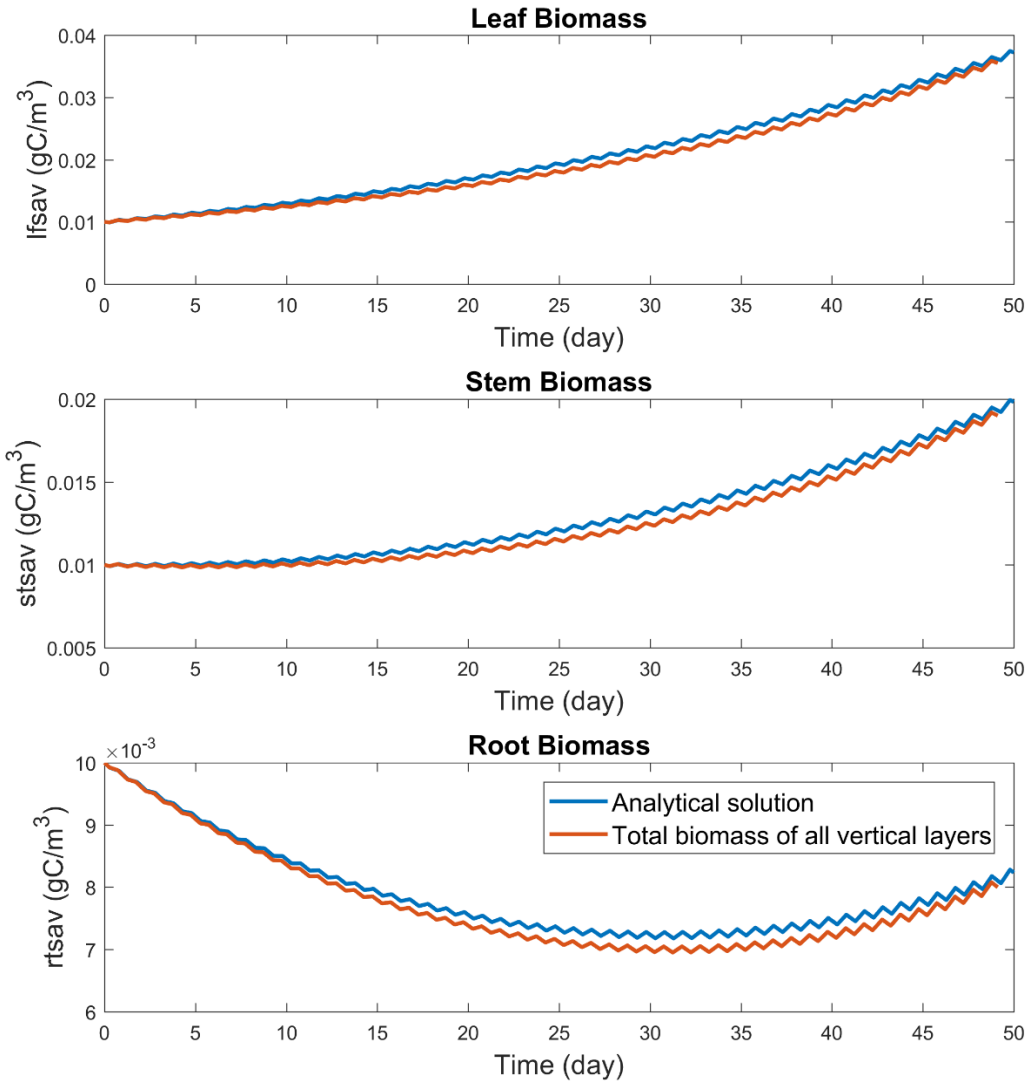

Figure 2-5: Comparison between modeled SAV biomass with analytical solution.

2.3.2 SAV Growth

2.3.2.1 Light Limitation on SAV Growth

In this test, the model simulation starts with an initial condition of biomass of 100 g/m^2 for each of the three tissues to test the effect of light attenuation at different depth (layers). To estimate the impact

of light supply on SAV growth, other limitations on SAV growth are deactivated except for temperature and light.

Figure 2-6(a) shows the light intensity (Iwc) at each vertical layer of SAV, where Layer 1 and Layer 7 denote surface and bottom respectively. The results indicate that the light intensities at Layer 5, 6 and 7, which are under the canopy, follow diurnal pattern of sunlight. These features suggest that the light attenuation is qualitatively captured. The sudden decline of light intensity at Layer 5 at certain times is because SAV canopy changes from Layer 5 to Layer 6 by water level change in this case. Figure 2-6(b) shows the light limitation function (fisav) from the surface to the bottom. The light near the bottom varies from 40% to 75% of the light available near the surface.

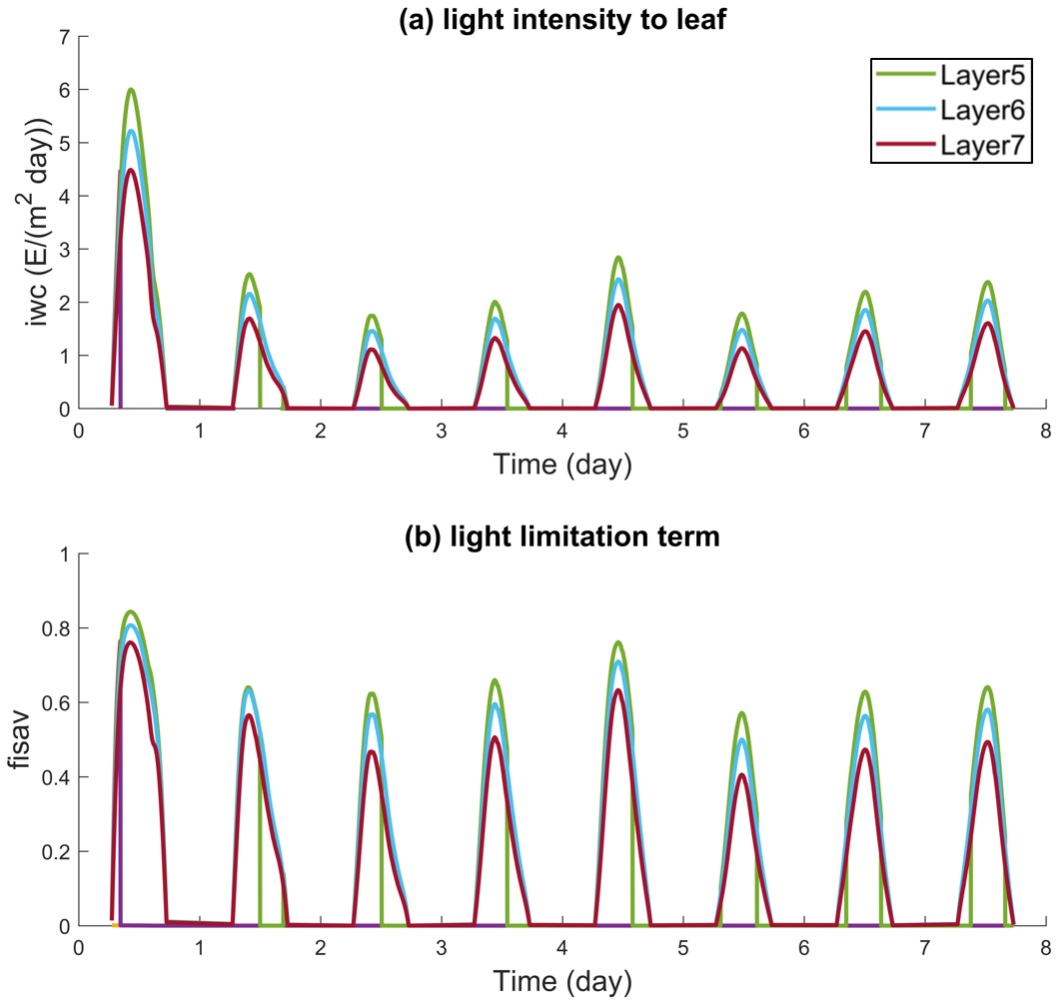

Figure 2-6: (a) The light intensity to leaf in each layer; (b) the light limitation function (range from 0 to 1) at each layer. Layers 1 to 7 are from surface to bottom, and there are seven lines in (a) and (b), but since SAV only occupies layers 5, 6, 7, non-zero values only occur in these three layers.

2.3.2.2 Nutrient Limitation on SAV Growth

In this test, the model simulation starts with an initial condition of biomass of 0.01 g/m^2 for each of the three tissues. To estimate the impact of nutrients on SAV growth, other limitations for SAV growth are deactivated, except for temperature and nutrients.

For a typical estuary, the nutrient concentration within the bottom sediment layer is much larger than that in the water column. Therefore, we expect that the nutrient limitation for SAV growth is minor

because SAV is able to uptake nutrients from sediment directly. Indeed, Figure 2-7 shows that nutrient limiting factor has a minor impact on SAV growth as it is close to saturation rate 1. The limitation functions for nitrogen and phosphorus (denoted by fnsav and fpsav) are plotted in the last two panels, where the blue line shows the limitation is very close to 1, as seen in Figure 2-7(e-f).

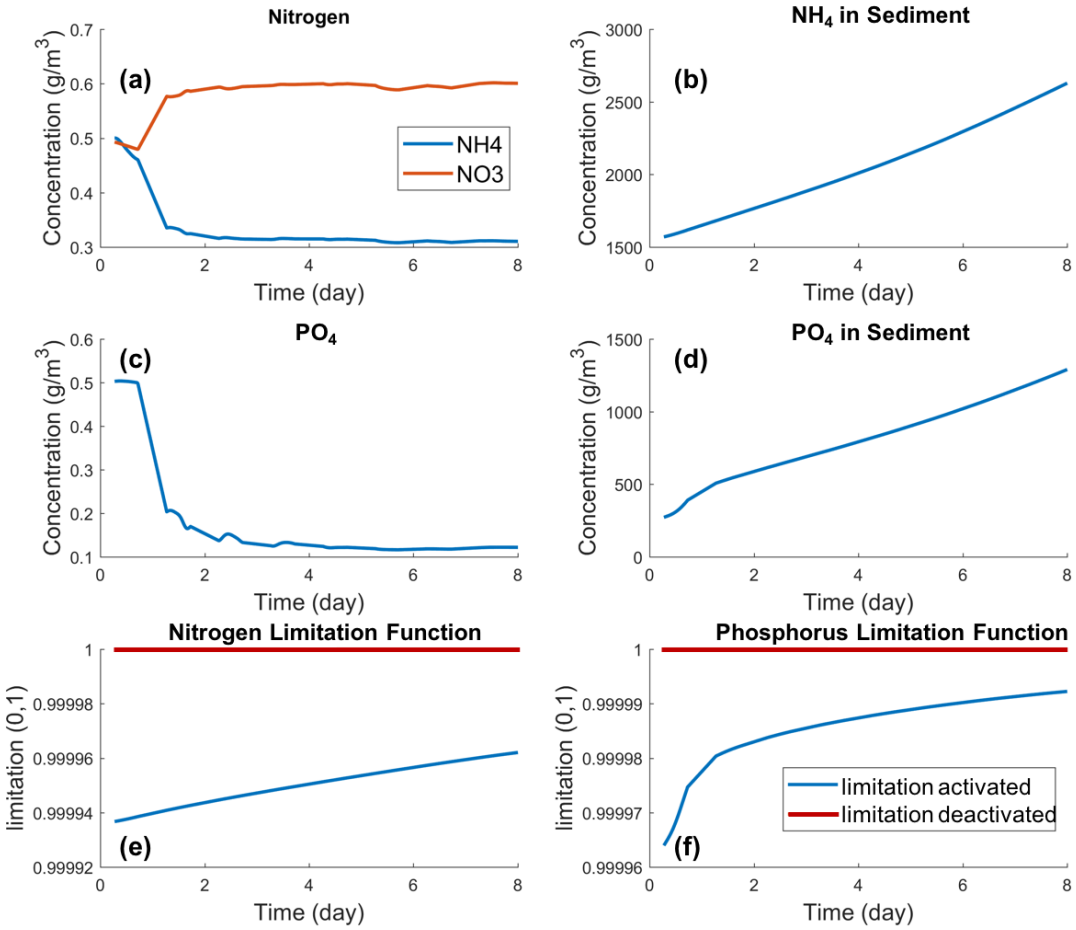

Figure 2-7: Concentration of (a) ammonia & nitrate and (c) phosphate in water column; and concentration of (b) ammonia and (d) phosphate in the sediment. (e) and (f): the activated nutrient limitation functions of nitrogen and phosphorus, which are close to the saturation value of 1.

2.3.3 SAV Impact

2.3.3.1 SAV Impact on Light Supply

In this test, the model simulation starts with an initial condition of biomass of 0.01 g/m^2 for each of the three tissues. To estimate the impact of SAV on light supply in the water column, other impacts from SAV are deactivated, except for light supply.

Figure 2-8 compares the light attenuation rates: background attenuation Kw and total attenuation Ke with or without SAV. It's clear that adding SAV will increase the light attenuation Ke inside canopy through shading compared with the background attenuation Kw. Without SAV, background attenuation and total attenuation are the same by definition, so the red line overlaps the blue line. The inset Figure shows that the background attenuation Kw with SAV (the orange line) is slightly smaller than that without SAV (the blue and red lines), because SAV shading leads to a lower concentration of phytoplankton below the canopy. Note that this benchmark test used a small initial biomass (0.01 g/m^2), and, therefore, the impact from SAV on light supply is relatively minor; in reality, this impact may be much larger as will be shown in Figure 3-10(a-b).

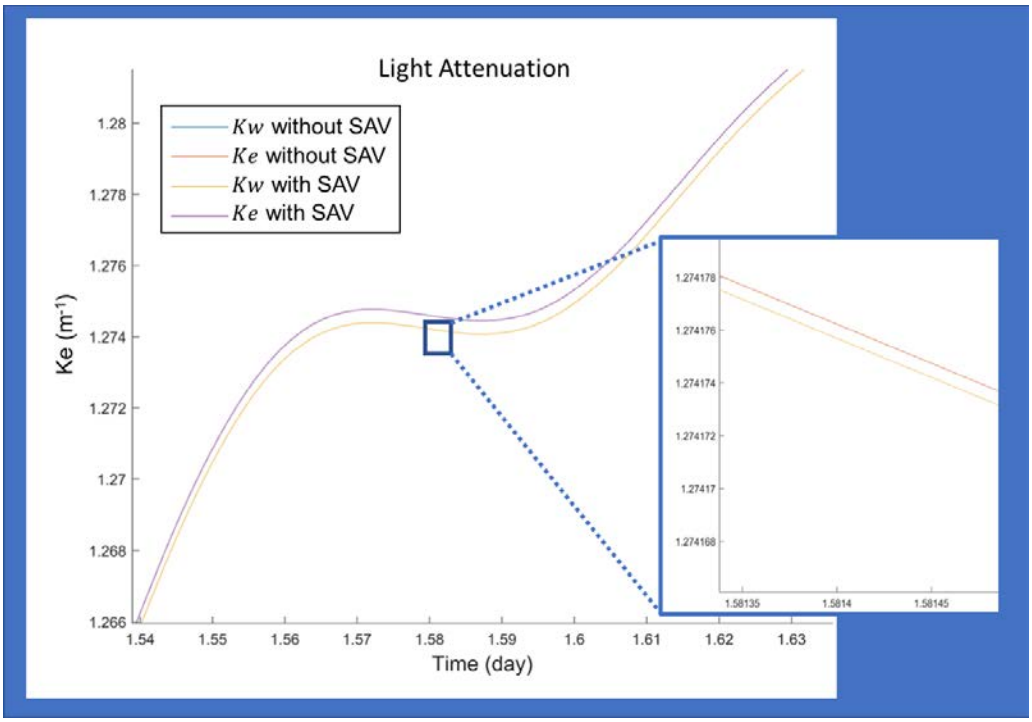

Figure 2-8: Comparison of light attenuation rates with and without SAV in bottom layer.

2.3.3.2 SAV Impact on Nutrient Budget

In this group of benchmark tests, we test the SAV impact on organic nutrient or inorganic nutrient in the water column and sediment separately. Main processes considered here include uptake of inorganic nutrients from water column and sediment to SAV, release of nutrients in water column and sediment from SAV, interaction between phytoplankton and nutrients, remineralization of organic matter to inorganic matter, and exchange of nutrients between water column and sediment due to the concentration gradients. The initial biomass concentrations for the three tissues are all set to be 100 g/m^2.

2.3.3.2.1 SAV Impact on Nitrogen and Phosphorus in Water Column

In this case, we deactivate the SAV impact on sediment nutrients, and activate/deactivate the SAV impact on water column nutrients. All other feedback loops are active. The light supply is kept as unlimited so as to exclude this factor in the following discussion.

SAV releases inorganic ammonia and phosphorus through metabolism, and uptakes them for growth. The diurnal pattern of nitrogen is obvious in Figure 2-9 due to the daily variability of photosynthesis and metabolism. As the half-saturation rate of phosphorus is 1/10 of nitrogen, the diurnal pattern of phosphate is not as obvious as ammonia and nitrate.

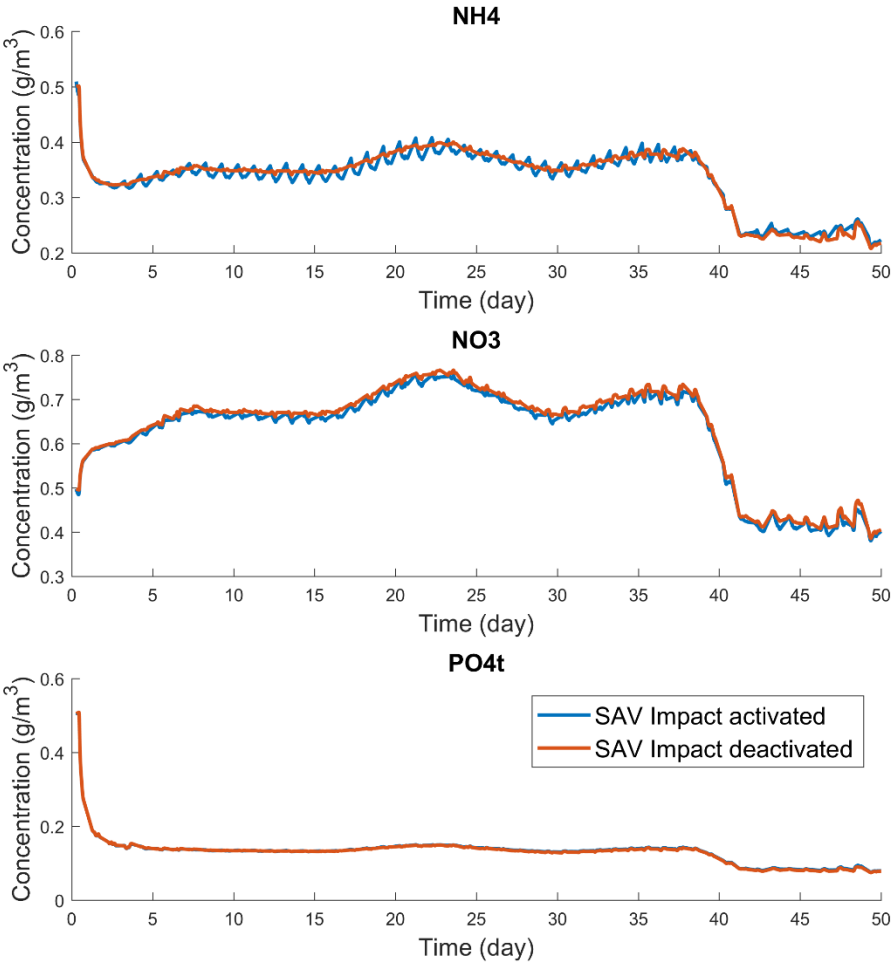

Figure 2-9: Differences of (a) ammonia, (b) nitrate and (c) phosphate concentrations in the water column when the effect of SAV on the nutrients in water column is activated/deactivated.

2.3.3.2.2 SAV Impact on Nutrients and Oxygen in Sediment

In this test, we deactivate the SAV impact on the water column nutrients, and activate/deactivate the SAV impact on the sediment. If deactivated, all the fluxes are zero. Again the light supply is kept unlimited.

In Figure 2-10, the total flux of inorganic N/P to leaf from the sediment follows a diurnal pattern. As SAV uptakes nutrients directly from bottom sediment during the growing season, the decreasing rate of DIN and DIP concentrations in the sediment is much faster than the accumulating rate of organic matter in sediment by SAV metabolism, as seen by comparing Figure 2-10(a-b) with (c-d) after the initial ramp-up period. In addition, the recycle of organic nutrients to the inorganic budget is slow, as diagenesis process is a slow process. Therefore SAV effectively slows down the sediment fluxes of nutrients.

SAV root deposits POC in the sediment, and the decay of organics increases sediment oxygen demand (SOD). In addition, SAV roots can directly uptake oxygen for metabolism. Overall, the magnitude of SAV-induced SOD is found to be in range of 1 to 1.5 g/(m^2 day) with SAV root biomass of ~100 g/m^3 (Figure 2-10(f)), which is confirmed by a simple estimate from equation 2-48. In other words, decay of SAV in the sediment can be a significant part of bottom oxygen consumption.

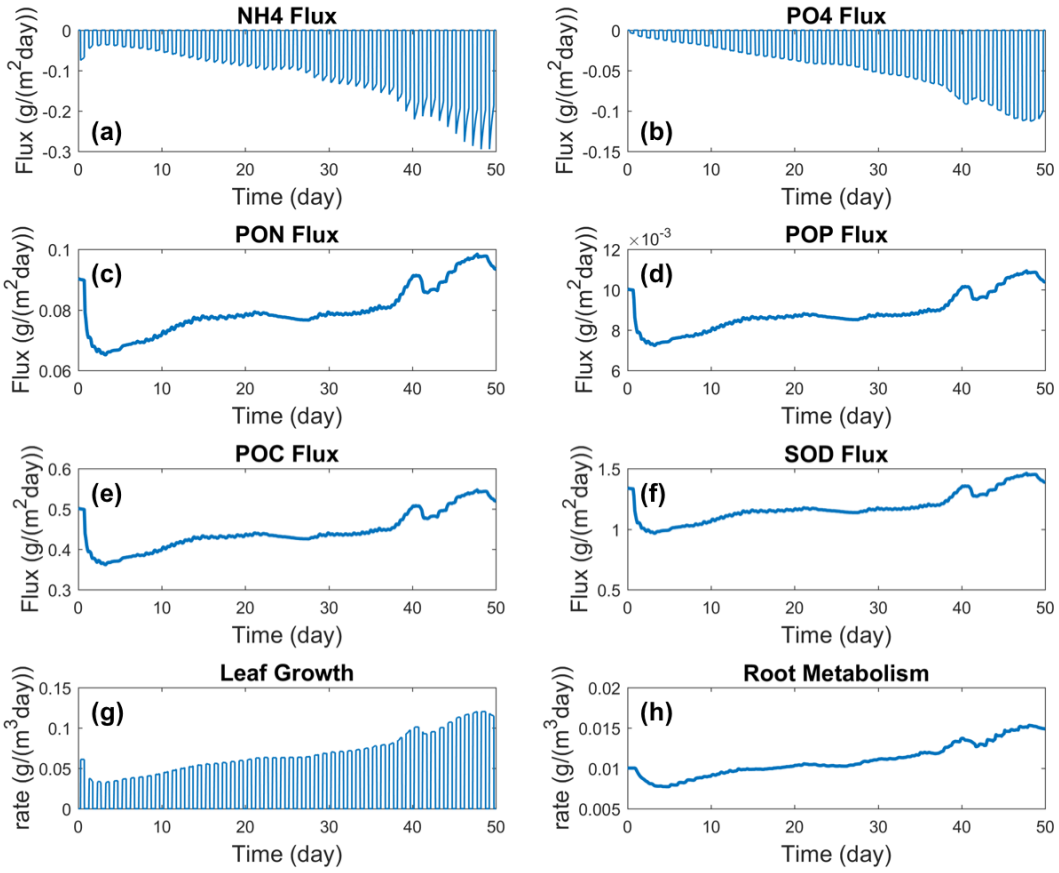

Figure 2-10: SAV sinks from nutrients in sediment and sources for the sediment depositional fluxes. (a) & (b): uptake of inorganic nitrogen and phosphorus, which are required by photosynthesis; (c) (d) (e): release of organic nitrogen, phosphorus and carbon; (f): oxygen demand required by SAV root metabolism in the sediment. (g): leaf growth rate; (h): root metabolism rate.

2.4. Conclusion

An SAV model is developed which is directly coupled within the SCHISM-ICM framework to account for feedback of SAV to the water quality variables. The new SAV model is developed based on the Chesapeake Bay water quality model (Cerco and Moore 2001; Cerco et al., 2002). Because we only need to simulate the freshwater species to simulate, only three state variables are simulated which represent leaf, root and stem components of SAV.

Compared with the Chesapeake Bay SAV model, the coupled SCHISM-ICM-SAV is characterized by several new features. Firstly, the effects from SAV on hydrodynamics are directly simulated and the SAV-induced drag force is incorporated in the momentum and turbulence equations. In the Chesapeake version, only the effects from SAV on sedimentation is simulated with an additional term as a function of SAV biomass added to the original settling velocity. Secondly, SCHISM can locally refine grid resolution with multiple vertical layers at each grid cell, which allows SAV to grow to different layers in the vertical. Therefore, the local horizontal and vertical sub-grid is no longer needed. Instead, the SAV biomass is distributed to multiple vertical layers, which allows for a more accurate simulation of the interactions between SAV and the surrounding environment. In addition, the light attenuation depends on the height of SAV and therefore the shading effect on itself and phytoplankton at different layers can be more adequately captured. In other words, this new version of the SAV model is able to simulate the competition for light supply between SAV and phytoplankton. Furthermore, the nutrient exchange between SAV and water column can be distributed into each layer based on the changing height of the SAV, and therefore the SAV impact on the vertical nutrient distribution is more accurately accounted for.

A series of benchmark tests on SAV biomass dynamics were conducted to validate numerical schemes used to simulate SAV growth and SAV impacts on both water column and bottom sediment nutrient budgets. The modeled SAV biomass matched the analytical solution, and gave reasonable distribution of light supply from upper to lower layers. The increased light attenuation by SAV is captured. The impact of SAV on nutrients in the water column was found to follow a diurnal pattern due to photosynthesis and respiration. Furthermore, the estimates of the magnitude of nutrient flux from/to sediment with SAV were consistent with other estimates, and demonstrated a much-reduced nutrient recycling from sediment to water column with the presence of SAV. The SAV root component was found to be a significant source of sediment oxygen demand.

Chapter 3 Application of SAV Model to Cache Slough Complex, Sacramento-San Joaquin Delta

3.1. Introduction

Liberty Island in Cache Slough Complex is an inundated and naturally restored island created by a levee failure in 1998, in the southern part of the Yolo Bypass (Lehman et al., 2010). Both tidal exposure and seasonal stream flow play a role in this area for its restoration (Marchetti and Moyle, 2001). It is an important source and sink of inorganic and organic material in the Delta, where tidal flow accounts for more than 90% of the material flux (Lehman et al., 2010).

Endemic species such as Delta Smelt use the flooded Liberty Island as dominant habitat (Whitley and Bollens, 2014). Liberty Island is also estimated to have a high aquatic habitat potential for abundant native species (Durand, 2017). However, the invasive SAV Egeria densa has the potential to damage the value of Liberty Island as a habitat for Delta Smelt (Brown and Michniuk, 2007). The SAV can colonize the shallow open-water areas, making it become structurally more complex habitat, which is not desirable for Delta Smelt, because such habitat make them vulnerable to predation (Brown, 2003). In addition, the SAV canopy is also favorable to certain fish species, and some of them are also predators for Delta Smelt (Durand, 2017). Therefore the state and federal agencies adopted the California Natural Resources Agency's Delta Smelt Resiliency Strategy to improve and expand habitat for Delta Smelt since 2016, including a proposal for chemical control on SAV in Cache Slough Complex. A pilot study of this proposal has already begun on two local flooded islands comparing a treatment site (Little Hastings Tract) to a non-treatment site (French Tract, excluded from the domain in this study).

Although SAV habitat is trophically decoupled from pelagic food webs, it has introduced higher phytoplankton and zooplankton levels in some minor channels by increasing the residence time (Grimaldo et al., 2009; Sommer and Mejia, 2013). In this sense, it is also important to estimate the impacts of SAV on the phytoplankton community, which is favorable for the entire food web.

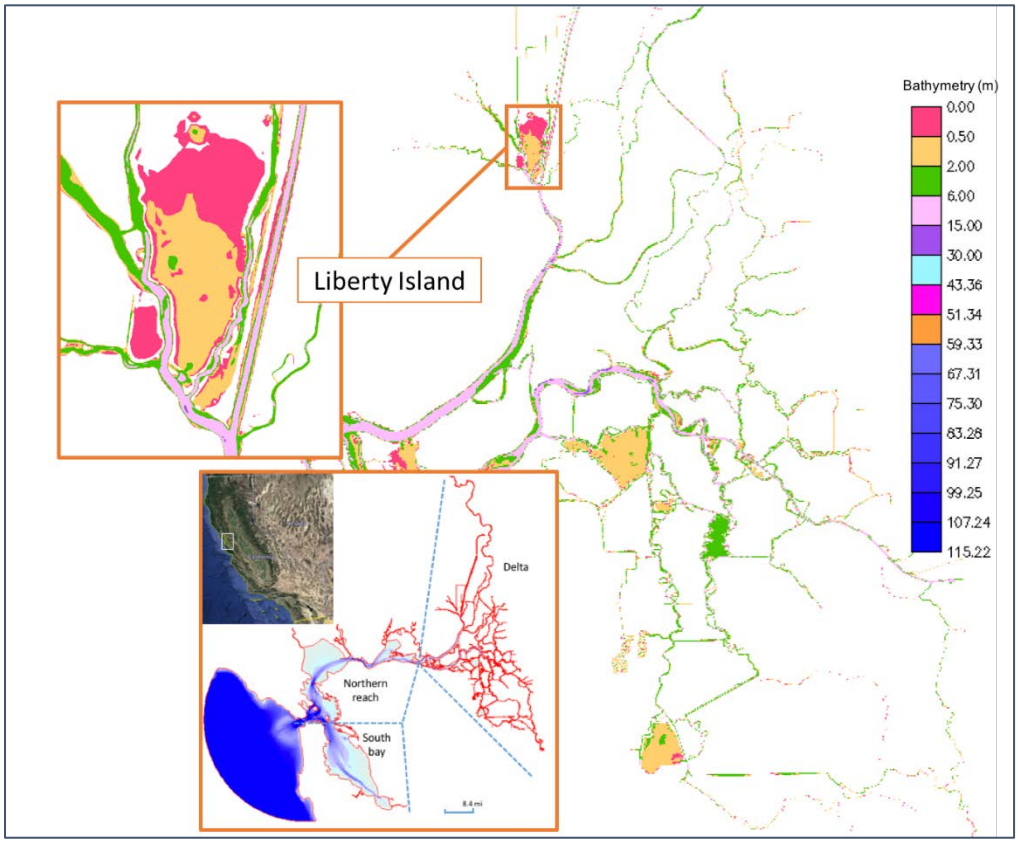

Figure 3-1: Map of Cache Slough Complex, Sacramento-San Joaquin Delta

3.2. Methods

3.2.1 Model Setup and Inputs

The Cache Slough Complex domain is cut from a larger domain encompassing the entire Bay-Delta (Zhang et al., submitted). This small grid contains 20226 triangular and quadratic elements. The horizontal resolution varies from 2.7m in some small narrow channels to 35m in some open water areas. This small domain uses a simper S vertical grid, with 8 levels covering a maximum 16m water depth in deep channels. The boundaries for the Cache Slough Complex domain are Lisbon Weir, Barker Slough Pumping Plant, Cache Slough at Ryer Island and Miner Slough at Hood (Figure 3-2). The boundary hydrodynamic forcing of water level, flow velocity and temperature are all taken from the boundary station observations (LIS, BKS, RYI, HWB) from 2015 to 2016. The water quality loading of nutrients

for both boundary and point/non-point sources are from available observation stations (WDL 145, USGS 11455315, USGS 11455350). Because this region is typically tidal fresh, cyanobacteria is not often observed and it is not simulated. The algal assemblage group, diatom (PB1) and green algae (PB2) are simulated in the model.

In the water quality model, the CN ratio is set to be 11.1 for SAV and 6.1 for phytoplankton (Cloern et al., 2002). The ratio of carbon to SAV dry weight is 0.38 and carbon to chlorophyll-a ratio is 32 (Cloern et al., 1995). The optimal temperature for SAV growth is 32^{o}C. The root half-saturation rates of nitrogen and phosphorus from sediment are 0.1 and 0.01. The initial biomass of SAV is 100 gm^{-2} for both leaf and stem, and 30 g m^{-2} for root, according to the estimated biomass fraction from Section 2.3.1. For the setup of static SAV feedback in the hydrodynamic model (i.e., the hydrodynamics sees a static, non-growing SAV), the diameter is 0.04 m, density is 20 (stem m^{-2}) and height is 0.8 m. The areas with static SAV feedback in hydrodynamics in Figure 3-2(b) follows the distribution of SAV observation reported by DWR (2017).

Due to the lack of observations in most areas of this domain, prior to conducting model experiments, the model with constant initial conditions of SAV and water quality variables was simulated for five years with the same boundary conditions before the ecosystem reaches a dynamic equilibrium.

Small-scale processes are found to be important in this system. However, due to the lack of supporting information required to refine the model for those processes, in this study we will focus mostly on system-wide dynamics using relatively simple assumptions on loadings, and leave the details of more localized dynamics to future study.

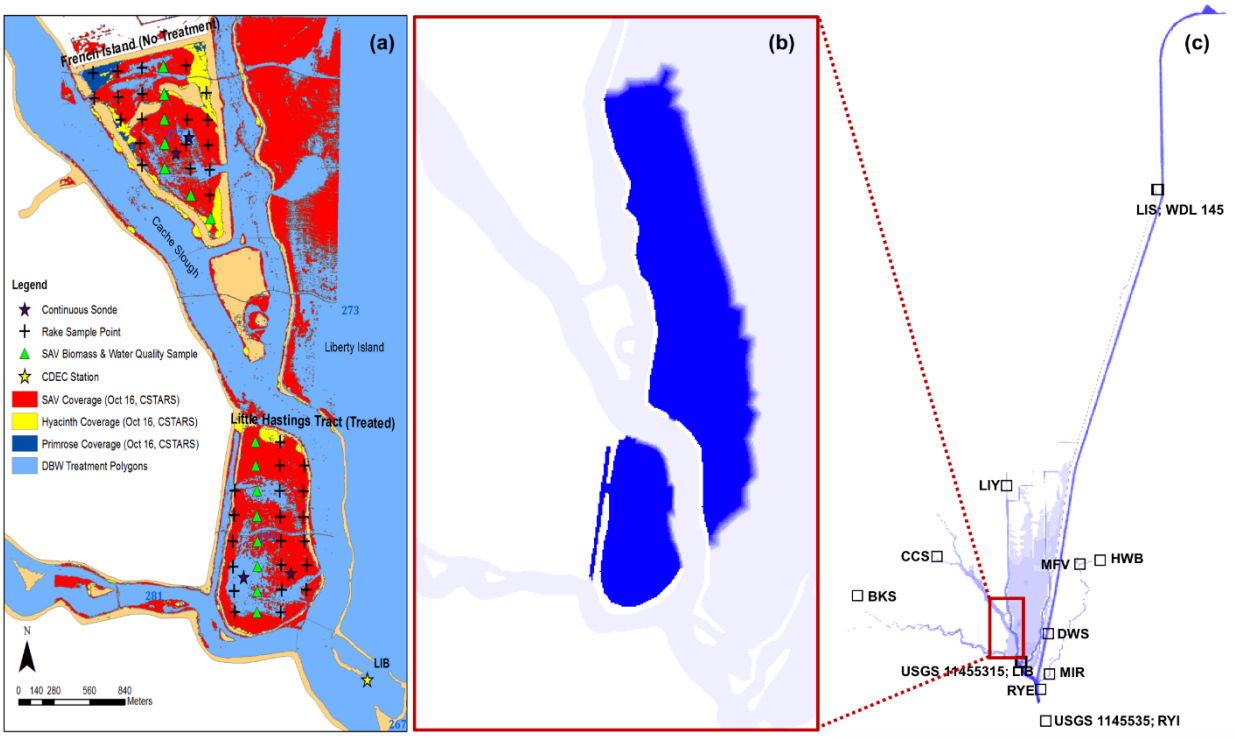

Figure 3-2: (a) UC Davis CSTARS estimated coverage for SAV, Water Hyacinth, and Water Primrose. (DWR et al., 2017). (b) Initial SAV distribution (in dark blue) used in static feedback experiment, based on the observation. (c) Cache Slough Complex domain with stations.

Table 3-1: Parameters for SAV model

Parameters in SAV Model			
Parameter	**Definition**	**Value**	**Unit**
Fam	fraction of production devoted to active metabolism	0.2	$[-]$
$FPlf$	fraction of production routed to leaf biomass	0.6	$[-]$
$FPst$	fraction of production routed to stem biomass	0.3	$[-]$
$FPrt$	fraction of production routed to root biomass	0.1	$[-]$
$Acdw$	plant carbon-to-dry-weight ratio	0.38	g C m^{-2} day^{-1}
$Pmbs$	coefficient for maximum growth rate function	0.1	g C g^{-1} DW
$Topt$	optimal temperature for SAV production	32	℃
$KTg1$	effect of temperature below $Topt$ on production	0.003	$℃^{-2}$
$KTg2$	effect of temperature above $Topt$ on production	0.005	$℃^{-2}$
α	initial slope of production versus irradiance curve	0.006	g C g^{-1} DW $\cdot$ (E $m^{-2})^{-1}$
Ksh	light attenuation by SAV	0.045	m^2 g^{-1} C
Tr	reference temperature for metabolism	20	℃
KTb	effect of temperature on metabolism	0.069	$℃^{-1}$
rlf	coefficients to transfer SAV biomass to canopy height	0.0036	m g^{-1}
rst	coefficients to transfer SAV biomass to canopy height	0.0036	m g^{-1}
rrt	coefficients to transfer SAV biomass to canopy height	0	m g^{-1}
$hcansav0$	coefficients to transfer SAV biomass to canopy height	0.054	m
Anc	SAV nitrogen to carbon ratio	0.09	g N g^{-1} C
$KHNwat$	half-saturation concentration of water column for nitrogen uptake	0.01	g N m^{-3}
$KHNsed$	half-saturation concentration of sediments for nitrogen uptake	0.1	g N m^{-3}
FNI	ammonium fraction of metabolic nitrogen release in water column	0.5	$[-]$
FND	DON fraction of metabolic nitrogen release in water column	0.3	$[-]$
$FNLP$	$RPON$ fraction of metabolic nitrogen release in water column	0.15	$[-]$
$FNRP$	$ORGN$ fraction of metabolic nitrogen release in water column	0.05	$[-]$
Apc	SAV phosphorus to carbon ratio	0.01	g P g^{-1} C
$KHPwat$	half-saturation concentration of water column for phosphorus uptake	0.001	g P m^{-3}
$KHPsed$	half-saturation concentration of sediments for phosphorus uptake	0.01	g P m^{-3}
FPI	phosphate fraction of metabolic nitrogen release in water column	0.5	$[-]$
FPD	$LDOP$ fraction of metabolic phosphorus release in water column	0.35	$[-]$
$FPLP$	$RDOP$ fraction of metabolic phosphorus release in water column	0.1	$[-]$
$FPRP$	$RPOP$ fraction of metabolic phosphorus release in water column	0.05	$[-]$
$Aocr$	mass ratio of oxygen to carbon produced in photosynthesis	2.67	g DO g^{-1} C
FDO	fraction of metabolism expressed as oxygen consumption	0.5	$[-]$
FCD	fraction of metabolism expressed as dissolved organic carbon	0.3	$[-]$
$FCLP$	fraction of metabolism expressed as labile particulate organic carbon	0.15	$[-]$
$FCRP$	fraction of metabolism expressed as refractory particulate organic carbon	0.05	$[-]$

3.2.2 Model Experiments: Reference Run and Experimental Scenarios

Basically, two groups of model experiments were conducted to investigate the effect of SAV removal: one with SAV and the other without SAV. For the experiments with SAV, there are three different tests – a) without feedback to hydrodynamics (i.e., the latter sees no SAV-induced friction feedback to hydrodynamics), b) with static feedback to hydrodynamics (i.e. the latter sees the effects of a non-growing SAV with constant height impacts hydrodynamics), c) with dynamic feedback to hydrodynamics (i.e. SAV growth (varying heights) directly impacts hydrodynamics). In this thesis, scenario run with static feedbacks is set to be reference run. All model simulations were conducted from January 2015 to November 2016 for Cache Slough Complex domain. These two years were chosen because water quality observations are relatively abundant since 2015. Model simulations incorporate both chlorophyll-a and SAV, as well as DO and nutrient dynamics. By comparing the results of these two groups of model experiments, the relative impact of SAV on chlorophyll-a, dissolved oxygen and nutrient budgets can be assessed. Because there is insufficient data for the spatial-temporal distributions of SAV biomass, the simulation of SAV biomass is started with a constant value largely consistent with the observation in the polygon shown in Figure 3-4(a), which contains the channels. The reason for containing the channels is to test the capability of the SAV model to simulate a reasonable SAV distribution as shown in Figure 3-4. However, the setup area for the static feedbacks to hydrodynamics excludes the channels to fit the reality. The model was further validated based on available observation data from the area shown in Figure 3-2(c) as well as station time series.

To quantify the impacts from the removal of SAV beds, besides the direct comparison between each selected state variable, differences with and without SAV for each water quality state variables were computed.

3.3. Model Validations

3.3.1 Comparison with Observations

The reference model (with static feedback) is calibrated to a normal performance with validation from the observations in this system (Figure 3-3). The elevation is mainly controlled by the boundary condition and fits the observation in Cache Slough. Salinity is minor in this area and the model simulation matches the observed temporal variations. The modelled temperature agrees with the observations.

Overall, the model catches the magnitude of the chlorophyll-a concentration. It matches both the pattern and magnitude of the dissolved oxygen. The nutrient concentrations agree with the observations well at each station with data available in terms of temporal variations and values. Unsurprisingly, the model skill is generally higher for physical variables than for biological variables, but the correlation coefficients for the latter are still above 0.7 at all stations except two (Figure 3-3), one of which (WDL145) has too few data points to make the statistics meaningful.

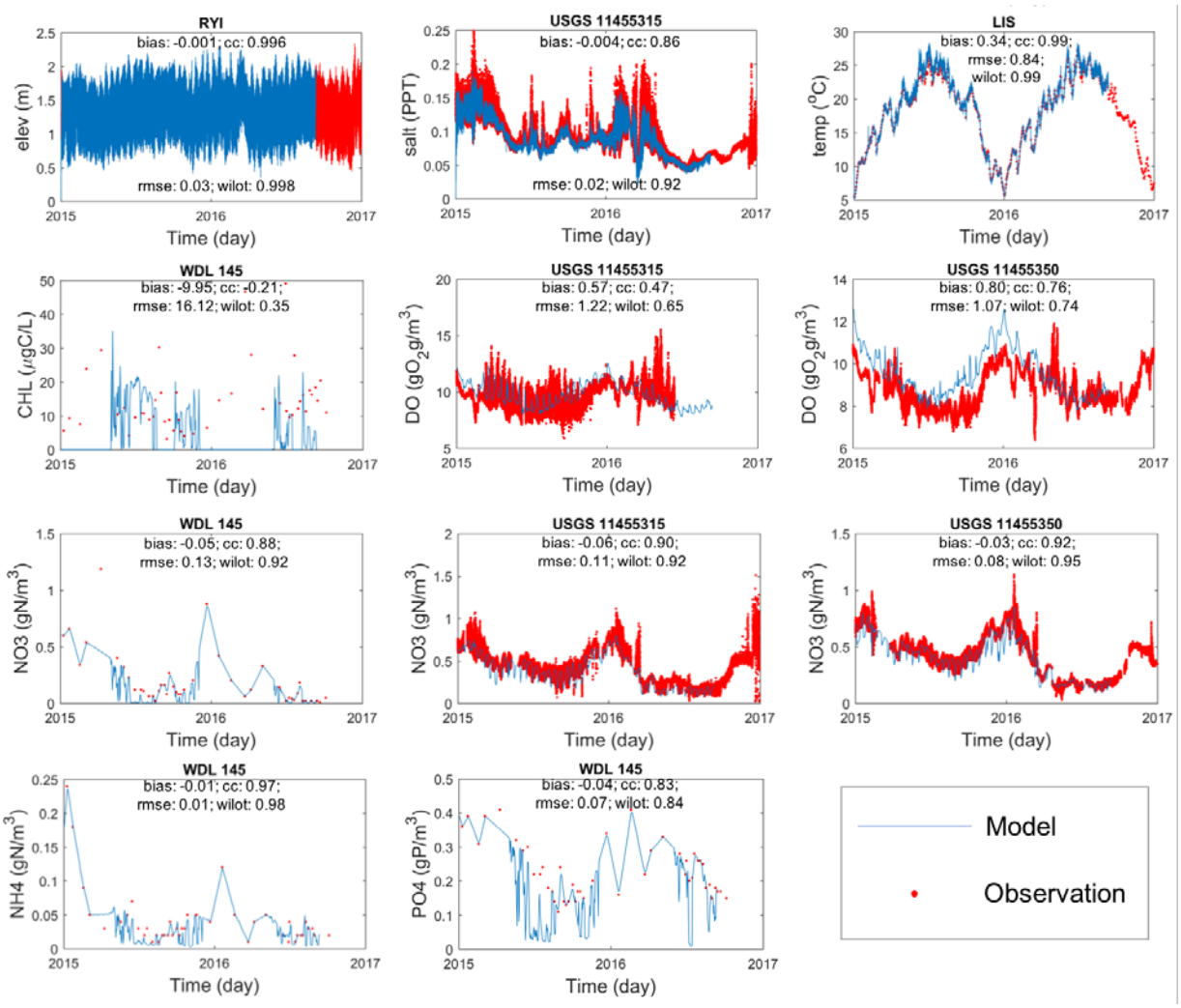

Figure 3-3: Comparison between model results and observation for physical and water quality variables. Errors statistics are shown in each panel ('cc' stands for correlation coefficient).

3.3.2 Evolution and Distribution of SAV

SAV growth is highly regulated by the available light but depends less on the nutrients in the water column as it can uptake the abundant nutrients from the bottom sediment. Light is unable to reach the bottom if water is too depth. Although the initial biomass of SAV is assumed to be constant within the polygon area (Figure 3-4(a)), the distribution of SAV will be dependent on the depth. The model results demonstrate that the model is able to adequately simulate the die-off process of SAV in the deep channels; Figure 3-4(a-f) shows the biomass, which presents the sequence of change of SAV throughout

the Delta system. The initial biomass in channels declines by half in 60 days and almost completely disappears in 180 days. The distribution of SAV after a one-year simulation (Figure 3-4(f)) is consistent with the observed distribution based on observation; the latter shows that SAV is abundant in shallow regions and spares in deep channel.

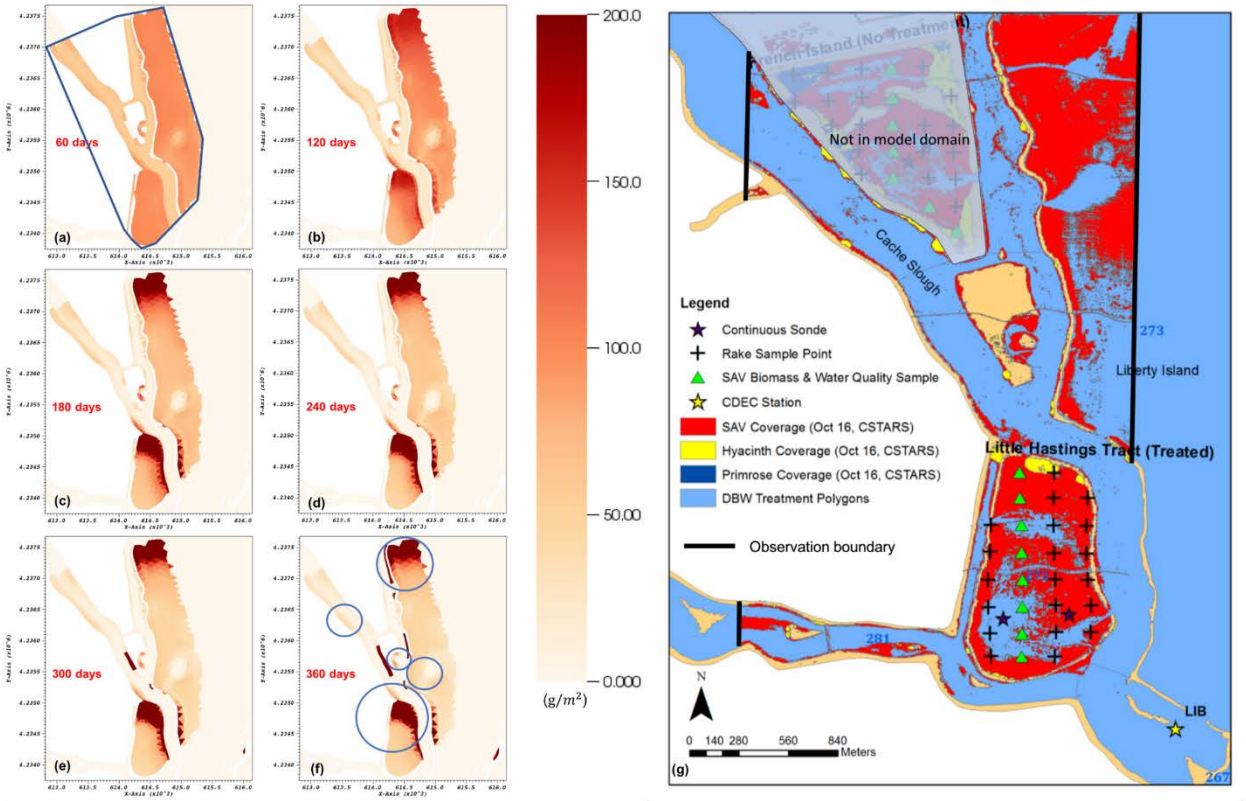

Figure 3-4: Biomass distribution every 60 days of SAV after an initiation of constant biomass inside the polygon shown in (a). (f): Highlights on matched SAV distribution with observations. (g) CSTARS estimated coverage for SAV (cf. Figure 3-2(c)).

3.4. Discussions

3.4.1 Spatial Variability of SAV Impacts

3.4.1.1 Overall Spatial Variabilities of SAV Biomass

After the model with same kinetic parameters and boundary conditions was repeatedly run for 5 years until it reaches dynamic equilibrium, the seasonal and spatial pattern of SAV biomass were

investigated from the results in the 5th year. The canopy height shown in Figure 3-5 illustrates the spatial-temporal variability of SAV. The canopy height increases a high level from spring to summer before going down in fall and winter. A large biomass of SAV is located in Hastings Tract to the west of the channel, which is an open body of water connected to the surrounding water through two main breaches and a number of sieve-like smaller ones, some of which are too small or poorly captured in elevation maps to include here – an omission that is becoming less tenable year by year. The northern part of this 'lake' has the highest biomass, while very little or no SAV is found in deep channel; low SAV biomass is also found in the middle of the areas in the east region of the channel, where the water depth is larger. Different levels of SAV biomass are largely correlated with bathymetry (Figure 3-6), and therefore we'll discuss the processes in 3 areas: shoal area (water depth <2m), median depth area (2~4m), and deep channels (>4m).

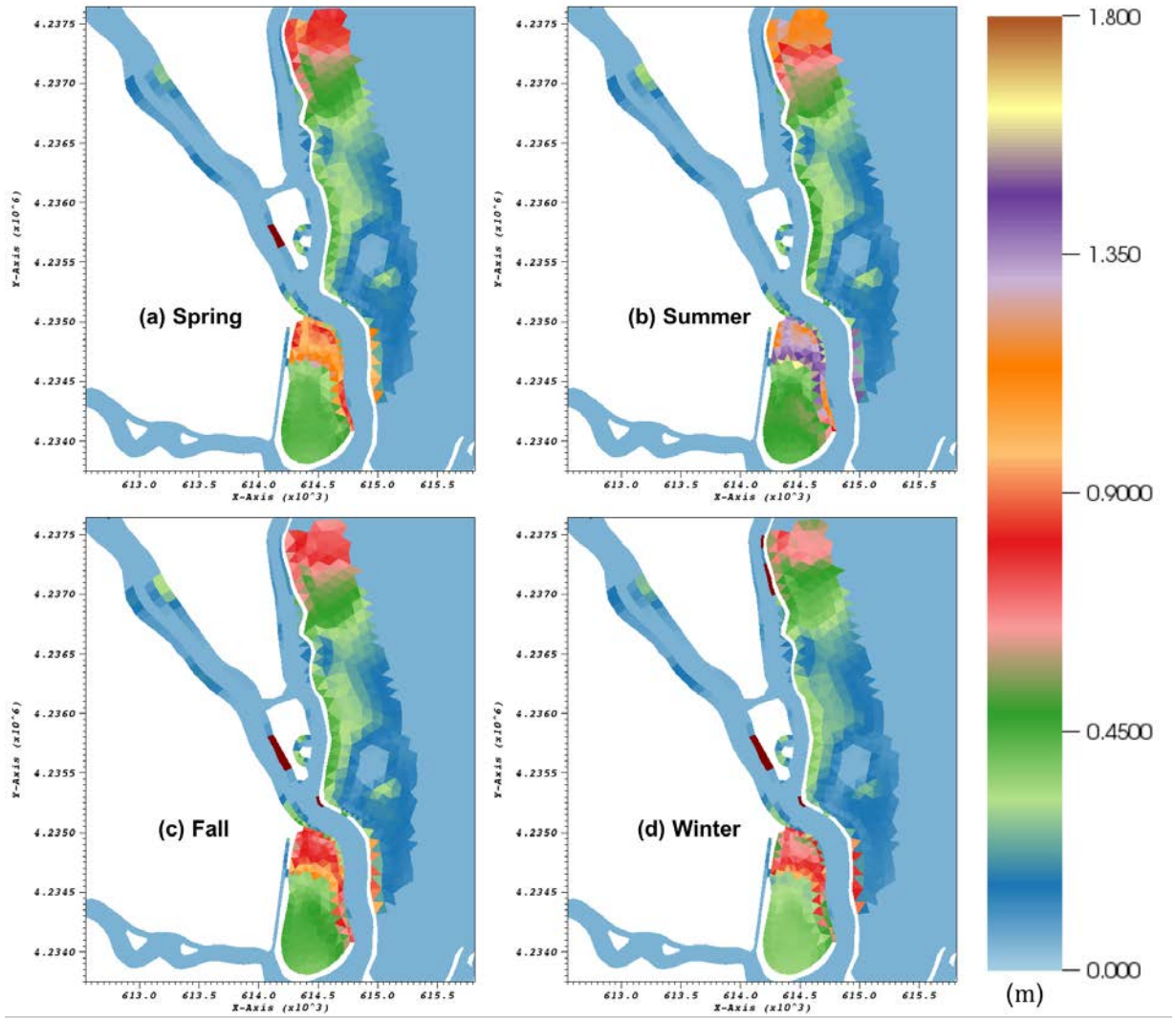

Figure 3-5: Canopy height (m) distribution over the four seasons: (a) Spring – Mar to May; (b) Summer – Jun to Aug; (c) Fall – Sep to Nov; (d) Winter – Dec to Feb.

To further investigate the change of SAV in these three regions, local transects and stations in the Cache Slough Complex Domain are selected (Figure 3-6) to examine the variation of SAV with respect to temperature and salinity, and changes in chlorophyll-a, dissolved oxygen and nutrients. The transects straddle two sides of Shag Slough (the deep part), one median depth section in Liberty Island and one in Little Hastings Tract and a shoal area in Little Hastings Tract. The average, minimum and maximum values of state variables are summarized in Tables 3-2, 3-3, and 3-4, and shed lights on the SAV dynamics in shoal, median depth and deep channel areas.

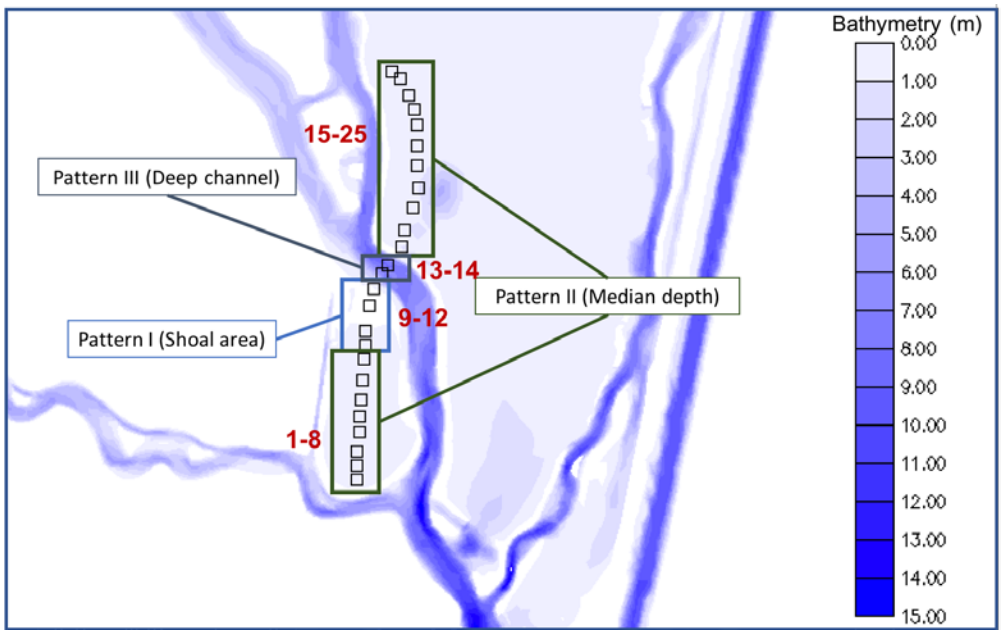

Figure 3-6: Three groups of stations along the SAV bed.

3.4.1.2 Shoal Area

As shown in Table 3-2, SAV leave biomass can reach over 455 g/m^2 in summer and drops to about 170 g/m^2 in winter. Stem has a peak biomass of 228 g/m^2 in summer and 85 g/m^2 through the winter. The peak biomass of root is around 76 g/m^2 in summer while it drops down to 28 g/m^2 in winter. The canopy can reach the water surface and float up and down along with the free surface. The canopy height can reach about 2 m at high tide.

With SAV slowing down the flow, the salinity in this area decreases slightly from 0.27ppt to 0.26ppt on average. The temperature decreases from 17.44℃ to 17.29℃ on average with SAV. The peak value of chlorophyll-a is smaller with SAV, but the average value is higher. Considering the shallow water depth and air reaeration, the DO concentration stays at a stable range around saturation value of 10 g/m^3, and therefore there is little difference in DO concentration with or without SAV. With large SAV biomass, especially large root biomass in the sediment, the metabolism of SAV consumes a large amount of oxygen. Therefore without SAV, the SOD produced by the diagenesis flux and other chemical

reactions is stable in a range of 0.5 to 1.8 g/(m^2 day), whereas with SAV growth (with static feedback to hydrodynamics), SOD can reach 3.57 g/(m^2 day) during bloom season and implicate on water column.

On average, ammonia decreases 11.8% with SAV. The range of ammonia concentration is 0.0085 to 0.39 g/m^3 without SAV, while with SAV, the range is 0.007 to 0.4 g/m^3. SAV plays an important role on blocking the nutrient recycling from the sediment. With SAV, the nutrient flux may be reversed from water column to the sediment because of the reversed nutrient concentration gradient. Without SAV, there is abundant ammonia flux from sediment into water column that peaked at the range of 0.1125 g/(m^2 day). A similar pattern can be concluded for other nutrients.

3.4.1.3 Median Depth Areas

For the run with SAV, the biomass magnitude of SAV is smaller than shoal area. SAV leave biomass can reach 112 g/m^2, with a drop of more than 100 g/m^2 in winter time. Peak stem biomass in summer is about 56 g/m^2, while in winter, the stem biomass on average is about 25 g/m^2. Concerning the root biomass, it is about 18 g/m^2 in summer bloom, while decreasing to 1.8 g/m^2 in winter. The canopy stays on a height of 0.35 to 0.5m under the water surface stably.

There is also a decrease of salinity as in shoal area, but the temperature slightly increases as shown in Table 3-3. Chlorophyll-a has a significant increase on average of 27.9% with SAV. The difference of dissolved oxygen is still slight. SOD slightly increased 0.3% on average with SAV in this area. With SAV, average SOD is 1.1269 g/(m^2 day).

On average, ammonia decreases by 55.58% with SAV. The range of ammonia concentration is 0.007 to 0.4277 g/m^3 without SAV, while with SAV, the range is 0.0016 to 0.381 g/m^3. Like in the shoal area, SAV plays an important role on blocking the nutrient recycling from the sediment: with SAV, the ammonia flux decreases from 0.029 to 0.0077 g/(m^2 day). Similar patterns can be found for other nutrients.

3.4.1.4 Deep Channel Areas

SAV does not survive in deep channels, as shown in Table 3-4. The changes in chlorophyll-a, DO, nutrient concentration and nutrient fluxes from sediment are all minor.

Table 3-2: Averaged, maximum and minimum values for each water quality state variable in scenarios of no SAV and with SAV in shoal area.

Shoal Area												
	Averaged				Maximum				Minimum			
	Diff = [SAV]-[no SAV]; Rat = ([SAV]-[no SAV])/[SAV] (%)											
Variables	With SAV	No SAV	Diff	Rat (%)	With SAV	No SAV	Diff	Rat (%)	With SAV	No SAV	Diff	Rat (%)
SAV Leaf (g/m^2)	315.1805	0	--	--	455.996	0	--	--	169.194	0	--	--
SAV Stem (g/m^2)	157.5927	0	--	--	228.001	0	--	--	84.5984	0	--	--
SAV Root (g/m^2)	52.5309	0	--	--	76.0005	0	--	--	28.1995	0	--	--
Canopy height (m)	1.3312	0	--	--	2	0	--	--	0.3932	0	--	--
Salinity (ppt)	0.2674	0.2709	-0.0035	-1.3083	0.3029	0.3092	-0.0063	-2.0922	0.215	0.2185	-0.0035	-1.6169
Temperature (℃)	17.299	17.4436	-0.1446	-0.8358	27.079	27.0245	0.0546	0.2016	3.8739	3.5561	0.3178	8.2029
Chlorophyll-a ($\mu g/L$)	21.2274	18.8365	2.3909	11.2631	57.4338	63.7229	-6.2891	-10.9501	0.0255	0.0144	0.0111	43.6478
DO (g/m^3)	10.1006	10.241	-0.1404	-1.3898	13.6911	14.0543	-0.3632	-2.6529	7.8685	7.8967	-0.0282	-0.3585
SOD ($g/(m^2 day)$)	-1.8538	-1.1094	-0.7444	40.1548	-0.8123	-0.5385	-0.2738	33.7049	-3.573	-1.7145	-1.8584	52.0135
NH_4(g/m^3)	0.1231	0.1377	-0.0146	-11.8488	0.4043	0.3909	0.0134	3.3207	0.0077	0.0085	-0.0008	-10.0427
NH_4 Flux ($g/(m^2 day)$)	-0.0059	0.0322	-0.0381	645.576	0.0341	0.1125	-0.0784	-229.5406	-0.0231	-0.0086	-0.0145	62.8938
NO_3 (g/m^3)	0.2442	0.2923	-0.0481	-19.7022	0.7296	0.7401	-0.0105	-1.4402	0.0013	0.0131	-0.0118	-931.8361
NO_3 Flux ($g/(m^2 day)$)	-0.0217	-0.0134	-0.0082	37.9954	0.0043	0.0116	-0.0072	-167.861	-0.0592	-0.0416	-0.0175	29.6519
PO_4 (g/m^3)	0.0633	0.0678	-0.0045	-7.067	0.1551	0.1575	-0.0024	-1.5758	0.0091	0.0079	0.0012	13.5043
PO_4 Flux ($g/(m^2 day)$)	-0.0093	-0.0062	-0.0031	32.9953	-0.002	-0.0008	-0.0012	61.5169	-0.0245	-0.0158	-0.0088	35.7589

Table 3-3: Averaged, maximum and minimum values for each water quality state variable in scenarios of no SAV and with SAV in median depth area.

Median Depth Area												
	Averaged				Maximum				Minimum			
	Diff = [SAV]-[no SAV]; Rat = ([SAV]-[no SAV])/[SAV] (%)											
Variables	With SAV	No SAV	Diff	Rat (%)	With SAV	No SAV	Diff	Rat (%)	With SAV	No SAV	Diff	Rat (%)
SAV Leaf (g/m^2)	51.0169	0	--	--	112.263	0	--	--	10.9177	0	--	--
SAV Stem (g/m^2)	25.5089	0	--	--	56.1327	0	--	--	5.4589	0	--	--
SAV Root (g/m^2)	8.503	0	--	--	18.7109	0	--	--	1.8197	0	--	--
Canopy height (m)	0.3295	0	--	--	0.6602	0	--	--	0.113	0	--	--
Salinity (ppt)	0.2657	0.2689	-0.0033	-1.2278	0.2992	0.3031	-0.0039	-1.304	0.1692	0.1874	-0.0182	-10.7804
Temperature (℃)	17.3568	17.267	0.0898	0.5174	27.8309	26.9998	0.831	2.986	2.1555	2.8269	-0.6714	-31.1478
Chlorophyll-a ($\mu g/L$)	28.9913	20.9001	8.0912	27.9092	99.3882	94.7808	4.6074	4.6358	0.0117	0.0126	-0.0009	-7.9452
DO (g/m^3)	10.3256	10.3643	-0.0387	-0.3744	16.8759	14.095	2.7809	16.4787	7.5991	8.0847	-0.4857	-6.3912
SOD ($g/(m^2 day)$)	-1.1269	-1.1229	-0.004	0.3513	-0.4826	-0.5259	0.0433	-8.9694	-1.9721	-1.7917	-0.1804	9.1487
NH_4(g/m^3)	0.0923	0.1464	-0.0541	-58.5825	0.381	0.4277	-0.0467	-12.2439	0.0016	0.007	-0.0054	-328.9828
NH_4 Flux ($g/(m^2 day)$)	0.0077	0.029	-0.0213	-276.7177	0.0941	0.1147	-0.0206	-21.8724	-0.0152	-0.01	-0.0052	34.2746
NO_3 (g/m^3)	0.1887	0.3129	-0.1242	-65.8069	0.6932	0.7871	-0.094	-13.5541	0	0.0059	-0.0059	--
NO_3 Flux ($g/(m^2 day)$)	-0.0087	-0.0149	0.0063	-72.3123	0.0166	0.0113	0.0052	31.629	-0.0454	-0.0483	0.0028	-6.2643
PO_4 (g/m^3)	0.0534	0.0689	-0.0155	-28.9416	0.1628	0.1639	-0.0011	-0.6833	0.0056	0.005	0.0006	10.7982
PO_4 Flux ($g/(m^2 day)$)	-0.0045	-0.0061	0.0016	-35.1005	-0.0006	-0.0003	-0.0003	51.5192	-0.0161	-0.0149	-0.0012	7.2169

Table 3-4: Averaged, maximum and minimum values for each water quality state variable in scenarios of no SAV and with SAV in deep channel area.

Deep Channel Area												
	Averaged				Maximum				Minimum			
	Diff = [SAV]-[no SAV]; Rat = ([SAV]-[no SAV])/[SAV] (%)											
Variables	With SAV	No SAV	Diff	Rat (%)	With SAV	No SAV	Diff	Rat (%)	With SAV	No SAV	Diff	Rat (%)
SAV Leaf (g/m^2)	0	0	--	--	0	0	--	--	0	0	--	--
SAV Stem (g/m^2)	0	0	--	--	0	0	--	--	0	0	--	--
SAV Root (g/m^2)	0	0	--	--	0	0	--	--	0	0	--	--
Canopy height (m)	0	0	--	0	0	0	--	--	0	0	--	--
Salinity (ppt)	0.2676	0.2701	-0.0025	-0.9411	0.3003	0.3016	-0.0013	-0.4342	0.2164	0.2203	-0.004	-1.8311
Temperature (℃)	17.6186	17.5874	0.0312	0.1771	27.1038	27.1497	-0.0459	-0.1693	3.8142	3.6603	0.1539	4.0348
Chlorophyll-a ($\mu g/L$)	18.9528	18.4461	0.5067	2.6736	56.3714	63.5894	-7.2179	-12.8042	0.0205	0.0168	0.0038	18.4087
DO (g/m^3)	10.4319	10.4226	0.0093	0.0889	15.3814	14.9822	0.3993	2.5958	7.8386	7.8499	-0.0113	-0.1447
SOD ($g/(m^2 day)$)	-1.3477	-1.3582	0.0105	-0.776	-0.6903	-0.6966	0.0063	-0.9146	-2.0054	-2.0321	0.0266	-1.3284
NH_4(g/m^3)	0.1184	0.1326	-0.0142	-11.9529	0.3867	0.3894	-0.0026	-0.6813	0.004	0.0058	-0.0018	-44.683
NH_4 Flux ($g/(m^2 day)$)	0.0429	0.0461	-0.0032	-7.4621	0.1345	0.1441	-0.0096	-7.1413	-0.0061	-0.0058	-0.0003	5.4245
NO_3 (g/m^3)	0.2564	0.2875	-0.0311	-12.1468	0.7181	0.7327	-0.0147	-2.0409	0.0065	0.0125	-0.006	-92.6848
NO_3 Flux ($g/(m^2 day)$)	-0.0131	-0.0159	0.0028	-21.109	0.0122	0.011	0.0012	9.5328	-0.0434	-0.0443	0.0009	-2.0364
PO_4 (g/m^3)	0.0673	0.0687	-0.0013	-1.9696	0.1653	0.1584	0.0069	4.2028	0.0102	0.008	0.0022	21.4089
PO_4 Flux ($g/(m^2 day)$)	-0.0076	-0.0079	0.0003	-4.4628	-0.0017	-0.0015	-0.0002	12.6674	-0.0188	-0.019	0.0001	-0.7214

3.4.1.5 Annually Averaged Differences

To investigate the change of water quality condition with and without SAV, the difference of model results with and without SAV for each state variable was computed and averaged for the 5th year. The spatial differences are analyzed over the entire domain to estimate the impacts.

The annually averaged difference is shown in Figure 3-7 for some state variables. This distribution pattern shows an overall influence of SAV on phytoplankton accumulation. The phytoplankton pattern appears to agree with the findings from previous studies that the SAV can increase the residence time and encourage accumulation of phytoplankton (Grimaldo et al., 2009; Sommer and Mejia, 2013). Large differences occur in the shallow area with high SAV growth. A detailed analysis of interactions between SAV and phytoplankton will be discussed in the next section. As a significant primary producer, SAV beds tend to have higher dissolved oxygen concentration. Dissolved organic nitrogen, as a product of the metabolism of phytoplankton and SAV, are found to be larger in the SAV beds area associated with high phytoplankton concentration. An overall decrease of inorganic nutrients near the SAV beds are observed, which are due to increased uptake by SAV and phytoplankton there.

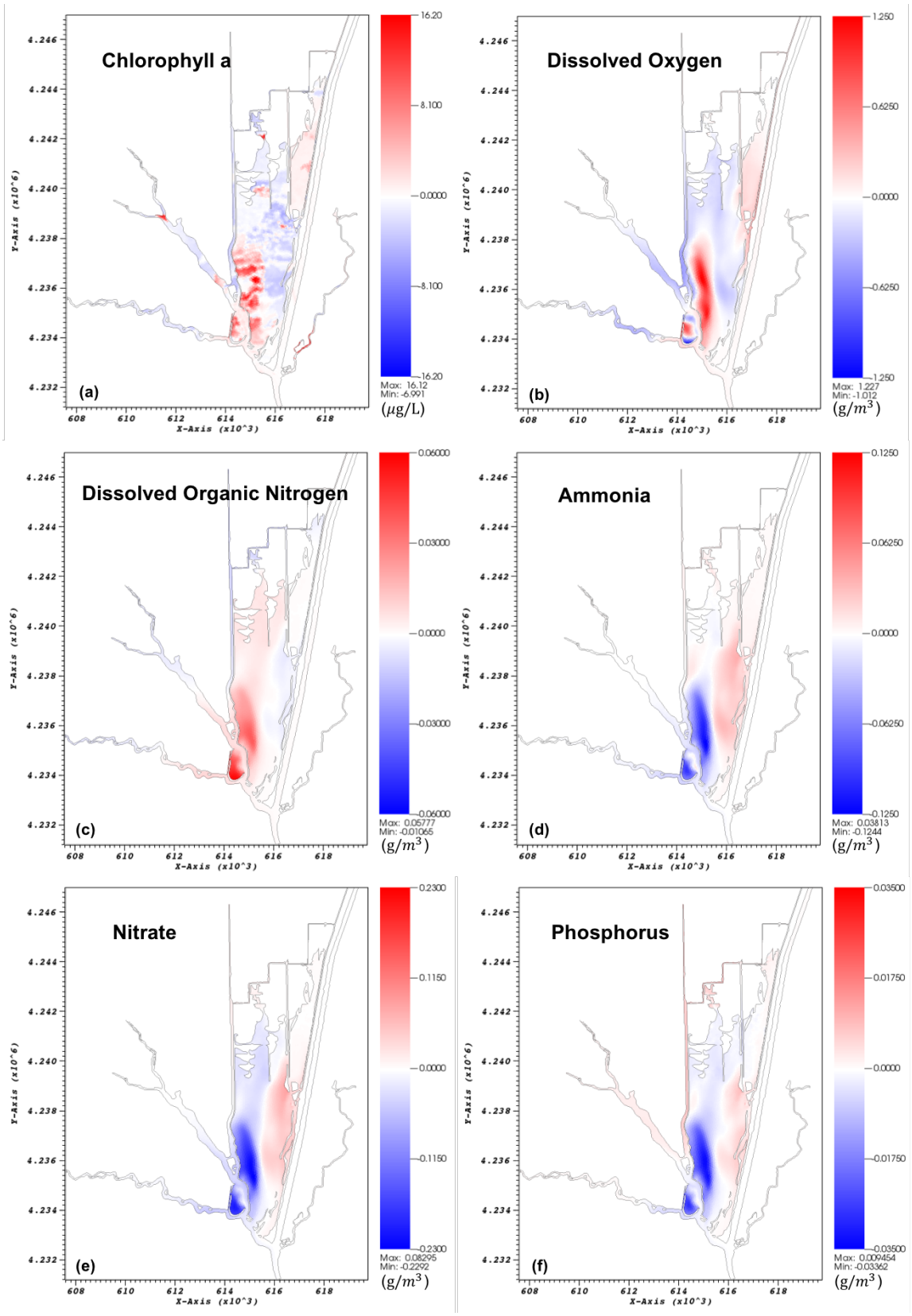

Figure 3-7: Spatial distributions of averaged differences of selected state variables ([SAV]-[No_SAV]) caused by SAV.

3.4.2 Seasonal Variabilities of SAV-Phytoplankton Interactions

SAV and phytoplankton are the main primary producers in the Delta region. And they interact with each other locally in several ways. Firstly, they compete for the nutrients in the water column, but only SAV can uptake nutrients directly from the sediment. Regarding the light supply, high concentration of phytoplankton increases the light attenuation in the water column when SAV has not reached to the surface, and it decreases the light supply to the SAV leaves; on the other hand, once SAV forms canopy, the shading of SAV will block the light supply to phytoplankton growth below the canopy. Besides these ecological interactions, the existence of SAV will increase friction for both the bottom and the water column that will feedback to the flow fields. It finally alters the dynamic conditions and local residence time. An increase of residence can result in accumulation of phytoplankton and increase of bloom in many areas (Figure 3-8).

To analyze the SAV-phytoplankton dynamics, rates of changes in the phytoplankton biomass are examined. The plots in this section show variables at 1m depth below surface at representative stations. Based on the model results along the transect of Cache Slough Complex domain (Figure 3-6), three distinctive patterns of SAV-phytoplankton interactions can be observed, which are related to the bathymetry– bloom coexistence in the shallows, SAV bloom in seasonal succession with phytoplankton decline at intermediate depths and no SAV in deep channels.

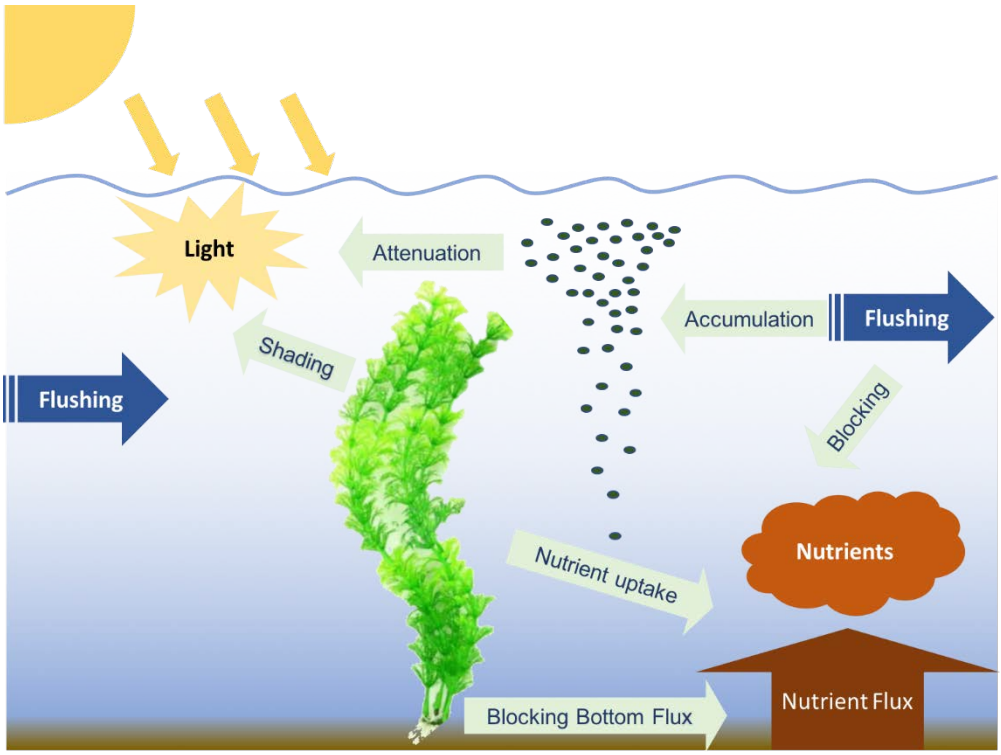

Figure 3-8: Local interactions between SAV and phytoplankton.

3.4.2.1 Pattern I: Bloom Coexistence in Shoal Area

As shown in Figure 3-9(a-j), in shoal areas, the SAV and phytoplankton tend to co-exist and bloom together. The biomasses are generally large for both. The canopy is right near the water surface, rising and falling along with elevation. In the presence of SAV, fluctuation of phytoplankton concentration due to tidal flushing is greatly reduced (Figure 3-9(c)). Figure 3-9(d) indicates that SAV slows down the tidal flow, which is favorable for phytoplankton accumulation. Figure 3-9(e) shows the surface elevation variation with clear spring-neap variation, which is mainly controlled by the boundary condition and does not depend on the presence of SAV. This indicates that the change of phytoplankton is mainly controlled by horizontal biomass transport. Figures 3-9(f-h) suggest that the nutrients are not limited for the growth of either SAV or phytoplankton. Referring to the bottom nutrient flux, SAV plays a

significant role on blocking the recycling of inorganic nutrients. In summary, emergent vegetation is dominant in this area with both SAV and phytoplankton blooming in summer.

To demonstrate the tidal scale variability, we plot out the hourly time series in a 15-day period from Aug 1 to Aug 16 in Figure 3-9(k-t). The tides in this area are predominantly semi-diurnal (Figure 3-9(o)). The presence of SAV induces large drag that not only slows down the flow but also causes a phase lag compared to the case without SAV (Figure 3-9(n)). For the case with SAV, the tidal fluctuation in Chlorophyll-a decreases because of smaller tidal flushing (Figure 3-9(m)). The decreased fluctuations of nutrients are results of both changed flow pattern and phytoplankton dynamics (Figure 3-9(p-r)). The changes in the nutrient concentrations further influence the bottom nutrient fluxes (Figure 3-9(s-t)). At the tidal scale, the variability of biological variables is intimately connected to that in the physical variables (in particular the flow), e.g., with a similar phase lag (Figure 3-9(k-t)).

Although the peak algal concentration is similar with and without SAV, it is still essential to compare algal growth rate under two different environments, with SAV and without SAV. The local growth rate of diatom and green algae is shown in Figure 3-10(a-b). The growth rates are much lower with SAV, which is mainly due to the decrease of light supply through the shades of SAV canopies (note that the nutrient is still unlimited; Figure 3-9). To reach a high concentration, phytoplankton requires a much longer residence time. Therefore, the lower flushing rate due to SAV is the main driver for the phytoplankton accumulation, even though the local growth rate is low. The accumulation of phytoplankton with SAV plays an important role on the phytoplankton blooms. In summary, both SAV and phytoplankton can coexist in the shallow water and bloom together in summer. However, the phytoplankton dynamics is different. To reach phytoplankton bloom, a high growth rate is needed to balance the high flushing without SAV. In contract, accumulation of phytoplankton due to reduced flushing plays the dominant role for phytoplankton bloom with SAV (with static feedback).

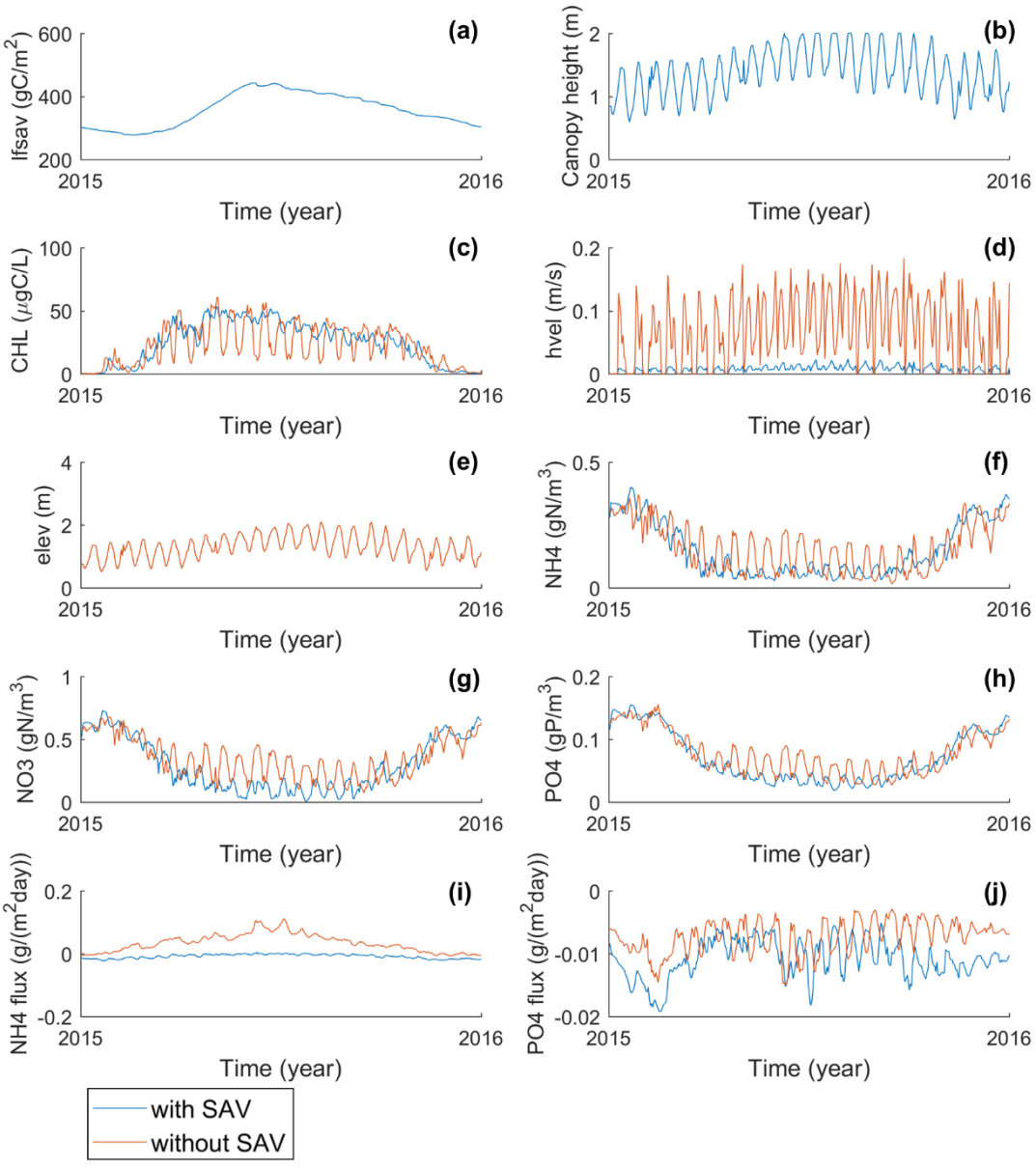
(a)
lfsav (gC/m2)
600
400
200
2015
2016
Time (year)
(b)
Canopy height (m)
2
1
0
2015
2016
Time (year)
(c)
CHL (μgC/L)
100
50
0
2015
2016
Time (year)
(d)
hvel (m/s)
0.2
0.1
0
2015
2016
Time (year)
(e)
elev (m)
4
2
0
2015
2016
Time (year)
(f)
NH4 (gN/m3)
0.5
0
2015
2016
Time (year)
(g)
NO3 (gN/m3)
1
0.5
0
2015
2016
Time (year)
(h)
PO4 (gP/m3)
0.2
0.1
0
2015
2016
Time (year)
(i)
NH4 flux (g/(m2day))
0.2
0
-0.2
2015
2016
Time (year)
(j)
PO4 flux (g/(m2day))
0
-0.01
-0.02
2015
2016
Time (year)
with SAV
without SAV

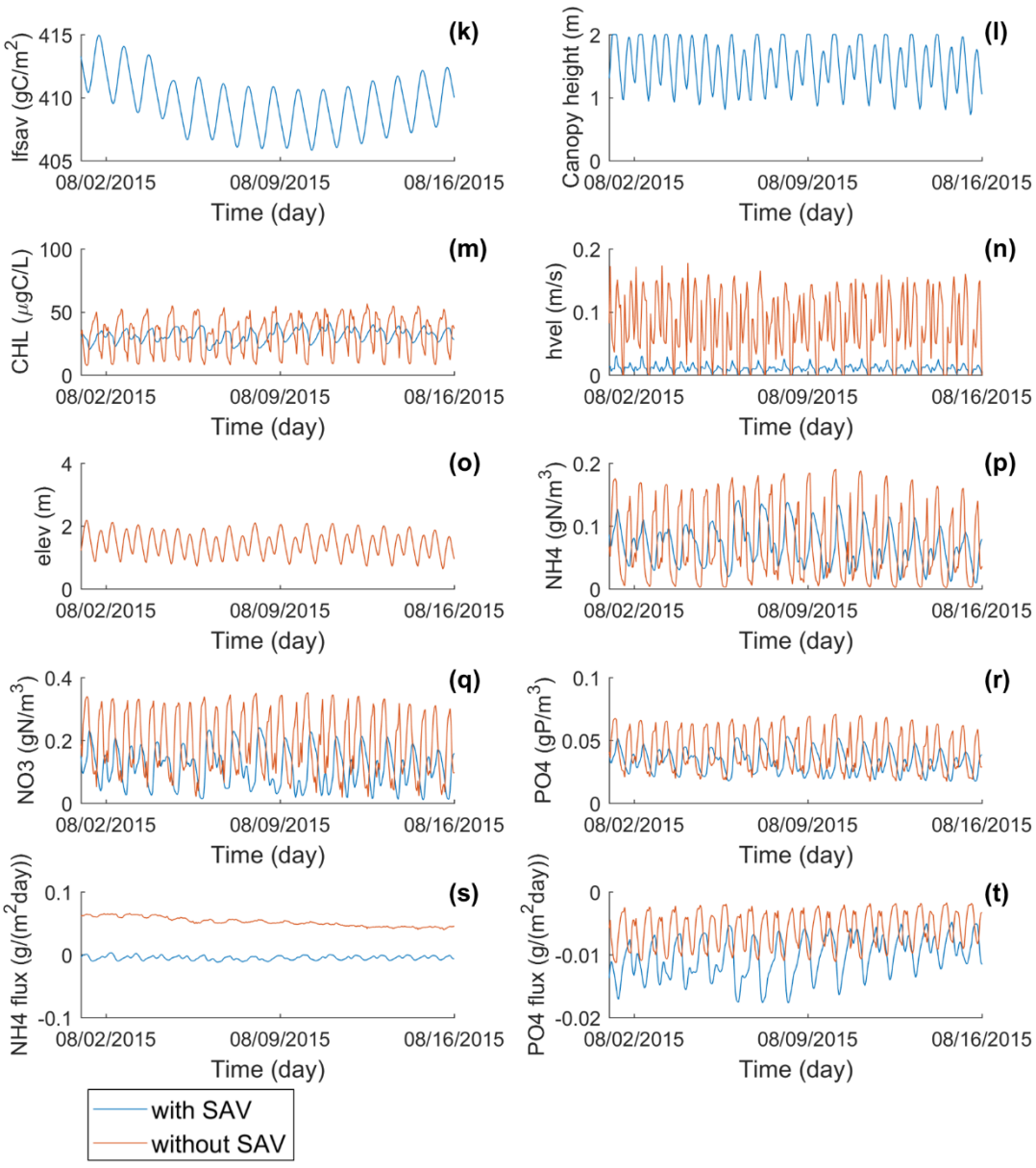

Figure 3-9: (a-j): Differences in water quality variables with and without SAV at the shoal station 10 (cf. Figure 3-6) over a year. (a-b): time series of SAV leaf biomass (stem and root biomasses are similar) and canopy height (note that the biomass is 0 without SAV). The elevation difference in (e) is very minor. (k-t): exemplary hourly time series of (a-j) for 15 days in summer.

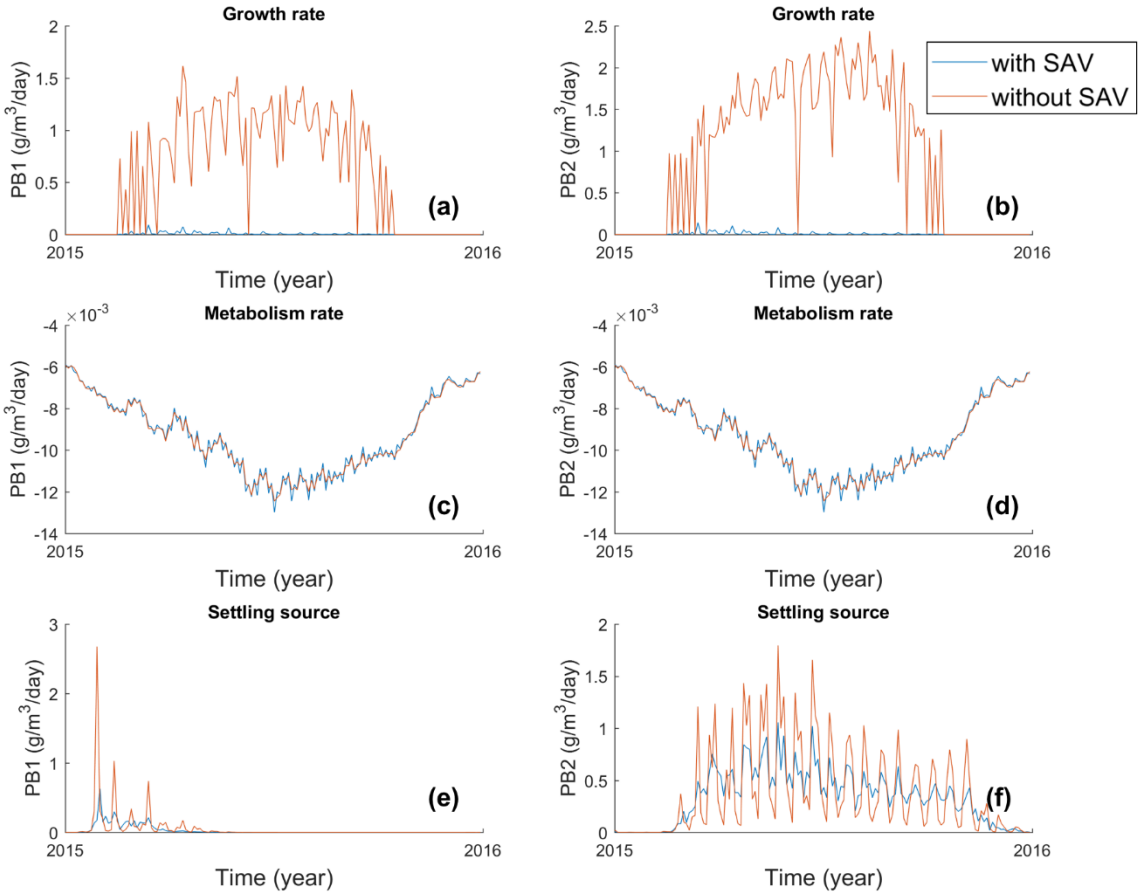

Figure 3-10: (a-b): Local growth rate of 2 groups of phytoplankton at the shoal station 10. (c-d): Local metabolism rate. (e-f): Settling source in 1m surface layer.

3.4.2.2 Pattern II: SAV Bloom in Seasonal Succession with Phytoplankton Decline in Median Depth Areas

As noted before, the biomass of SAV tends to be smaller in the median depth areas, which is confirmed by Figure 3-11(a-b). The canopy stays at a submerged level of less than 0.5m in height. In this case, SAV does not limit the light supply to the phytoplankton in the water column above the canopy. The biomass of phytoplankton tends to have different trends with or without SAV. In the presence of SAV, the phytoplankton has a higher bloom in the winter, while its concentration is lower in summer. With SAV the nutrient level is lower from winter to early spring but still unlimited for the phytoplankton

bloom, while in summer, the nutrients are used up and chlorophyll-a concentration decreases, suggesting that nutrient supply limits the growth of both SAV and phytoplankton. When nutrients are not limiting in winter, phytoplankton has a higher winter-spring bloom with SAV. The reason is the same as in the shallow water area as, i.e. due to SAV-induced accumulation, which is evidenced by the reduced velocity with SAV (Figure 3-11(d)). However, phytoplankton cannot reach its summer bloom when there is SAV due to nutrient limitation. Since SAV can uptake the nutrients directly from the sediment, the sediment flux of nutrients, which is the main mechanism for recycling inorganic nutrients in summer, decreases with the presence of SAV in these areas. As a result, SAV tends to have advantage in the competition for nutrient supplies. During fall and early winter, phytoplankton blooms again when nutrient become available with SAV included in the simulation, which is likely to be a result of the recycling of nutrients as SAV decreases.

On the tidal cycle scale, the phase lag and the reduction of flow magnitude are similar to the shoal case (Figure 3-11(n-o)). Nutrient limits the phytoplankton growth in this area as analyzed in last paragraph; however, during each diurnal cycle, there is recycling of inorganic nutrients (ammonia and phosphate) at nighttime by phytoplankton, SAV and bottom flux (Figure 3-11(p,r)). And in daytime, these recycled nutrients will be quickly used up by phytoplankton.

The differences in local kinetic processes of phytoplankton between environments with and without SAV are investigated as shown in Figure 3-12. In early Spring, the phytoplankton has a similar local growth rate with or without SAV because there is not much light or nutrient limitation caused by SAV during that period, which indicates the growth rates in both scenarios are mainly controlled by due to SAV. In summer, the growth rate of phytoplankton is much lower with SAV because of nutrient competition; while shading should not be a major factor because the canopy does not reach the surface. SAV has little influence on the metabolism rate of phytoplankton. Settling gain, which means the settling source from surface to this layer, largely correlates with the phytoplankton biomass dynamics, so there is

relatively higher settling gain during winter-spring time while it is lower during summer-fall time with SAV (Figure 3-12(e-f)).

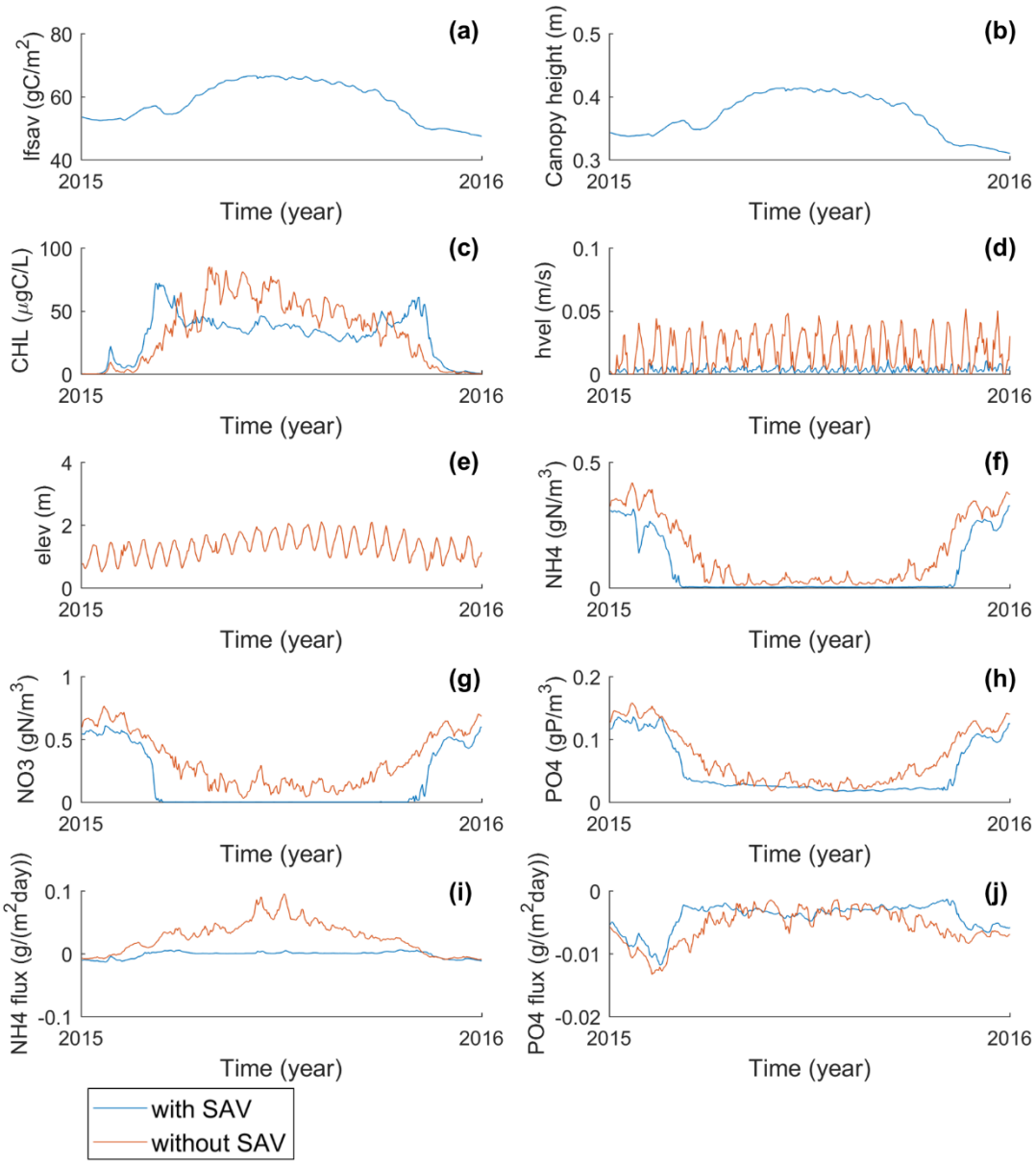

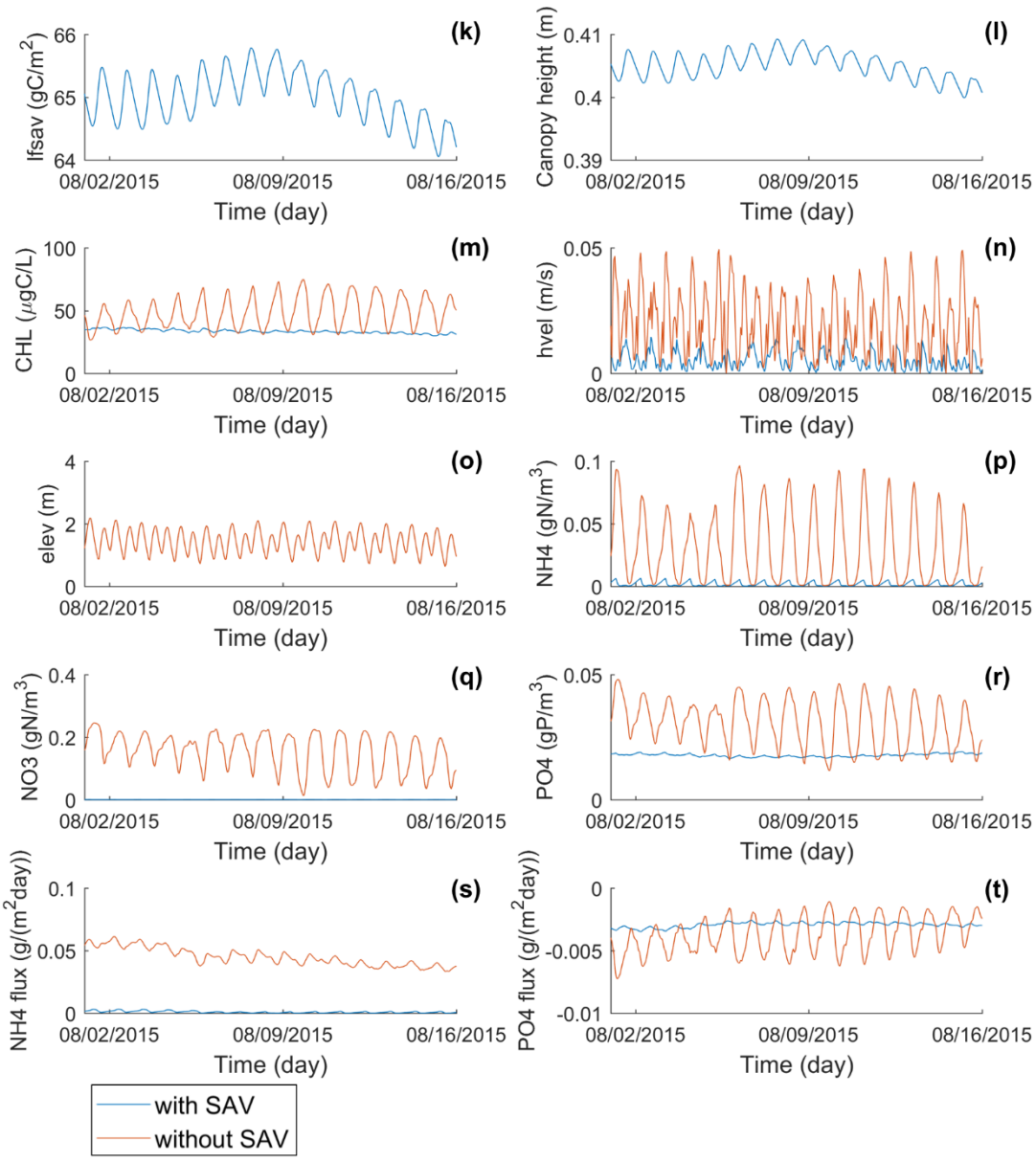

Figure 3-11: (a-j): differences in water quality variables with and without SAV at the median depth station 1 (cf. Figure 3-6). (a-b): time series of SAV leaf biomass (stem and root biomasses are similar) and canopy height (note that the biomass is 0 without SAV). (k-t): hourly time series of (a-j) for 15 days in summer.

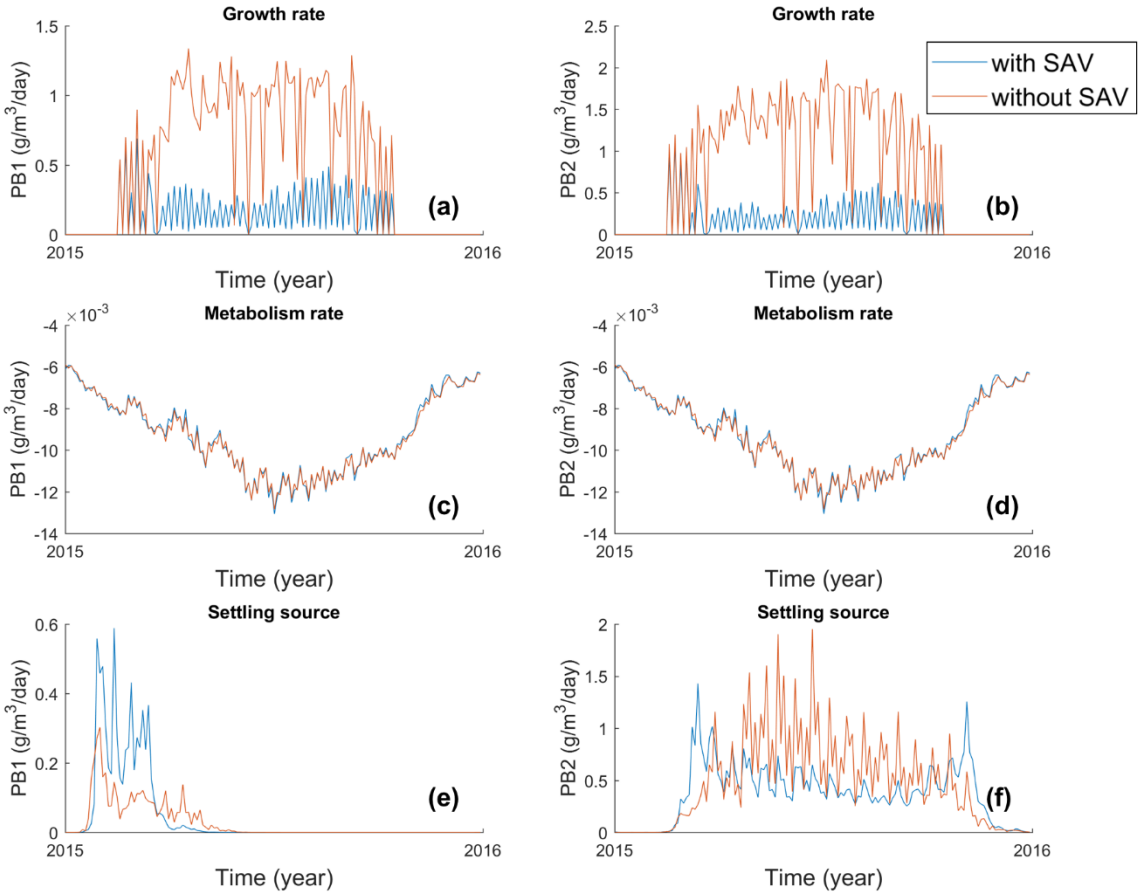

Figure 3-12: (a-b): Local growth rate of 2 groups of phytoplankton at the median depth station 1. (c-d): Local metabolism rate. (e-f): Settling source in 1m surface layer.

3.4.2.3 Pattern III: Non SAV Survival in Deep Channel Areas

Overall the SAV impact is rather minor in this area because SAV cannot survive in deep channels due to light limitation (Figure 3-13(a-b)). There is a small decrease in the phytoplankton concentration. The flow velocity, on the other hand, is larger in channels with SAV, as the presence of SAV in other areas effectively channelizes the flow (Zhang et al., submitted). Larger tidal flushing with SAV, as well as horizontal advection, is responsible for the minor decrease in the phytoplankton biomass. There is a slight increase of nutrients when SAV is removed because the SAV in surrounding areas consumes the

nutrients. The changes are much smaller than those at the other 2 areas, at either seasonal or tidal cycle scales (Figure 3-13(k-t)).

Not surprisingly, phytoplankton has similar growth/decay rates in cases with or without SAV because locally there is little or no SAV (Figure 3-14). SAV exerts its impact on these variables mainly through its effects on the hydrodynamics or through an indirect effect in the neighboring areas. For example, the local net growth rates show some differences in the case with SAV because of changes in the flow pattern, which in turn changes the light and nutrient supplies.

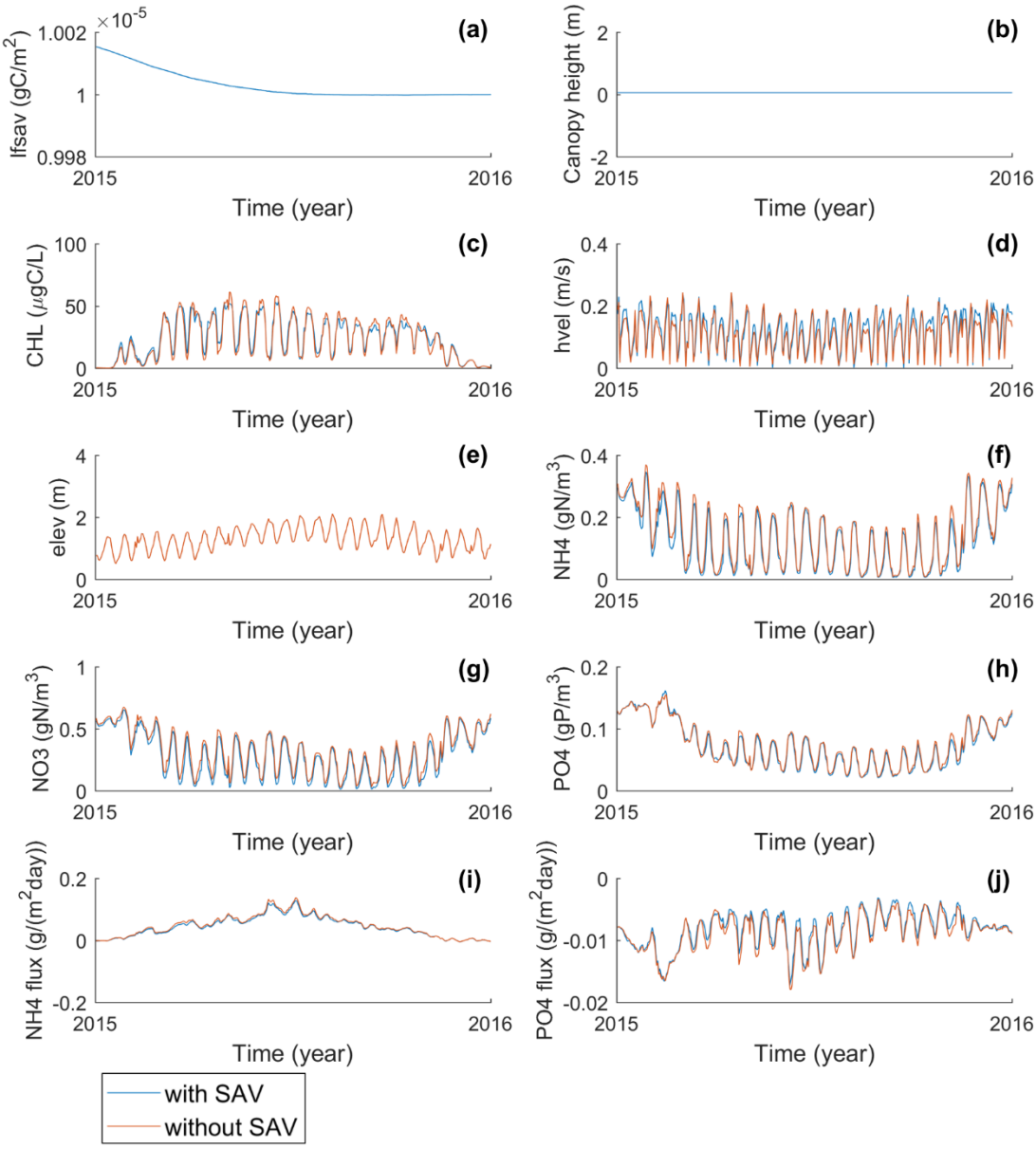
(a)
lfsav (gC/m2)
×10-5
1.002
1
0.998
2015
2016
Time (year)
(b)
Canopy height (m)
2
0
-2
2015
2016
Time (year)
(c)
CHL (μgC/L)
100
50
0
2015
2016
Time (year)
(d)
hvel (m/s)
0.4
0.2
0
2015
2016
Time (year)
(e)
elev (m)
4
2
0
2015
2016
Time (year)
(f)
NH4 (gN/m3)
0.4
0.2
0
2015
2016
Time (year)
(g)
NO3 (gN/m3)
1
0.5
0
2015
2016
Time (year)
(h)
PO4 (gP/m3)
0.2
0.1
0
2015
2016
Time (year)
(i)
NH4 flux (g/(m2day))
0.2
0
-0.2
2015
2016
Time (year)
(j)
PO4 flux (g/(m2day))
0
-0.01
-0.02
2015
2016
Time (year)
with SAV
without SAV

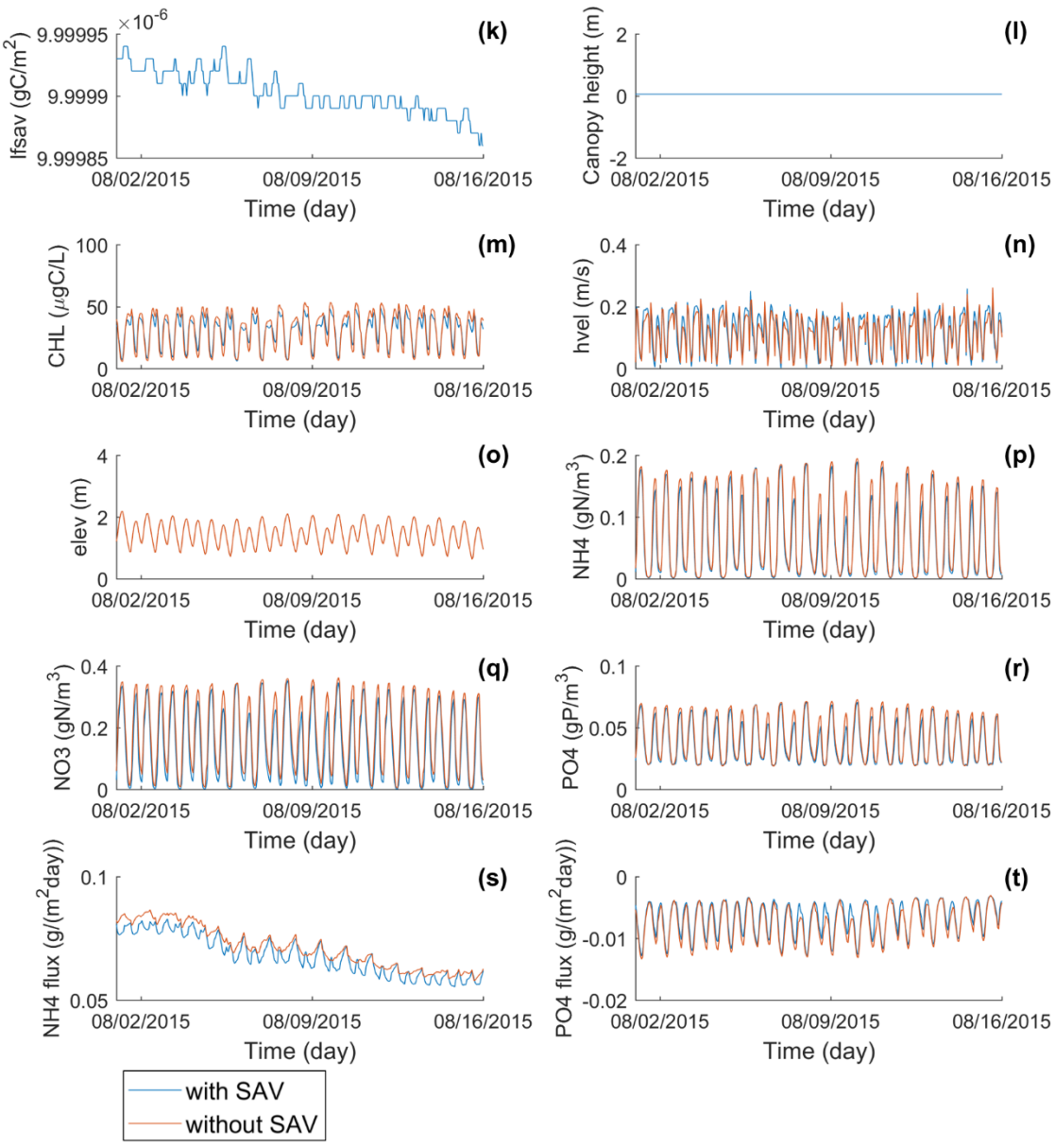

Figure 3-13: (a-j): differences in water quality variables with and without SAV at the channel station 13 (cf. Figure 3-6). (a-b): time series of SAV leaf biomass (stem and root biomasses are similar) and canopy height (note that the biomass is 0 without SAV). (k-t): hourly time series of (a-j) for 15 days in summer.

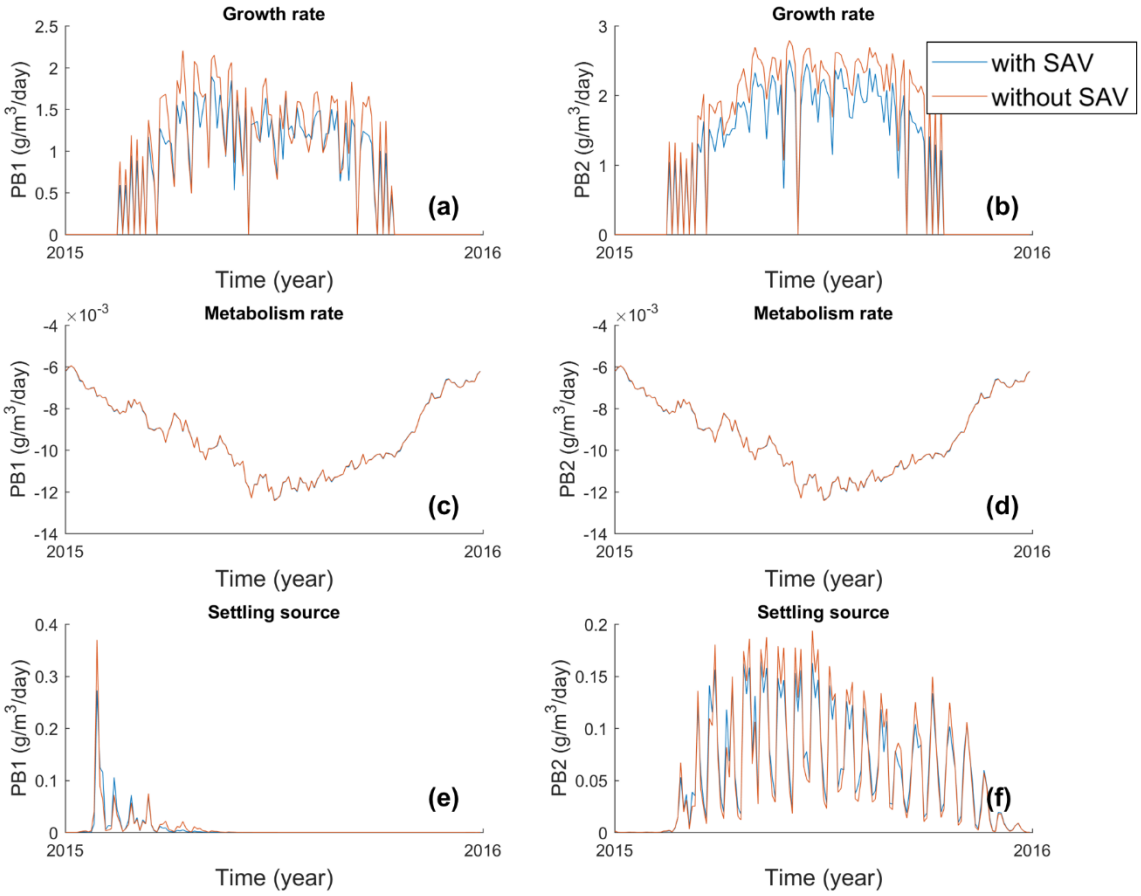

Figure 3-14: (a-b): Local growth rate of 2 groups of phytoplankton at the channel station 13. (c-d): Local metabolism rate. (e-f): Settling source in 1m surface layer.

3.4.3 SAV-Driven Effects on Biological Processes of Dissolved Oxygen and Nutrients

The biological impact of SAV on the nutrients and oxygen is not only from direct photosynthesis and respiration of SAV itself, but also from indirect effects on phytoplankton dynamics. Both change the oxygen concentration and the nutrient budget through photosynthesis and respiration (Figure 3-15). Also, changes in dissolved oxygen can affect some kinetic processes of nutrients, such as nitrification, but this effect is expected to be minor. Overall, DO budget is relatively stable because of the reaeration and vertical mixing in this relatively shallow water system. The removal of SAV does not result in a decrease or increase of DO or nutrient budgets everywhere during the simulation period because both biological

processes and physical advection effect the budgets. By comparing the simulation results with and without SAV for each biological process and its contribution to nutrient and DO budget, we can diagnose processes that receive the most impact from SAV. As in Section 3.4.2, this analysis is also conducted at selected representative stations in each of the three areas. Both DO and ammonia are chosen for the analysis. We plot the components of each process and compare the difference between the model results with and without SAV. As there is no SAV survival in the deep channel area (Figure 3-13), the changes in DO and nutrient budgets are minor, therefore, changes in the deep channel are not discussed further.

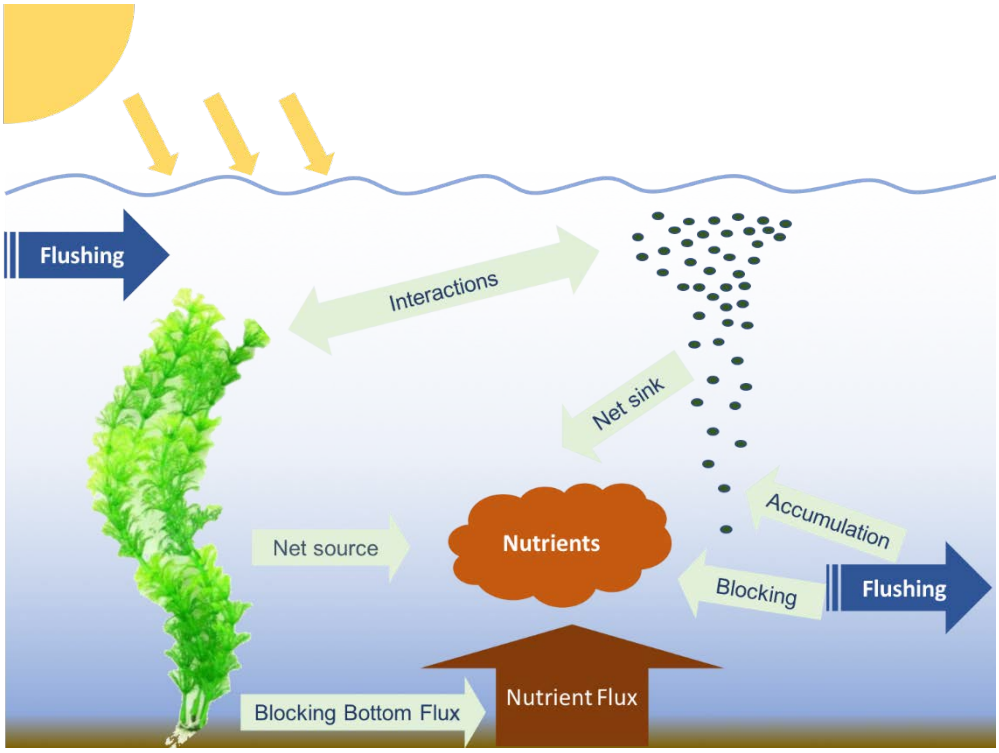

Figure 3-15: Local biological processes of nutrient budget.

3.4.3.1 Shoal Area

Because of high primary production of SAV, DO is supersaturated in this area for most of the time as shown in Figure 3-16(a). Among the kinetic components of DO, SAV is a large producer of oxygen, and the magnitude of its net oxygen production (Figure 3-16(f)) is three times larger than the phytoplankton production without SAV (Figure 3-16(b)). Net oxygen production by phytoplankton with

SAV is almost negligible due to its lower local growth rate. There is more oxygen consumption used for DOC mineralization as there is more DOC produced with SAV. Although SAV is a net producer of oxygen, it also induces large SOD via its root metabolism. However, there is no large change in DO level, which is dominated by aeration.

Using ammonia budget as an example of nutrient dynamics, we see that SAV alters the source or sink for the budget (Figure 3-17). SAV does not change the ammonia source from predation much as in Figure 3-17(b). The direct impact from SAV photosynthesis and metabolism can give ammonia a net positive/increasing rate in the water column, i.e. SAV transfers ammonia from sediment to the water column (Figure 3-17(f)). The reduction of sediment flux by SAV is one of the most important pathways through which SAV effects the nutrient budget; it generally blocks the source of ammonia from the sediment flux. Because SAV changes the phytoplankton growth dynamics through the shading effect, the net uptake rate of ammonia by phytoplankton is reduced. Overall, the amount of ammonia is on the same order in the water column with or without SAV, but the amplitude of variation is reduced with SAV.

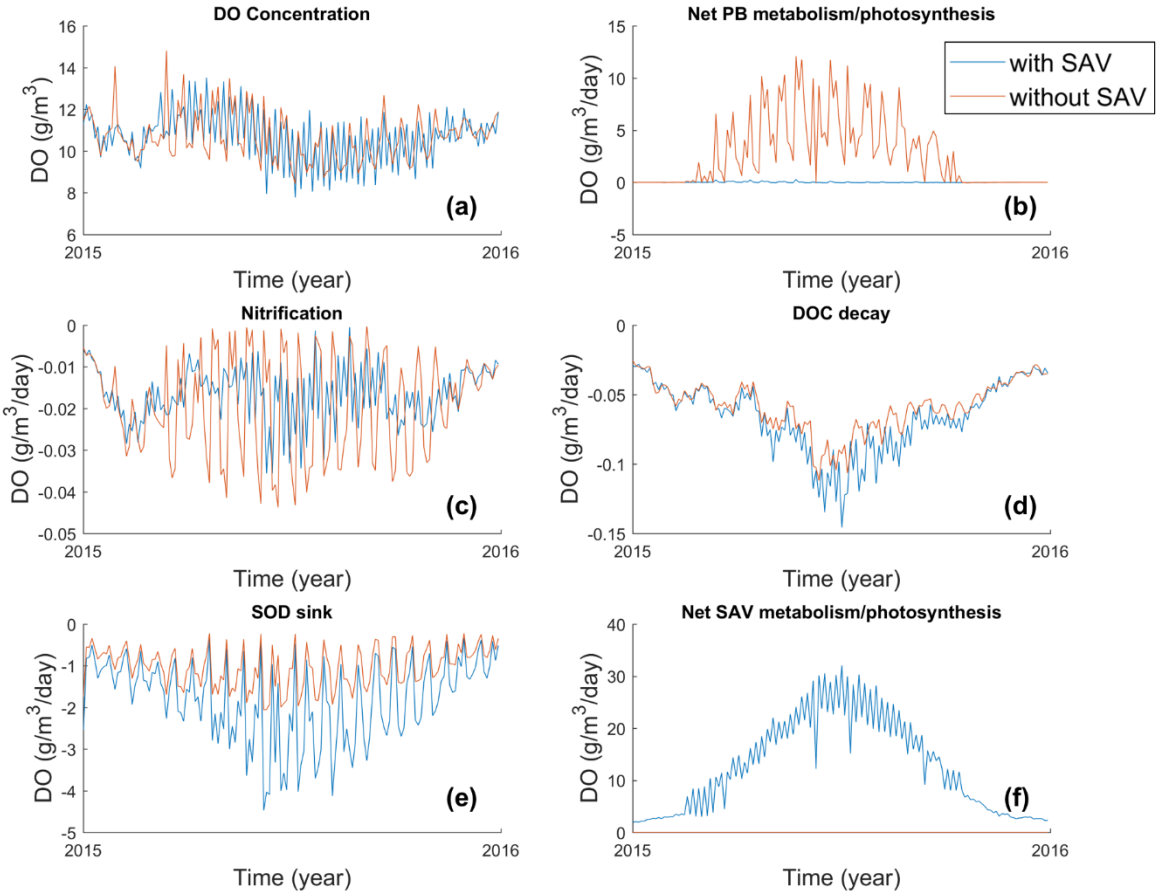

Figure 3-16: Impact of SAV on total DO and individual process for oxygen budget at the shoal station 10. (a): Time series of dissolved oxygen concentration. (b, f): Local net oxygen source from phytoplankton and SAV, where the DO production of photosynthesis minus the consumption of metabolism. (c, d): local DO consumption on nitrification and DOC decay. (e): local DO consumption rate on the transfer to sediment oxygen demand.

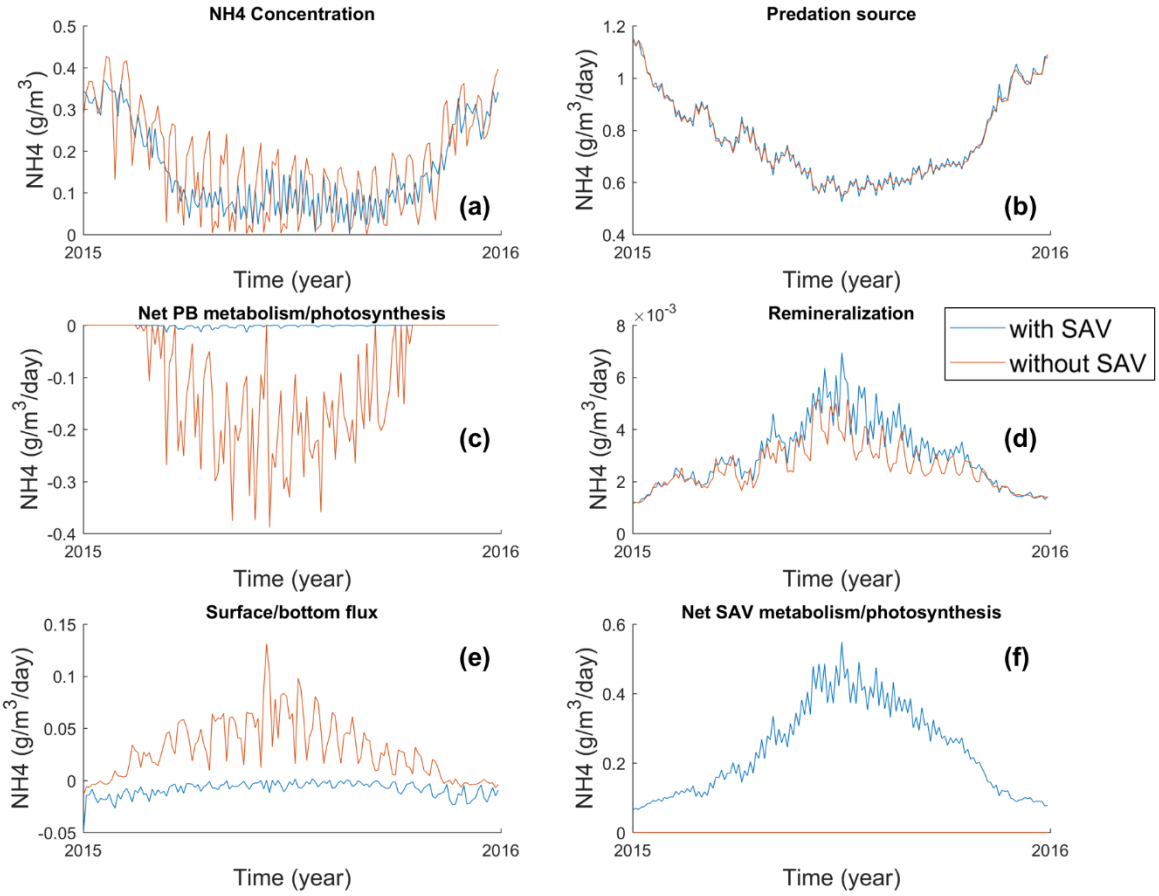

Figure 3-17: Impact of SAV on ammonia and individual processes of ammonia budget at the shoal station 10. (a): Time series of ammonia concentration. (b, d, e): Local ammonia source from predation, remineralization and surface/bottom flux. (c, f): Local net ammonia source/sink from phytoplankton and SAV, where the ammonia release of metabolisms minus the consumption of photosynthesis.

3.4.3.2 Median Depth Area

At 1m below the surface, even though SAV produces a large portion of oxygen, the oxygen concentration decreases in summer because the net oxygen production from phytoplankton is lower with SAV (Figure 3-18). The decrease of DO consumption due to the nitrification process is consistent with the reduced available ammonia in the water column (Figure 3-19(c)). In addition, as SAV produces more organic matter, the oxygen consumption due to DOC decay increases a little with SAV. However, there is

not a large change of SOD compared to shallow areas. The winter dissolved oxygen concentration becomes higher with SAV along with the high phytoplankton bloom when nutrient is available.

Besides the net release of ammonia from SAV in the water column (Figure 3-19(f)), SAV reduces sediment flux of ammonia through direct uptake of ammonia in the sediment (Figure 3-19(e)). The lower phytoplankton biomass and decreased local growth in summer reduces the ammonia uptake by phytoplankton. The mineralization of increasing organic nitrogen results in an increase of ammonia in water column with SAV (Figure 3-19(d)). Overall, the ammonia is limited in spring to fall with SAV (Figure 3-19(a)). The ammonia concentration in water column drops to almost zero in spring, it limits the local growth of phytoplankton. Although SAV transfers ammonia from bottom sediment to water column due to decay, the recycled ammonia will be consumed by phytoplankton immediately, resulting in almost zero concentration starting in late spring.

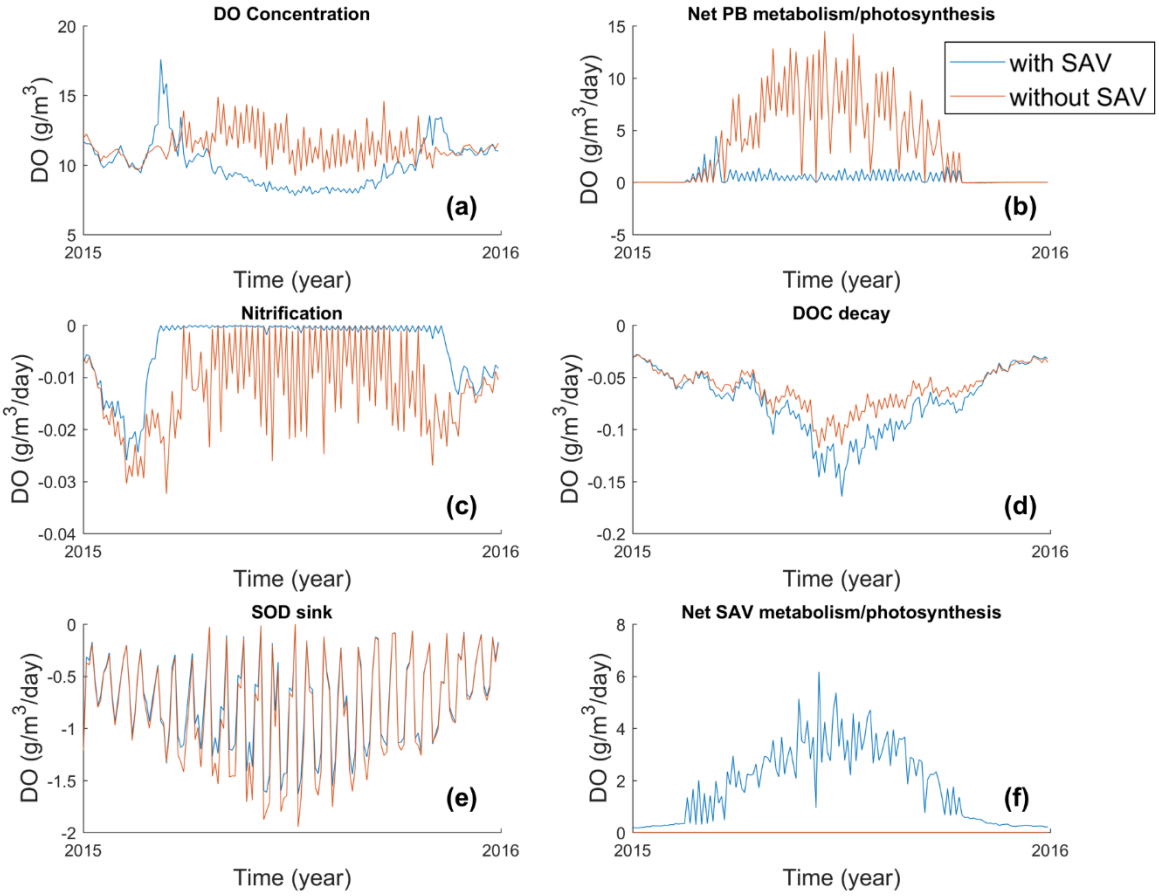

Figure 3-18: Impact of SAV on total DO and individual process for oxygen budget at the median depth station 1. (a): Time series of dissolved oxygen concentration. (b, f): Local net oxygen source from phytoplankton and SAV, where the DO production of photosynthesis minus the consumption of metabolism. (c, d): local DO consumption on nitrification and DOC decay. (e): local DO consumption rate on the transfer to sediment oxygen demand.

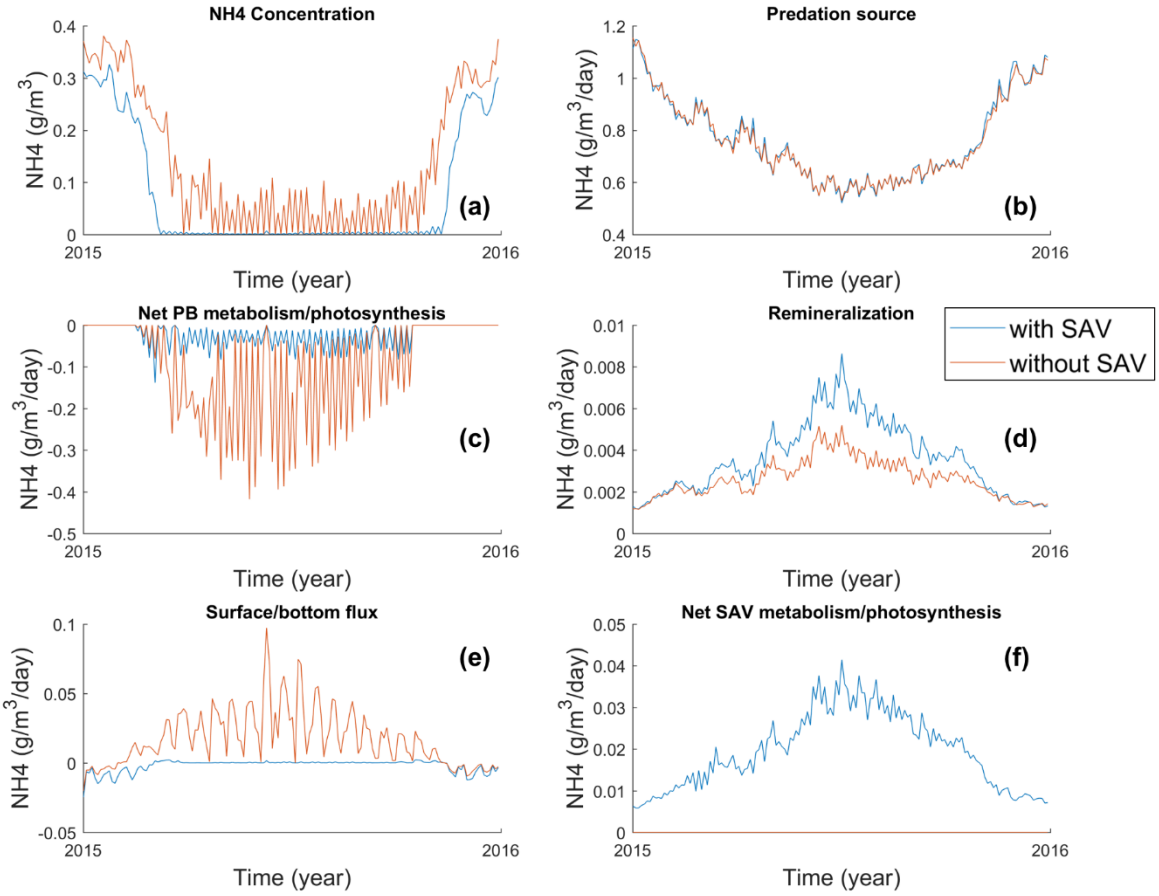

Figure 3-19: Impact of SAV on ammonia and individual processes of ammonia budget at the median depth station 1. (a): Time series of ammonia concentration. (b, d, e): Local ammonia source from predation, remineralization and surface/bottom flux. (c, f): Local net ammonia source/sink from phytoplankton and SAV, where the ammonia release of metabolisms minus the consumption of photosynthesis.

3.4.4 SAV Feedback to Hydrodynamics and Subsequent Feedback to Water Quality

3.4.4.1 SAV Impacts on Flow Patterns

Previous SAV modeling work did not consider the impact of SAV and SAV density on hydrodynamics. As SAV density increases and becomes taller, the increase of friction can alter the dynamic field and change local flushing and residence time. During model development, the SAV module was developed individually: SAV impacts on hydrodynamics and water quality through ecological

interactions are considered separately first. Then changes of SAV biomass and canopy height are coupled to the hydrodynamic model to account for the feedback of SAV to the hydrodynamics and feedback of resultant flow on the ecological model. Two sensitivity tests of feedbacks were conducted: one is a static feedback and the other is dynamic feedback. With the static feedback, the canopy height, SAV stem diameter and density are fixed in the hydrodynamics calculation. With the dynamic feedback, the canopy height simulated in the SAV model is passed on to the hydrodynamic model (SAV density remains unchanged), which could further improve the simulation on the seasonal scale.

Up until now, the data support for the calibration of SAV biomass simulation or the feedback function is not sufficient and difficult to get, but comparing simulation results with and without including feedback can shed light on the underlying mechanisms and inspire future monitoring.

Four model simulations were conducted: (a) the baseline simulation without SAV, (b) simulation with SAV with no feedback on hydrodynamics, (c) simulation with SAV with static feedback, and (d) simulation with SAV and dynamic feedback. Figure 3-20 shows the depth-averaged horizontal velocity magnitude and directions for both flood tide and ebb tide for scenarios (a,c,d); note that (a) and (b) have the same flow patterns as SAV has no impact on hydrodynamics. It is obvious that in both runs with SAV, the SAV alter flow distribution. Strong currents are focused into a narrow region and velocities decrease in shallow area. But the current with dynamic feedback is slightly weaker than that with static feedback. With static feedback, the canopy height (a constant 0.8m) increases friction in the hydrodynamics part, and the impact of feedback is higher than most areas in the SAV beds for the dynamic feedback except for the northern part of the region located on the western side of the channel according to the simulation. The dynamic feedback results in a weaker channelized flow on the eastern side of the channel whereas distinguished low flow region is formed on the western side because of the huge SAV biomass there.

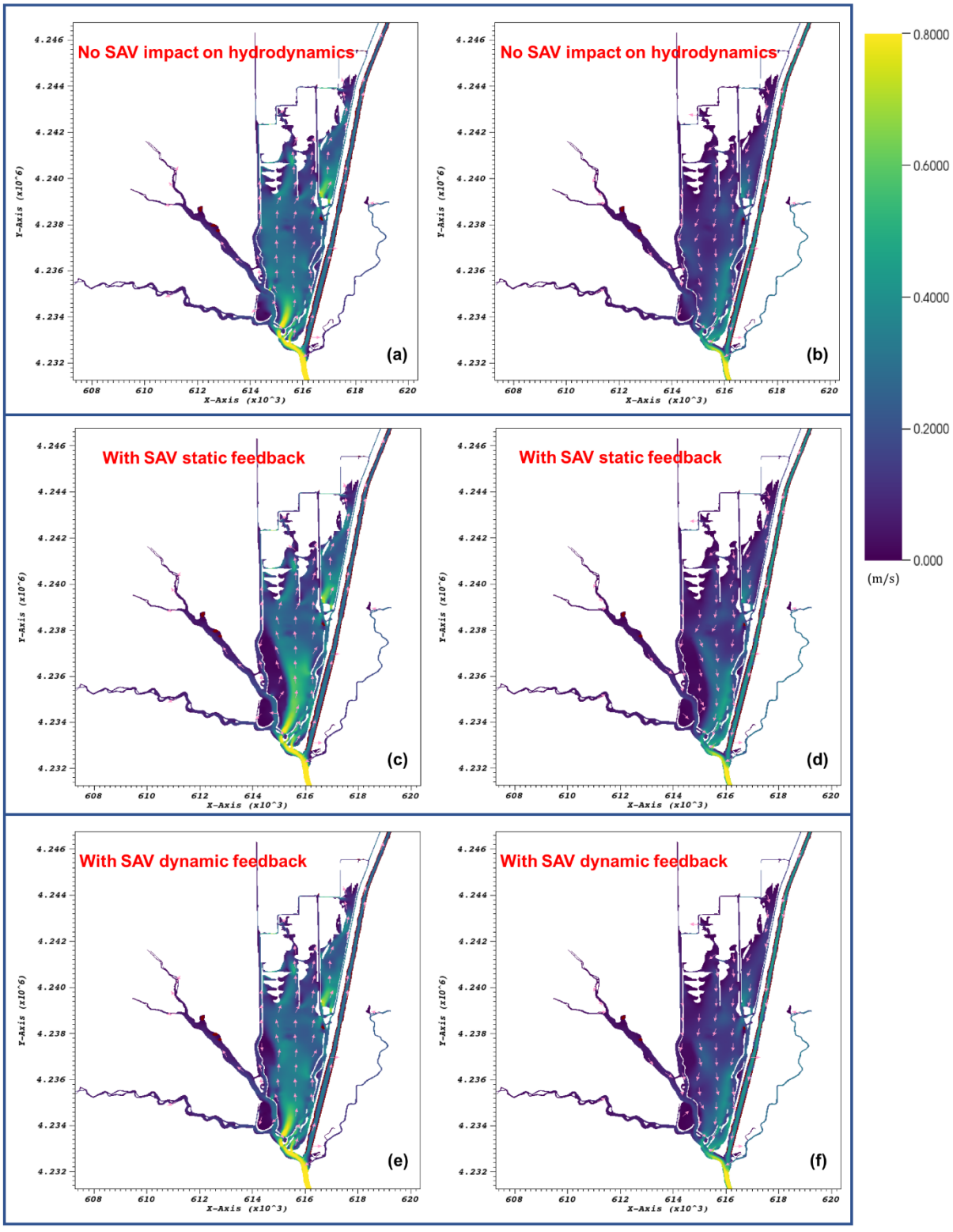
No SAV impact on hydrodynamics
No SAV impact on hydrodynamics
With SAV static feedback
With SAV static feedback
With SAV dynamic feedback
With SAV dynamic feedback
(a)
(b)
(c)
(d)
(e)
(f)
Y-Axis (x10^6)
X-Axis (x10^3)
0.8000
0.6000
0.4000
0.2000
0.000
(m/s)

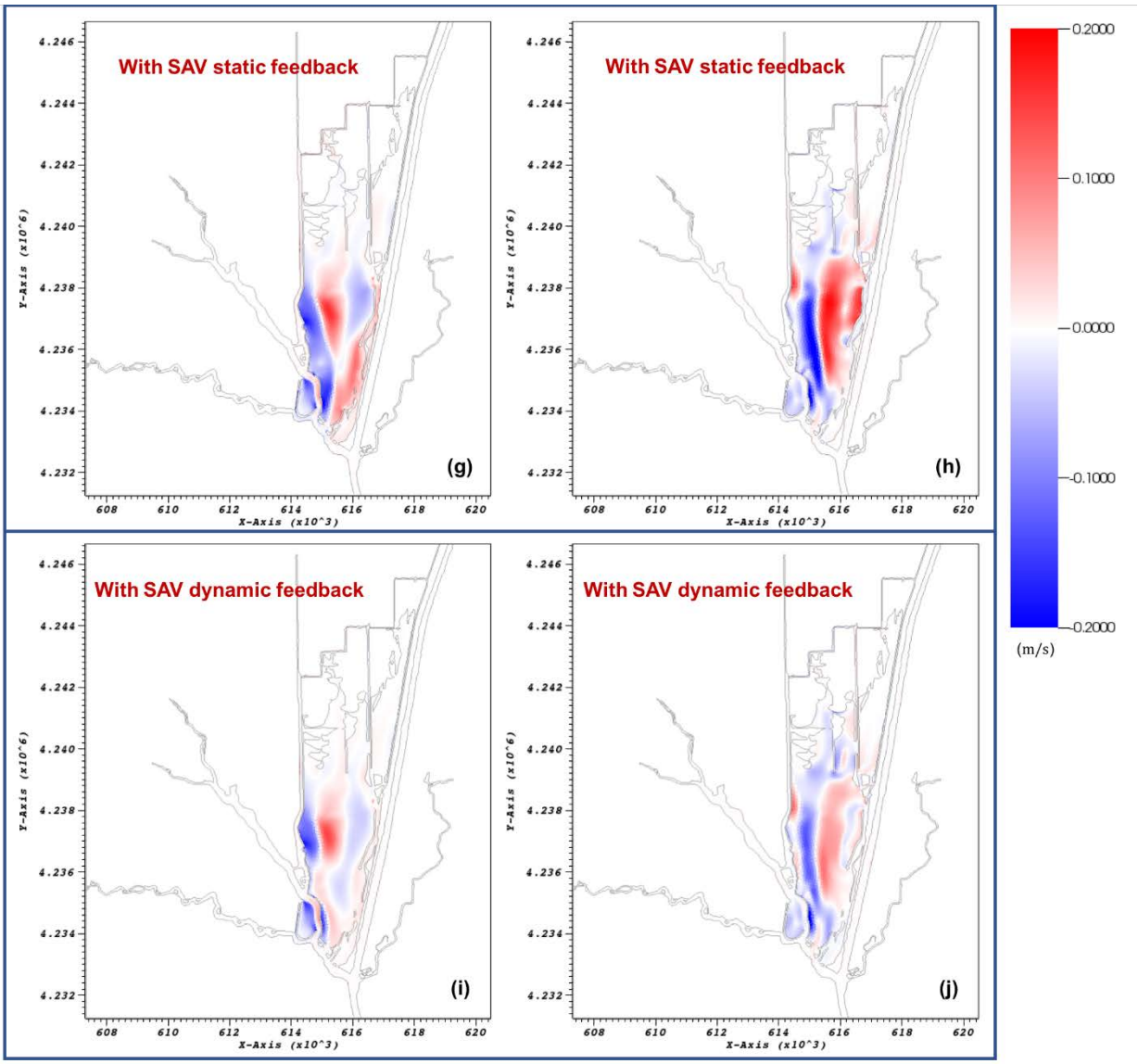

Figure 3-20: Flood (a, c, e) and ebb (b, d, f) patterns from results of no-SAV, with SAV static feedback, with SAV dynamic feedback at 12 a.m. on Jun 30, 2015 and Jul 5, 2015. (g, h): flow magnitude difference between (c, d) and (a, b), etc. c-a and d-b. (i, j): flow magnitude difference between (e, f) and (a, b)

3.4.4.2 SAV Biomass Response to SAV with Feedback to Hydrodynamics

As the dynamic feedback of SAV heights to hydrodynamics changes the flow pattern, it made some difference to the entire aquatic system. Comparing the SAV biomass distribution in the middle of the year, SAV biomass was larger overall when feedback to hydrodynamics was considered in Figure 3-

21. This was found to be caused by a number of factors; for example, the different flow patterns changed the nutrient distribution and this in turn changed the growth patterns of SAV in ways that depended on water depth. More discussion will be conducted in the following sections.

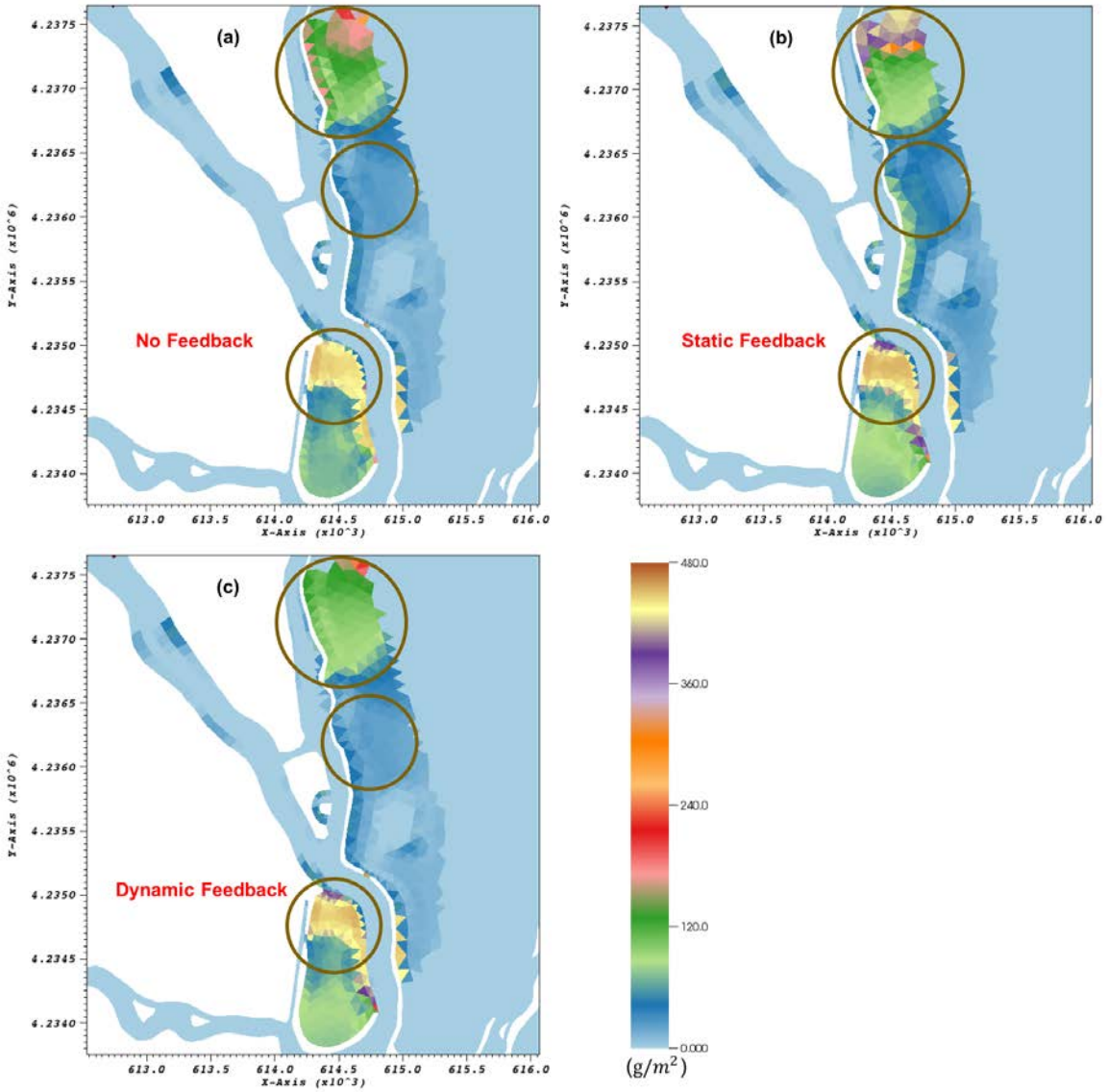

Figure 3-21: SAV biomass distributions on Jun 29, 2015 during summer bloom from the results of no SAV impact on hydrodynamics, with SAV static feedback, and with SAV dynamic feedback.

3.4.4.3 Importance of SAV Feedback to Hydrodynamics for Ecosystem Components

To study the importance of SAV feedback to hydrodynamic and its impacts to water quality, two scenarios are investigated. The first is that of no feedback from SAV to hydrodynamics (Figure 3-22) and the second has a static feedback with constant SAV height, density transferred to hydrodynamics.

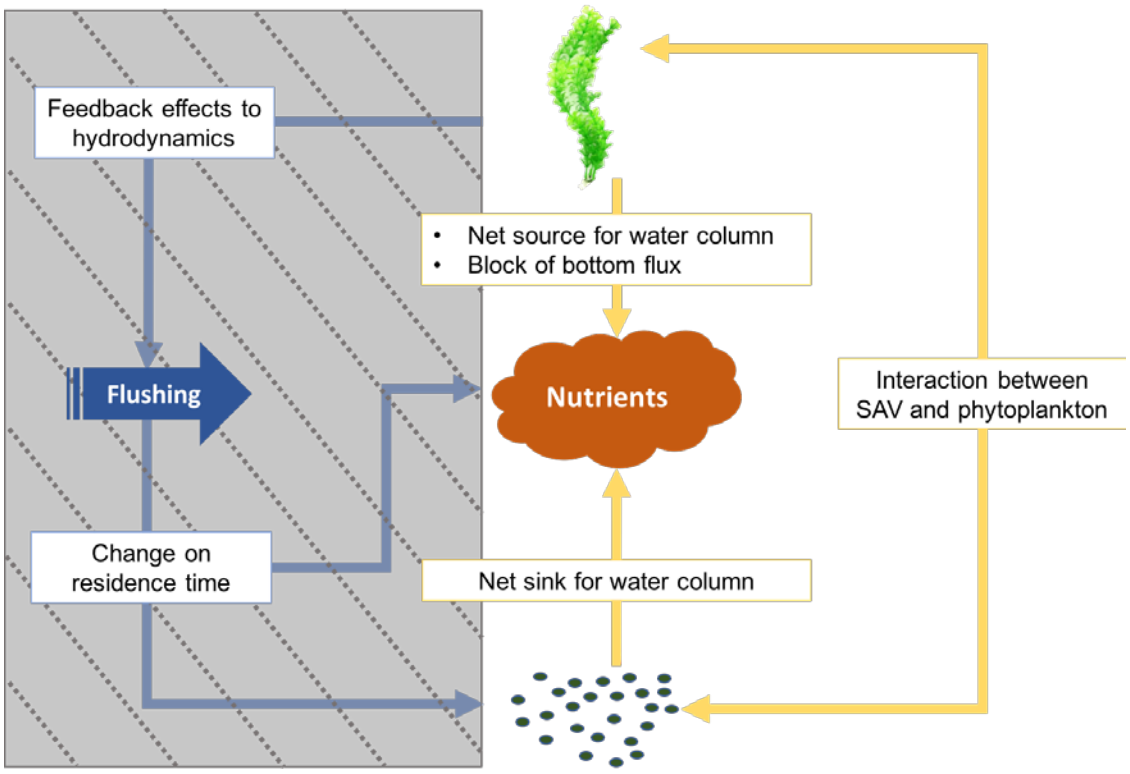

Figure 3-22: Local system with and without feedback from SAV to hydrodynamics. In the case of no feedback, the left subsystem with gray hatching is turned off.

The annually averaged differences made by SAV to chlorophyll-a, dissolved oxygen, and ammonia in the two scenarios are shown in the difference maps of Figure 3-23. Without feedback, SAV tends to decrease the chlorophyll-a concentration almost everywhere relative to the no-SAV case. However, the difference caused by SAV in the no feedback case is still less than 18.5% of the difference caused by SAV in the static feedback scenario (Figure 3-23(a)). In other words, the feedback effects through hydrodynamics accounts for more than 81.5% of the changes of phytoplankton. Without the accumulation caused by weak tidal flushing, the phytoplankton tends to be lower because of competition

from SAV on nutrient or light supplies, which is further analyzed in the following paragraphs. Referring to Section 3.4.2, it can be concluded that feedback effects of SAV to hydrodynamic model reduce fluxes in dense SAV region and promote phytoplankton accumulation.

In Figure 3-23(c), there tends to be an overall decrease of dissolved oxygen in most areas, but the difference is still minor – less than 21.6% of the DO difference in the static feedback scenario. The SAV beds have an even larger decrease of dissolved oxygen because of its metabolism and decay. The difference in ammonia caused by SAV in the no feedback scenario is less than 6.4% of the difference in static feedback scenario (Figure 3-23(e-f)). SAV beds tends to provide more ammonia in the no feedback run, while in the static feedback scenario, ammonia has a net decrease in the SAV beds. In conclusion, the feedback of SAV to hydrodynamics accounts for about 80% of the changes in water quality, and it can reach up to more than 90% for certain variables.

Detailed analysis on time series of the water quality state variables is presented in the following sections, and discussions focus on shoal area and median depth area. As there is no SAV in deep channels, the impact on this area is negligible. As the DO budget is dominated by reaeration for each scenario, further discussions on DO budget is also omitted.

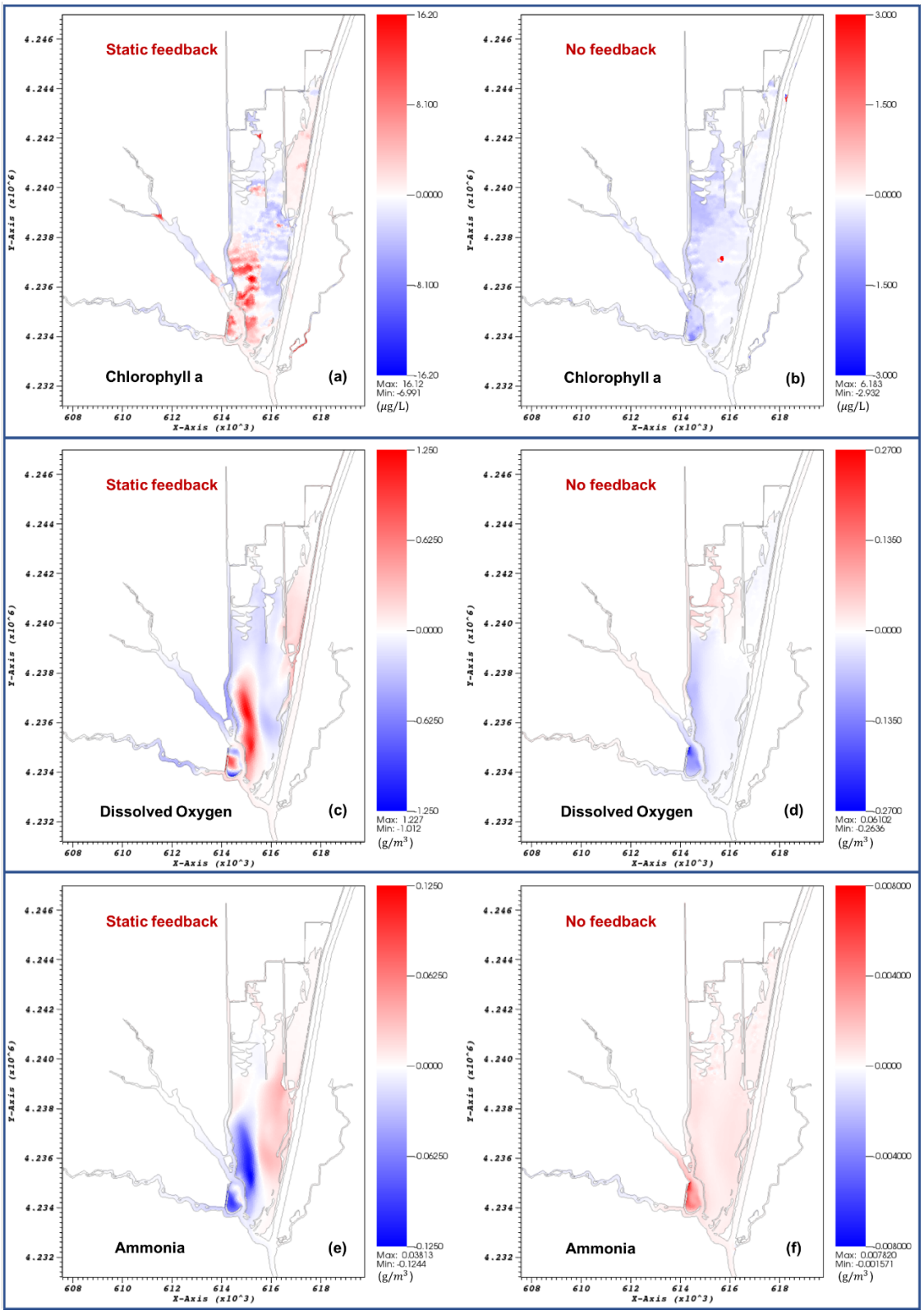

Figure 3-23: (a, c, e): Spatial distribution of averaged differences ([SAV]-[No_SAV]) caused by SAV in scenario of static feedback, (cf. Figure 3-7- (a, b, d)). (b, d, f): Spatial distribution of averaged differences ([SAV]-[No_SAV]) caused by SAV in scenario of no feedback to hydrodynamic.

In the shoal area, without SAV feedback to hydrodynamics the SAV biomass is similar to the biomass for the case with static feedback (Figure 3-24(a)). Phytoplankton biomass is similar between no SAV and with SAV but no feedback but is very different from the case of SAV with static feedback (Figure 3-24(c)); the static feedback effects on hydrodynamics directly influence the phytoplankton biomass.

The nutrients in the water column are similar between the cases of no feedback to hydrodynamics and without SAV, even though SAV decreases the bottom nutrient fluxes (Figure 3-24(i-j)). In the case of static feedback, inclusion of feedback affects the flow field so much so that it has a large impact on nutrient dynamics; the altered tidal flow tends to reduce nutrient supply resulting in decrease of nutrient concentration (Figure 3-24(f-h)).

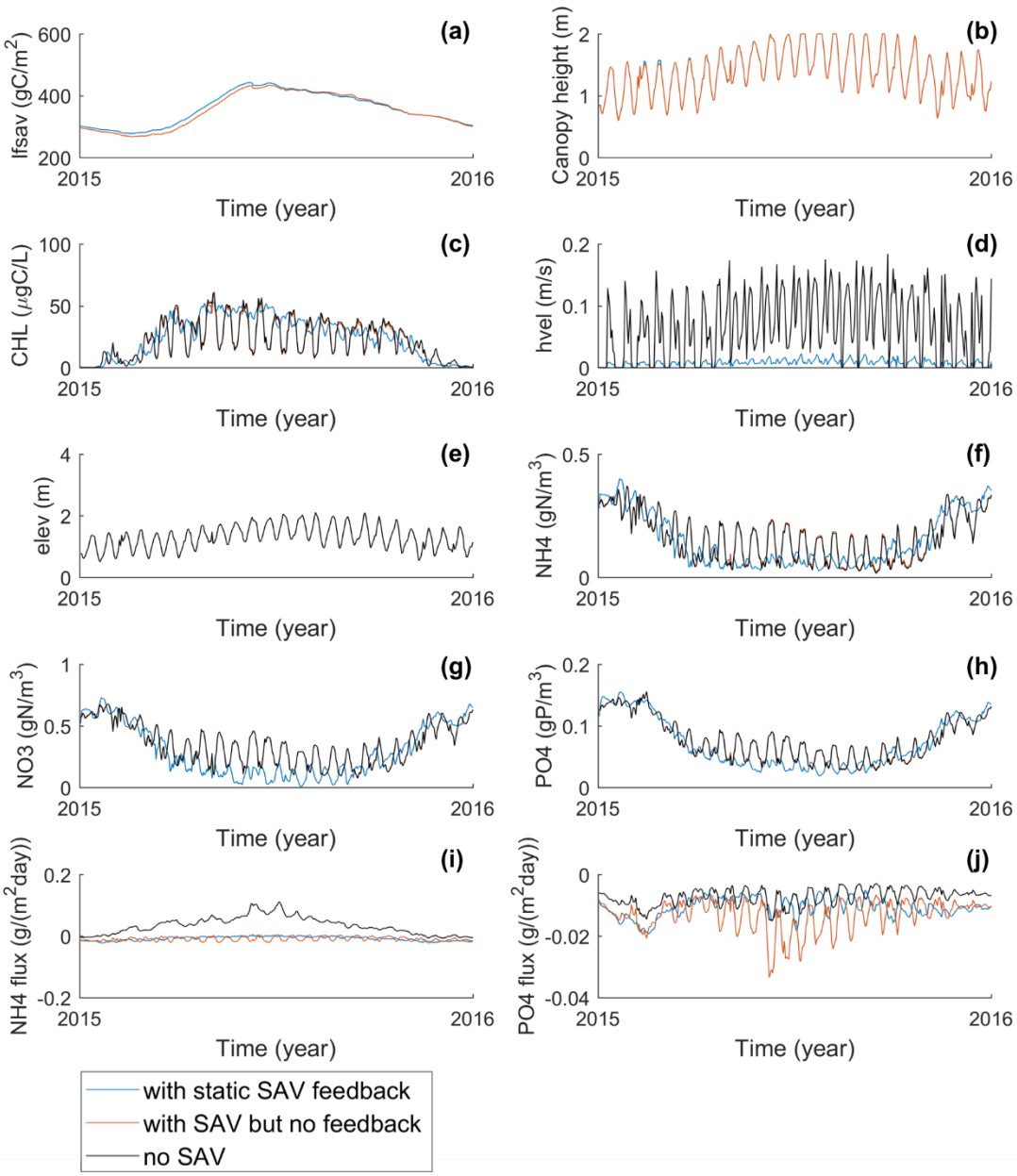

Figure 3-24: Differences in water quality variables without SAV, with SAV but no feedback and with static SAV feedback at the shoal station 10 (cf. Figure 3-6). (a-b): Time series of SAV leaf biomass (stem and root biomasses are similar) and canopy height (note that the biomass is 0 without SAV).

In median depth area, it is more complex to describe simply the effect of feedback on water quality time series. As shown in Figure 3-25, phytoplankton has a very different distribution for the scenarios with and without feedback (3-25(c)). With the static feedback, phytoplankton has a large bloom

during winter-spring period when nutrients are available while SAV biomass is still low. The reduced flushing enables the bloom to accumulate. As SAV becomes more abundant, phytoplankton has to compete with SAV nutrients, which makes the phytoplankton bloom crash in summer. As SAV biomass decreases in fall and nutrients again become available, a second phytoplankton bloom occurs. For the scenario without feedback, SAV gains more biomass and phytoplankton bloom can sustain in summer because flushing transfer more nutrient supply through advection. For both no feedback and static feedback scenarios, SAV decreased the local bottom nutrient flux to different degrees. However, different nutrient levels drive the different bloom patterns in these two scenarios.

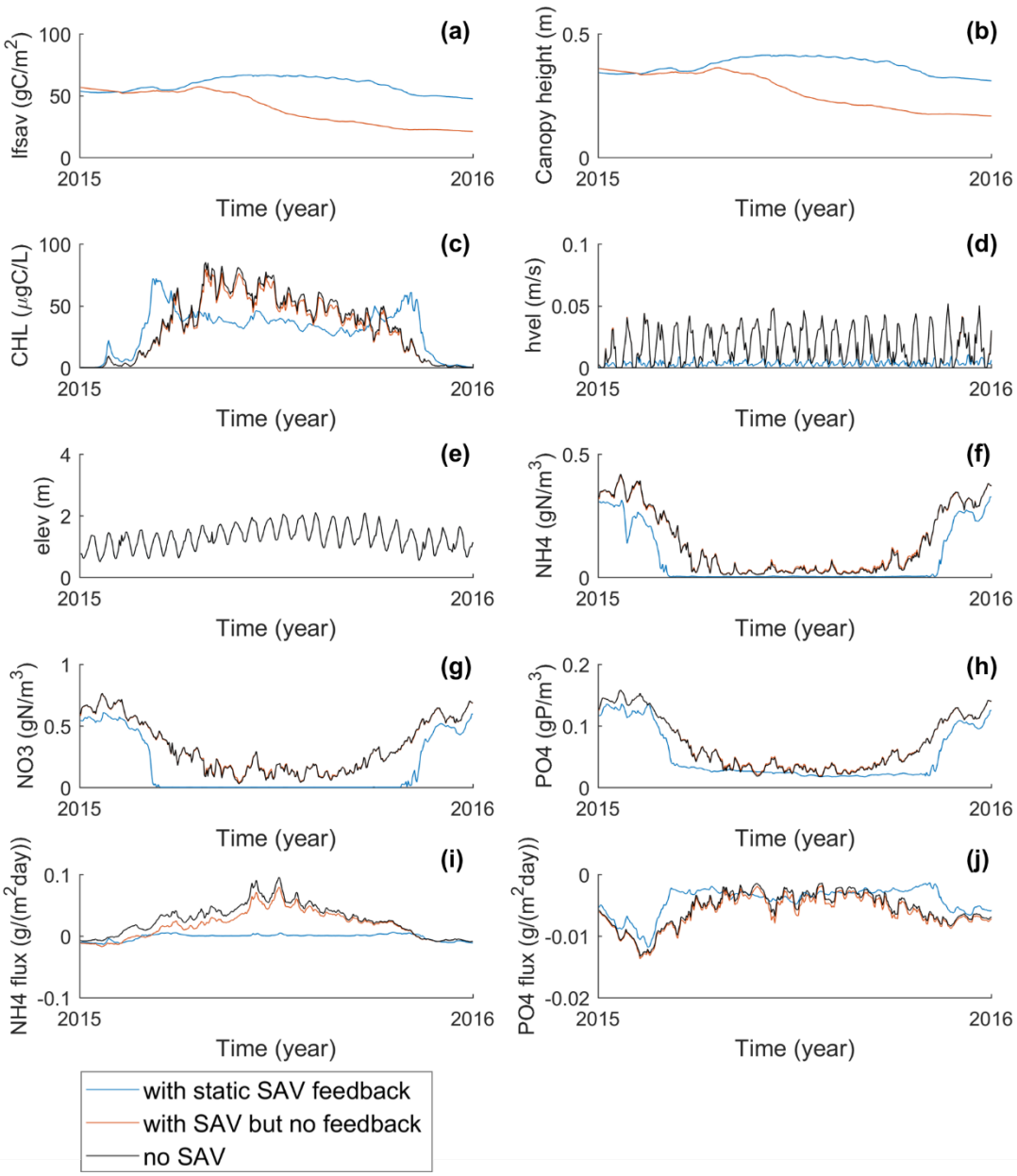

Figure 3-25: Differences in water quality variables without SAV, with SAV but no feedback and with static SAV feedback at the shoal station 10 (cf. Figure 3-6). (a-b): Time series of SAV leaf biomass (stem and root biomasses are similar) and canopy height (note that the biomass is 0 without SAV).

3.4.4.4 Sensitivity Tests for Static feedback and Dynamic Feedback

The distribution and concentration of the phytoplankton, dissolved oxygen and nutrient budgets are also different under these two scenarios – static feedback and dynamic feedback. Overall a lower impact can be seen with the dynamic feedback (Figure 3-26).

As far as the phytoplankton is concerned, increase in the phytoplankton concentration is lower on the SAV beds with the dynamic feedback than static feedback. As most of the canopy height calculated in the dynamic feedback scenario is lower than the constant 0.8m used in the static feedback scenario, the accumulation of phytoplankton due to reduced advection by tidal flushing is lower. For the dynamic feedback scenario, lower SAV and phytoplankton biomass both contributed to the lower production of dissolved oxygen and lower uptake of nutrients. Therefore, the increase in the dissolved oxygen concentration and decrease in the ammonia concentration are less over the SAV bed with the dynamic feedback than with the static feedback.

With the dynamic feedback, areas with changes of DO and nutrients are less confined. The reason for this is that, with the static feedback, the more channelization of flow makes the SAV beds more isolated to the surrounding area, while with dynamic feedback, the effect from the SAV beds tends to spread out (Figure 3-26).

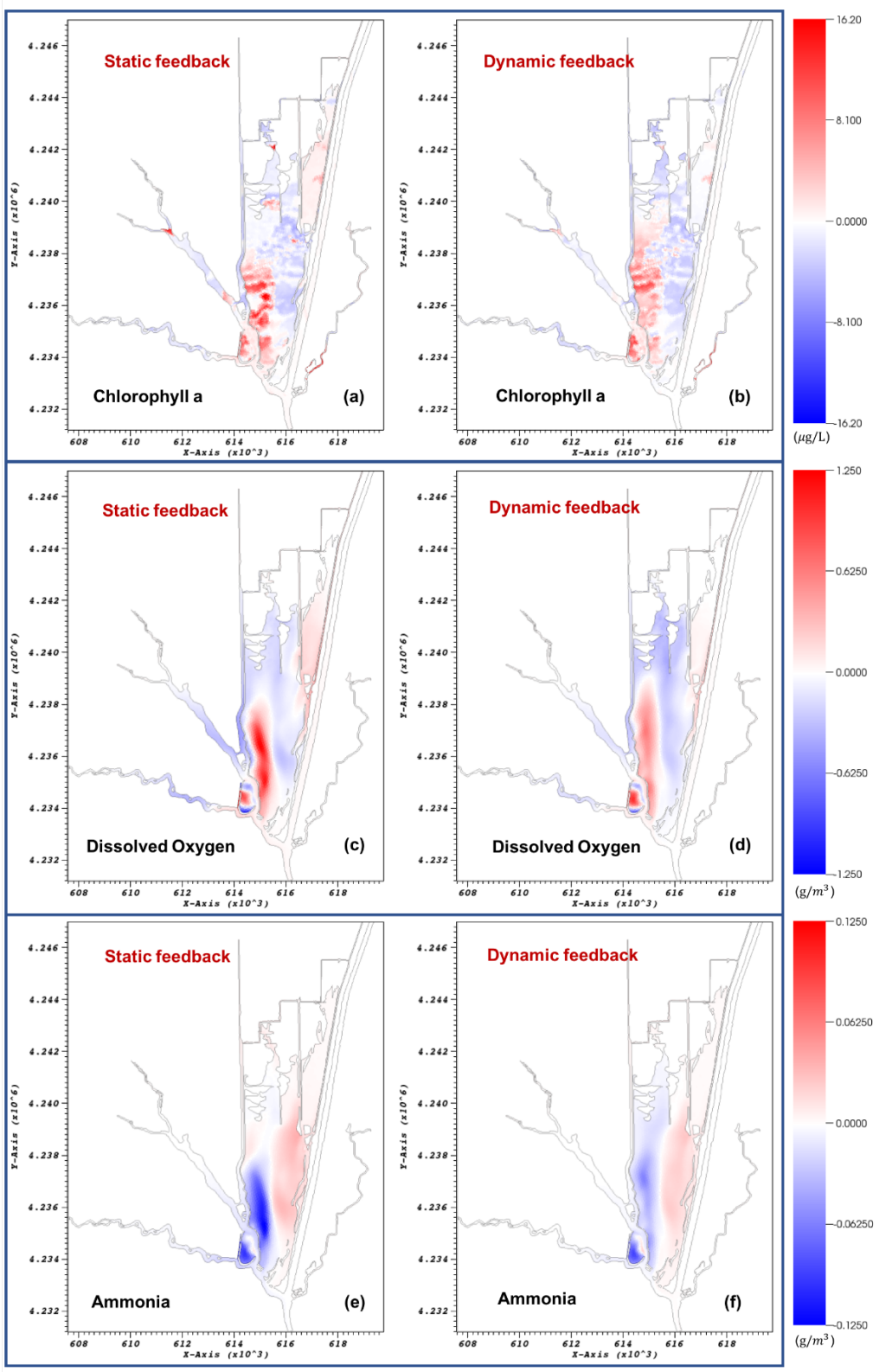

Figure 3-26: (a, c, e): Spatial distribution of averaged differences ([SAV]-[No_SAV]) caused by SAV in scenario of static feedback (cf. Figure 3-7- (a, b, d)). (b, d, f): Spatial distribution of averaged differences ([SAV]-[No_SAV]) caused by SAV in scenario of dynamic feedback to hydrodynamic.

3.5. Conclusion

We applied the new SAV model to the study of Cache Slough Complex in the Delta region of the San Francisco Bay, and validated it with observational data. The overall pattern and magnitude of chlorophyll-a, dissolved oxygen, and nutrient concentrations matched the observations reasonably well. The modeled SAV distribution was also in agreement with the observed SAV distribution, and successfully captured the uneven distribution of SAV among shoal and channel areas.

The annually averaged differences were used to study the SAV impacts on the water quality state variables (chlorophyll-a, dissolved oxygen, and nutrients). The overall pattern of differences suggests that there is an increase of phytoplankton, dissolved oxygen and organic nutrients, and a decrease of inorganic nutrients over the SAV beds. This difference was found to be due to the presence of SAV itself and the SAV-induced changes in phytoplankton biomass.

The SAV biomass tends to vary with bathymetric depth. To study the seasonal patterns of the SAV impact on the whole system, detailed analysis was conducted at representative stations along different transects associated with different depths across the SAV beds. Time series of these stations were analyzed to study the interaction between SAV and phytoplankton. The overall pattern in each area is summarized in Figure 3-27. In the shoal area, the local growth rate of phytoplankton is lower with SAV because of the shading and to a lesser extent, competition for nutrients; on the other hand, the phytoplankton biomass increases locally because of the prolonged residence time, which is caused by the reduced flow due to frictional effects of SAV as a result of feedback to hydrodynamic fields. In the median depth area, SAV outcompetes the phytoplankton for both light and nutrient supplies in summer-fall time and thus suppresses the phytoplankton growth, while during winter-spring and fall-winter, SAV enhances phytoplankton bloom due to the reduced flow with SAV and available nutrients with SAV decay. A double bloom of phytoplankton was found that exhibits a seasonal succession pattern. In deep channels, the impact on the phytoplankton is minor as SAV cannot survive there.

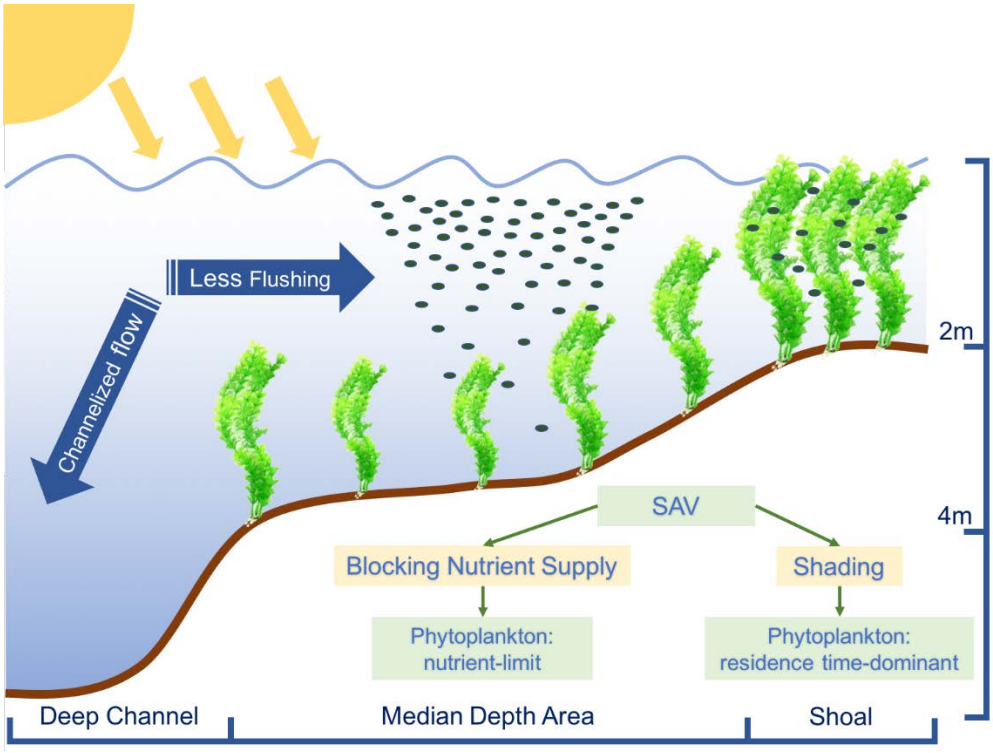

Figure 3-27: Summary of SAV-phytoplankton interaction in different water depths

Among the local kinetic processes of DO and nutrient budgets, the changes of these state variables can be directly induced by SAV or indirectly induced by phytoplankton, which is under the impact of SAV. The net production of oxygen from SAV photosynthesis and metabolism contribute a significant source to the DO budget. But DO concentration stays stable due to air-sea exchange and advection. The SAV contributes to transfer certain amount of inorganic matter to the water column as a net result of its photosynthesis and metabolism, but the magnitude of this value is at a low level. Instead, SAV changes the nutrient budgets mostly by reducing the sediment fluxes due to its advantage of taking up nutrients directly from the sediment.

The SAV impact on hydrodynamics accounts for more than 80% of the differences for the water quality state variables, including nutrients and phytoplankton. Comparing model results for scenarios without feedback and with feedbacks to the hydrodynamics, the flow pattern changes significantly. The flow is more channelized in the with-feedback scenario, while the flow velocity is reduced significantly

over the SAV bed, thus suppressing the tidal flushing. The overall SAV biomass increases with the SAV feedbacks to hydrodynamics, at the same time, it encourages the accumulation of phytoplankton biomass. However, in certain areas where water depth is relatively large, SAV can suppress the summer phytoplankton bloom by reducing nutrient source from advection and bottom flux at the same time. Furthermore, the presence and growth of SAV alters the flow pattern, which in turn can have a wide range of impacts on biochemical processes of the habitat through several complex nonlinear feedback loops. Our results highlight the importance of incorporating all of these feedback loops in a model in order to correctly account for these complex hydrodynamic and biogeochemical processes.

Chapter 4 Summary and Future Work

The major contribution of this thesis includes two parts. The first is to develop a new version of SAV model and incorporate it into the fully coupled hydrodynamic-water quality framework of SCHISM-ICM. The second part is to apply the new SAV model to the Cache Slough Complex located in the Sacramento-San Joaquin Delta in California to study potential impacts of removal of SAV on the aquatic system.

Compared with the previous efforts, the coupled SCHISM-ICM-SAV is able to directly simulate the effects of SAV on hydrodynamics by incorporating SAV-induced drag force in the momentum and turbulence equations. In addition, the new SAV model can simulate the competition between SAV and phytoplankton for light and nutrient supplies.

The new SAV model is first validated with a series of benchmark tests for SAV dynamics and impacts of SAV growth on the surrounding environment. The simulated biomass matches analytical solution well. The model can successfully simulate the die-off process of SAV where habitat is not favorable. Magnitudes of SAV-induced nutrient flux and oxygen budget agree with the change of SAV biomass, suggesting that mass conservation is achieved.

We applied the SAV model to the Cache Slough Complex domain to study the impacts of SAV removal on the ecosystem through numerical experiments. The model is validated by the comparisons with available observations. In particular, the distribution of SAV biomass matches observation well. A series of model experiments were then conducted to study the scenarios with and without SAV. Through the analysis of these model results, we can diagnose the potential influences of SAV on the ecosystem. The SAV biomass is in different magnitude in areas with different water depth. Overall, the annually averaged differences caused by SAV indicate that SAV tends to increase the concentration of phytoplankton, dissolved oxygen and organic nutrients, while decrease the inorganic nutrients over the SAV bed. SAV tends to encourage the phytoplankton accumulation by prolonging the residence time

while suppressing local primary production of the phytoplankton through competition for light and nutrient supply. The local kinetic changes on dissolved oxygen and nutrients can be directly induced by SAV itself or indirectly affected through phytoplankton. Overall, SAV is a significant oxygen producer. The blocking of sediment flux to the water column caused by SAV accounts for an important change of the nutrient budgets, which reduces the nutrient supply for phytoplankton to grow.

The SAV feedback to hydrodynamics is significant as it accounts for more than 80% of the changes of water quality state variables. Without feedback to the hydrodynamics, the difference made by SAV directly or indirectly to the water quality is mostly minor. In some cases, SAV helps to reduce the summer algae bloom to a healthier level through competition on the ecological side and also by its impact on hydrodynamics. Furthermore, the presence and growth of SAV alters the flow pattern, which in turn can have a wide range of impacts on biochemical processes of the habitat through complex nonlinear feedback loops. Our results therefore suggest the importance of incorporating all of these feedback loops in a model in order to correctly account for these complex hydrodynamic and biogeochemical processes.

In this study the feedback from SAV to hydrodynamics is primarily through the canopy height, with SAV diameter and density unchanged. Competition between plant species is not included in the model. To further improve this model, we plan to add new capability to simulate the SAV propagation and also possibly competition between plant species if ongoing monitoring work by CADWR and USGS suggests niches are identifiable (say, between the median depth and shoal regimes identified in this thesis). The verification of the current model is limited by complexity of the system we envision and the availability of observation, and so more data support for the model development would further improve the model. At the same time, the hypotheses and ambiguities of the present work should help inform further monitoring work.

References

Allanson, B.R., 1973. The fine structure of the periphyton of Chara sp. and Potamogeton natans from Wytham Pond, Oxford, and its significance to the macrophyte-periphyton metabolic model of RG Wetzel and HL Allen. *Freshwater Biology*, *3*(6), pp.535-542.

Alpine, A.E. and Cloern, J.E., 1992. Trophic interactions and direct physical effects control phytoplankton biomass and production in an estuary. *Limnology and Oceanography*, 37(5), pp.946-955.

Bach, Hanne K. "A dynamic model describing the seasonal variations in growth and the distribution of eelgrass (Zostera marina L.) I. Model theory." *Ecological Modelling* 65.1-2 (1993): 31-50.

Boynton, W.R., Kemp, W.M. and Keefe, C.W., 1982. A comparative analysis of nutrients and other factors influencing estuarine phytoplankton production. In *Estuarine comparisons* (pp. 69-90).

Branquart, E., Stiers, I., Triest, L., Vanderhoeven, S., Van Landuyt, W., Van Rossum, F. & Verloove, F., 2013. Egeria densa - Brazilian waterweed. http://ias.biodiversity.be/species/show/54. Last accessed 01-08-2014.

Brown, L.R., 2003. Will tidal wetland restoration enhance populations of native fishes?. *San Francisco Estuary and Watershed Science*, *1*(1).

Brown, L.R. and Michniuk, D., 2007. Littoral fish assemblages of the alien-dominated Sacramento-San Joaquin Delta, California, 1980–1983 and 2001–2003. *Estuaries and Coasts*, *30*(1), pp.186-200.

Carpenter, S.R. and Lodge, D.M., 1986. Effects of submersed macrophytes on ecosystem processes. *Aquatic botany*, 26, pp.341-370.

Center, W.R.C., 2010. Historical climate information. Reno, NV: Desert Research Institute, Western Regional Climate Center. Web site viewed on March, 30, p.2010.

Cerco, C.F. and Cole, T., 1993. Three-dimensional eutrophication model of Chesapeake Bay. *Journal of Environmental Engineering*, *119*(6), pp.1006-1025.

Cerco, C.F. and Cole, T.M., 1994. *Three-Dimensional Eutrophication Model of Chesapeake Bay. Volume 1: Main Report* (No. WES/TR/EL-94-4). Army engineer waterways experiment station Vicksburg MS environmental lab.

Cerco, C.F. and Moore, K., 2001. System-wide submerged aquatic vegetation model for Chesapeake Bay. *Estuaries*, *24*(4), pp.522-534.

Cerco, C.F., Johnson, B.H. and Wang, H.V., 2002. *Tributary Refinements to the Chesapeake Bay Model (CD-ROM)* (No. ERDC-TR-02-4). Engineer research and development center Vicksburg MS.

Cerco, C., Kim, S.C. and Noel, M., 2010. The 2010 Chesapeake Bay Eutrophication Model. A Report to the US Environmental Protection Agency Chesapeake Bay Program and to the US Army Engineer Baltimore District. US Army Engineer Research and Development Center, Vicksburg, MS.

Te Chow, V., 1959. Open-channel hydraulics (Vol. 1). New York: McGraw-Hill.

Cloern, J.E., 1987. Turbidity as a control on phytoplankton biomass and productivity in estuaries. *Continental Shelf Research*, 7(11-12), pp.1367-1381.

Cloern, J.E., Canuel, E.A. and Harris, D., 2002. Stable carbon and nitrogen isotope composition of aquatic and terrestrial plants of the San Francisco Bay estuarine system. *Limnology and oceanography*, 47(3), pp.713-729.

Cloern, J.E., Cole, B.E., Wong, R.L. and Alpine, A.E., 1985. Temporal dynamics of estuarine phytoplankton: a case study of San Francisco Bay. In *Temporal Dynamics of an Estuary: San Francisco Bay* (pp. 153-176). Springer, Dordrecht.

Cloern, J.E., Grenz, C. and Vidergar -Lucas, L., 1995. ratio -Limnology and Oceanography, 40(7), pp.1313- 1321.

Conomos, T.J. and Peterson, D.H., 1977. Suspended-particle transport and circulation in San Francisco Bay: an overview. In *Estuarine processes: Circulation, Sediments, and transfer of material in the estuary* (pp. 82-97).

Dahm, C.N., 2016. Delta nutrients: Sources, sinks, sags, soups, and sensors. https://mavensnotebook.com/2016/11/10/delta-nutrients-sources-sinks-sags-soups-and-sensors/

Dale, H.M. and Gillespie, T.J., 1977. The influence of submersed aquatic plants on temperature gradients in shallow water bodies. *Canadian Journal of Botany*, *55*(16), pp.2216-2225.

Darby, S.E., 1999. Effect of riparian vegetation on flow resistance and flood potential. *Journal of Hydraulic Engineering*, *125*(5), pp.443-454.

Darrin, H., 2009. Brazilian Elodea, Egeria densa, Anacharis, Philotria densa, Giant Elodea, Brazilian waterweed. Washington Department of Ecology: Aquatic Weeds, United States of America.

De Boer, W.F., 2007. Seagrass–sediment interactions, positive feedbacks and critical thresholds for occurrence: a review. *Hydrobiologia*, *591*(1), pp.5-24.

Dennison, W.C., Orth, R.J., Moore, K.A., Stevenson, J.C., Carter, V., Kollar, S., Bergstrom, P.W. and Batiuk, R.A., 1993. Assessing water quality with submersed aquatic vegetation. *BioScience*, *43*(2), pp.86-94.

Dierberg, F.E., DeBusk, T.A., Jackson, S.D., Chimney, M.J. and Pietro, K., 2002. Submerged aquatic vegetation-based treatment wetlands for removing phosphorus from agricultural runoff: response to hydraulic and nutrient loading. *Water research*, *36*(6), pp.1409-1422.

DiToro, D.M. and Fitzpatrick, J.J., 1993. Chesapeake Bay sediment flux model. Prepared for the US Army Corps of Engineers, WES Environmental Laboratory, Vicksburg, Mississippi by HydroQual. *Inc., Mahwah, NJ*.

Dugdale, R.C., Wilkerson, F.P., Hogue, V.E. and Marchi, A., 2007. The role of ammonium and nitrate in spring bloom development in San Francisco Bay. *Estuarine, Coastal and Shelf Science*, 73(1), pp.17-29.

Durand, J.R., 2017. Evaluating the Aquatic Habitat Potential of Flooded Polders in the Sacramento-San Joaquin Delta. *San Francisco Estuary and Watershed Science*, *15*(4).

Feijoó, C.S., Momo, F.R., Bonetto, C.A. and Tur, N.M., 1996. Factors influencing biomass and nutrient content of the submersed macrophyte Egeria densa Planch. in a pampasic stream. *Hydrobiologia*, 341(1), pp.21-26.

Feyrer, F., Nobriga, M.L. and Sommer, T.R., 2007. Multidecadal trends for three declining fish species: habitat patterns and mechanisms in the San Francisco Estuary, California, USA. *Canadian Journal of Fisheries and Aquatic Sciences*, *64*(4), pp.723-734.

García, M.H., López, F., Dunn, C. and Alonso, C.V., 2004. Flow, turbulence, and resistance in a flume with simulated vegetation. *Riparian vegetation and fluvial geomorphology*, pp.11-27.

Glibert, P.M., 2010. Long-term changes in nutrient loading and stoichiometry and their relationships with changes in the food web and dominant pelagic fish species in the San Francisco Estuary, California. *Reviews in Fisheries Science*, 18(2), pp.211-232.

Glibert, P.M., Dugdale, R.C., Wilkerson, F., Parker, A.E., Alexander, J., Antell, E., Blaser, S., Johnson, A., Lee, J., Lee, T. and Murasko, S., 2014. Major–but rare–spring blooms in 2014 in San Francisco Bay-Delta, California, a result of the long-term drought, increased residence time, and altered nutrient loads and forms. *Journal of Experimental Marine Biology and Ecology*, 460, pp.8-18.

Glibert, P.M., Fullerton, D., Burkholder, J.M., Cornwell, J.C. and Kana, T.M., 2011. Ecological stoichiometry, biogeochemical cycling, invasive species, and aquatic food webs: San Francisco Estuary and comparative systems. *Reviews in Fisheries Science*, 19(4), pp.358-417.

Grimaldo, L.F., Stewart, A.R. and Kimmerer, W., 2009. Dietary segregation of pelagic and littoral fish assemblages in a highly modified tidal freshwater estuary. *Marine and Coastal Fisheries*, *1*(1), pp.200-217.

Haynes, R.R., 1988. Reproductive biology of selected aquatic plants. *Annals of the Missouri Botanical Garden*, pp.805-810.

Hestir, E.L., Schoellhamer, D.H., Greenberg, J., Morgan-King, T. and Ustin, S.L., 2016. The effect of submerged aquatic vegetation expansion on a declining turbidity trend in the Sacramento-San Joaquin River Delta. *Estuaries and Coasts*, 39(4), pp.1100-1112.

Howard-Williams, C. and Allanson, B.R., 1981. Phosphorus cycling in a dense Potamogeton pectinatus L. bed. *Oecologia*, *49*(1), pp.56-66.

Ikeda, S. and Kanazawa, M., 1996. Three-dimensional organized vortices above flexible water plants. *Journal of Hydraulic Engineering*, *122*(11), pp.634-640.

Jassby, A., 2008. Phytoplankton in the upper San Francisco Estuary: recent biomass trends, their causes, and their trophic significance. *San Francisco Estuary and Watershed Science*, 6(1).

Jassby, A.D. and Cloern, J.E., 2000. Organic matter sources and rehabilitation of the Sacramento-San Joaquin Delta (California, USA). *Aquatic Conservation: Marine and Freshwater Ecosystems*, *10*(5), pp.323-352.

Jassby, A.D. and Platt, T., 1976. Mathematical formulation of the relationship between photosynthesis and light for phytoplankton. *Limnology and oceanography*, *21*(4), pp.540-547.

Jin, K.R., Ji, Z.G. and James, R.T., 2007. Three-dimensional water quality and SAV modeling of a large shallow lake. *Journal of Great Lakes Research*, 33(1), pp.28-45.

Jolliff, J.K., Kindle, J.C., Shulman, I., Penta, B., Friedrichs, M.A., Helber, R. and Arnone, R.A., 2009. Summary diagrams for coupled hydrodynamic-ecosystem model skill assessment. *Journal of Marine Systems*, *76*(1), pp.64-82.

Kemp, W.M., Twilley, R.R., Stevenson, J.C., Boynton, W.R. and Means, J.C., 1983. The decline of submerged vascular plants in upper Chesapeake Bay: Summary of results concerning possible causes. *Marine Technology Society Journal*, *17*(2), pp.78-89.

Kimmerer, W., 2004. Open water processes of the San Francisco Estuary: from physical forcing to biological responses. *San Francisco Estuary and Watershed Science*, 2(1).

Knight, R.L., Gu, B., Clarke, R.A. and Newman, J.M., 2003. Long-term phosphorus removal in Florida aquatic systems dominated by submerged aquatic vegetation. *Ecological Engineering*, *20*(1), pp.45-63.

Latta, Marilyn, and Natalie Cosentino-Manning. "San francisco bay subtidal habitat goals report: setting 50 year conservation goals for olympia oyster research, restoration, and management in the san francisco bay." in Journal of Shellfish Research, vol. 31, no. 1, pp. 310-310. c/o Dr. Sandra E. Shumway, Univ Connecticut, Natl Shellfisheries Assoc, 2012.

Lehman, P.W., Mayr, S., Mecum, L. and Enright, C., 2010. The freshwater tidal wetland Liberty Island, CA was both a source and sink of inorganic and organic material to the San Francisco Estuary. *Aquatic ecology*, *44*(2), pp.359-372.

López, F. and García, M.H., 2001. Mean flow and turbulence structure of open-channel flow through non-emergent vegetation. *Journal of Hydraulic Engineering*, *127*(5), pp.392-402.

Lund, J., Hanak, E., Fleenor, W., Howitt, R., Mount, J. and Moyle, P., 2007. Envisioning futures for the Sacramento-San Joaquin delta. *Public Policy Institute of California, San Francisco*, p.324.

Madden, C.J. and Kemp, W.M., 1996. Ecosystem model of an estuarine submersed plant community: calibration and simulation of eutrophication responses. *Estuaries and Coasts*, *19*(2), pp.457-474.

Maglio, C. and Hershorin, A., 2013. Nearshore berm discussion environmental impacts. Engineer Research and Development Center Vicksburg MS coastal and hydraulics lab.

Marchetti, M.P. and Moyle, P.B., 2001. Effects of flow regime on fish assemblages in a regulated California stream. *Ecological Applications*, *11*(2), pp.530-539.

Mazzeo, N., Rodríguez-Gallego, L., Kruk, C., Meerhoff, M., Gorga, J., Lacerot, G., Quintans, F., Loureiro, M., Larrea, D. and García-Rodríguez, F., 2003. Effects of Egeria densa Planch. beds on a shallow lake without piscivorous fish. *Hydrobiologia*, *506*(1-3), pp.591-602.

Mendez, F.J. and Losada, I.J., 2004. An empirical model to estimate the propagation of random breaking and nonbreaking waves over vegetation fields. *Coastal Engineering*, *51*(2), pp.103-118.

Moore, K.A., 2004. Influence of seagrasses on water quality in shallow regions of the lower Chesapeake Bay. *Journal of Coastal Research*, pp.162-178.

Moore, K.A., Wetzel, R.L. and Orth, R.J., 1997. Seasonal pulses of turbidity and their relations to eelgrass (Zostera marina L.) survival in an estuary. *Journal of Experimental Marine Biology and Ecology*, *215*(1), pp.115-134.

Nadaoka, K. and Yagi, H., 1998. Shallow-water turbulence modeling and horizontal large-eddy computation of river flow. *Journal of Hydraulic Engineering*, 124(5), pp.493-500.

Naot, D., Nezu, I. and Nakagawa, H., 1996. Hydrodynamic behavior of partly vegetated open channels. *Journal of Hydraulic Engineering*, *122*(11), pp.625-633.

Nepf, H.M. and Vivoni, E.R., 2000. Flow structure in depth -limited, vegetated flow. *Journal of Geophysical Research: Oceans*, *105*(C12), pp.28547-28557.

Nichols, F.H., Cloern, J.E., Luoma, S.N. and Peterson, D.H., 1986. The modification of an estuary. *Science(Washington)*, *231*(4738), pp.567-573.

Oremland, R.S. and Taylor, B.F., 1977. Diurnal fluctuations of O2, N2, and CH4 in the rhizosphere of Thalassia testudinum. *Limnology and Oceanography*, *22*(3), pp.566-570.

Owens, M., Learner, M.A. and Maris, P.J., 1967. Determination of the biomass of aquatic plants using an optical method. *The Journal of Ecology*, pp.671-676.

Park, K., Kuo, A.Y., Shen, J. and Hamrick, J.M., 1995. A three-dimensional hydrodynamic-eutrophication model (HEM-3D): description of water quality and sediment process submodels. *Special Report in Applied Marine Science and Ocean Engineering*, *327*.

Peterson, D.H., Conomos, T.J., Broenkow, W.W. and Doherty, P.C., 1975. Location of the non-tidal current null zone in northern San Francisco Bay. *Estuarine and Coastal Marine Science*, *3*(1), pp.1-11.

Pokorný, J. and Rejmánková, E., 1983. Oxygen regime in a fishpond with duckweeds (Lemnaceae) and Ceratophyllum. *Aquatic Botany*, *17*(2), pp.125-137.

Q-bank invasive plants, 2014. http://www.q-bank.eu/Plants/. Last accessed 16-07-2014.

Qin, Q. and Shen, J., 2017. The contribution of local and transport processes to phytoplankton biomass variability over different timescales in the Upper James River, Virginia. Estuarine, *Coastal and Shelf Science*, 196, pp.123-133.

Rodrigues, R.B. and Thomaz, S.M., 2010. Photosynthetic and growth responses of Egeria densa to photosynthetic active radiation. *Aquatic Botany*, *92*(4), pp.281-284.

Santos, M.J., Anderson, L.W. and Ustin, S.L., 2011. Effects of invasive species on plant communities: an example using submersed aquatic plants at the regional scale. *Biological Invasions*, *13*(2), pp.443-457.

Schaeffer, K., K. McGourty, and N. Cosentino-Manning (eds.) 2007. *Report on the subtidal habitats and associated biological taxa in San Francisco Bay.* NOAA Santa Rosa Office.

Schoellhamer, D.H., Wright, S.A. and Drexler, J., 2012. A conceptual model of sedimentation in the Sacramento–San Joaquin Delta. *San Francisco Estuary and Watershed Science*, 10(3).

Shimizu, Y. and Tsujimoto, T., 1993. Comparison of flood-flow structure between compound channel and channel with vegetated zone. In *Proceedings of the congress-international association for hydraulic research* (Vol. 1, pp. 97-97).

Shimizu, Y. and Tsujimoto, T., 1994. Numerical analysis of turbulent open-channel flow over a vegetation layer using a k-ε turbulence model. *Journal of hydroscience and hydraulic engineering*, *11*(2), pp.57-67.

Smith, L.H., 1987. *A review of circulation and mixing studies of San Francisco Bay, California*. Department of the Interior, US Geological Survey.

Sommer, T. and Mejia, F., 2013. A place to call home: a synthesis of Delta Smelt habitat in the upper San Francisco Estuary. *San Francisco Estuary and Watershed Science*, *11*(2).

Staehr, P.A., Testa, J.M., Kemp, W.M., Cole, J.J., Sand-Jensen, K. and Smith, S.V., 2012. The metabolism of aquatic ecosystems: history, applications, and future challenges. *Aquatic Sciences*, 74(1), pp.15-29.

Stow, C.A., Jolliff, J., McGillicuddy, D.J., Doney, S.C., Allen, J.I., Friedrichs, M.A., Rose, K.A. and Wallhead, P., 2009. Skill assessment for coupled biological/physical models of marine systems. *Journal of Marine Systems*, 76(1), pp.4-15.

Su, X. and Li, C.W., 2002. Large eddy simulation of free surface turbulent flow in partly vegetated open channels. *International Journal for Numerical Methods in Fluids*, 39(10), pp.919-937.

Thayer, G.W., Kenworthy, W.J. and Fonseca, M.S., 1984. *Ecology of Eelgrass Meadows of the Atlantic Coast: a community profile* (No. FWS/OBS-84/02). National Marine Fisheries Service, Beaufort, NC (USA). Beaufort Lab.; Virginia Univ., Charlottesville (USA). Dept. of Environmental Sciences.

Tschirky, P., Hall, K. and Turcke, D., 2001. Wave attenuation by emergent wetland vegetation. In *Coastal Engineering* 2000 (pp. 865-877).

TSUJIMOTO, T. and KITAMURA, T., 1995. Lateral Bed-load Transport and Sand-Rigde Formation Near Vegetation Zone in an Open Channel. *Journal of hydroscience and hydraulic engineering*, *13*(1), pp.35-45.

Umlauf, L. and Burchard, H., 2003. A generic length-scale equation for geophysical turbulence models. *Journal of Marine Research*, 61(2), pp.235-265.

Westlake, D.F., 1964. Light extinction, standing crop and photosynthesis within weed beds: With 4 Figures and 2 tables in the text. *Internationale Vereinigung für theoretische und angewandte Limnologie: Verhandlungen*, 15(1), pp.415-425.

Wetzel, R.G., 1960. Marl encrustation on hydrophytes in several Michigan lakes. *Oikos*, 11(2), pp.223-236.

Wetzel, R.L. and Neckles, H.A., 1986. A model of Zostera marina L. photosynthesis and growth: simulated effects of selected physical-chemical variables and biological interactions. *Aquatic Botany*, *26*, pp.307-323.

Whitley, S.N. and Bollens, S.M., 2014. Fish assemblages across a vegetation gradient in a restoring tidal freshwater wetland: diets and potential for resource competition. *Environmental biology of fishes*, *97*(6), pp.659-674.

Wu, C.H., Yuan, H. and Young, C.C., 2008. Non-hydrostatic modeling of vegetation effects on wave and flow motions. In *Estuarine and Coastal Modeling* (2007) (pp. 304-321).

Yarrow, M., Marin, V.H., Finlayson, M., Tironi, A., Delgado, L.E. and Fischer, F., 2009. The ecology of Egeria densa Planchon (Liliopsida: Alismatales): A wetland ecosystem engineer. *Revista Chilena de Historia Natural*, *82*(2), pp.299-313.

Zhang, Y. and Baptista, A.M., 2008. SELFE: a semi-implicit Eulerian–Lagrangian finite-element model for cross-scale ocean circulation. *Ocean modelling*, 21(3), pp.71-96.

Zhang, Y.J., Ateljevich, E., Yu, H.C., Wu, C.H. and Jason, C.S., 2015. A new vertical coordinate system for a 3d unstructured-grid model. *Ocean Modelling*, 85, pp.16-31.

Zhang, Y.J., Ye, F., Stanev, E.V. and Grashorn, S., 2016. Seamless cross-scale modeling with SCHISM. *Ocean Modelling*, 102, pp.64-81.

Zhang, Y., Gerdts, N., Ateljevich, E., Nam, K. (submitted) Simulating the 3D effects of vegetation on flows using unstructured grids, *Ocean Modelling.*

Zimmerman, R.C., Reguzzoni, J.L. and Alberte, R.S., 1995. Eelgrass (Zostera marina L.) transplants in San Francisco Bay: role of light availability on metabolism, growth and survival. *Aquatic Botany*, 51(1-2), pp.67-86.

VITA

Xun Cai

Born in Changshu, Jiangsu, China, Dec 2, 1992. Earned a B.S. in Oceanography from Nanjing University in 2015. Entered the M.S. program at the Virginia Institute of Marine Science / College of William and Mary School of Marine Science in 2015.